Doctoral Dissertation

Charging and Discharging Performances of Advanced Li-ion Batteries Using Eco-friendly Active Materials

環境配慮型活物質を用いる
次世代リチウムイオン電池の充放電特性

Akita University
September, 2023

Yusuke ABE
安部 勇輔

Abstract

Li-ion batteries (LIBs) featuring Li transition metal oxide cathodes and carbonaceous anodes have emerged as powerful energy storage devices. These LIBs have extensive applications in areas such as zero-emission vehicles and renewable energy-powered grids, contributing to the realization of a carbon-neutral society. The demand for component materials in LIBs is expected to increase drastically in the next decade. For LIB cathodes, Li transition metal oxides with abundant rare metals have been utilized to achieve high cathodic potential and adequate lithiation specific capacity. Notably, ternary Li transition metal oxide cathode active materials, comprising Li, Ni, Co, and Mn, are widely employed in automotive applications. However, the supply chains for these rare metals can be significantly impacted by international affairs. Consequently, there has been growing interest in recycling these metals to establish a sustainable LIB production system. Meanwhile, graphite has been the primary choice for LIB anodes since their commercialization in the 1990s due to its low and stable anodic potential. Over time, a wealth of technical experience in using graphite for LIBs has been accumulated. Nevertheless, next-generation LIBs require anode materials with higher lithiation specific capacity, improved rate and cycling performances, and extended cycle life. To address these technical requirements, the in-depth exploration into sustainable production methods for LIB electrode active materials is now essential. Consequently, this dissertation focuses on the charging and discharging performances of LIBs using eco-friendly active materials derived from agricultural waste and rare metals recovered from spent LIBs.

Rare metals, such as Li, Ni, Co, and Mn, are significant components of LIB cathode active materials. To address the uncertain future supply chains of these metals, it is crucial to establish reliable and efficient recycling methods for waste LIBs. One practical recovery process for Ni, Co, and Mn from spent LIBs involves pyrolyzing whole battery stacks without exposure to air, ensuring higher safety and time-efficient preprocessing. In this process, the “black mass,” a pyrolysis residue of LIB stacks, is purified and converted into hydroxides of Ni, Co, and Mn

with impurities. These metal hydroxides are mixed with Li carbonate and sintered in air, producing recycled $LiNi_{1/3}Co_{1/3}Mn_{1/3}O_2$. The cathode using recycled $LiNi_{1/3}Co_{1/3}Mn_{1/3}O_2$, containing metallic impurities, such as Al, Cu, and Fe totaling 4 mass%, as well as excessive Li and residual F, was electrochemically characterized in half- and full-cell configurations. The recycled $LiNi_{1/3}Co_{1/3}Mn_{1/3}O_2$ exhibited slightly lower lithiation specific capacity but much higher capacity retention (91.2% after 1000 cycles at 2 C) compared to the commercial LIB cathode active material $LiNi_{0.5}Co_{0.2}Mn_{0.3}O_2$. The results indicate that, while the lithiation specific capacity is marginally reduced, the co-existing metallic impurities have minimal adverse effects on the LIB cathode. This suggests that $LiNi_{1/3}Co_{1/3}Mn_{1/3}O_2$ cathode active materials recovered from pyrolyzed LIB stacks can be effectively used in LIBs.

Composite materials are known to possess superior electrochemical properties when used as LIB anodes. In this study, hard carbon (HC) and nanosized-Si (N-Si) were mixed at a mass ratio of 8:2 and used as the LIB anode active material. Galvanostatic electrochemical evaluations in a half-cell configuration revealed that the composite anode exhibited a high capacity (531 mAh g^{-1}) at 0.1 C and excellent stability against increased current density from 0.1 to 10 C. To assess its practical LIB anode performance, charge-discharge cycling tests were conducted on $LiNi_{0.5}Co_{0.2}Mn_{0.3}O_2$|8:2 HC/N-Si full cells. Before assembling the full cells, the composite anodes were prelithiated with different cutoff anodic specific capacities (200–600 mAh g^{-1}). The effects of excessive prelithiation on the composite anodes in the LIB full cells were examined. By setting the cutoff anodic specific capacities at 500 mAh g^{-1} or higher during the prelithiation process, the full cells using the 8:2 HC/N-Si composite anode demonstrated the highest capacity retention (>62%) over 200 cycles at 2 C. These findings emphasize the importance of selecting an appropriate prelithiation level for composite LIB anodes.

To achieve sustainable and eco-friendly fabrication of LIB anodes, agricultural waste rice husk (RH) was considered. Around 150 million metric tons of RH are produced worldwide annually, with their utilization currently limited to some agricultural and livestock fields. In Japan,

approximately 30% of discharged RH is not effectively utilized. Composites of RH-derived carbon (C) and silicon oxides (SiO_x) were produced, and their electrochemical properties as LIB anodes were evaluated. C/SiO_x composites were produced by heating raw RH at 600 °C under inert conditions, followed by washing or partial or complete removal of SiO_x in a NaOH solution. They were then heated again at 1000 °C, resulting in three types of C/SiO_x containing 45, 24, and 5 mass% SiO_x. The LIB anodic performances of these composites were investigated in half- and full-cell configurations, and the role of SiO_x in C/SiO_x was examined. In the half-cell configuration, the specific capacities of the carbon and SiO_x components were determined to be 375 and 475 mAh g^{-1}, respectively. The full-cell test demonstrated that stable anodic operation of C/SiO_x composites required a prelithiation process. LIB full cells consisting of a $LiNi_{0.5}Co_{0.2}Mn_{0.3}O_2$ cathode and prelithiated C/SiO_x anode exhibited high initial Coulombic efficiency (~85%). As the charging and discharging current density increased, capacity retention improved with higher SiO_x content. During the cycling test, the full cell with the highest SiO_x content showed the largest decrease in cell-specific capacity. Considering the performance variations due to different SiO_x levels and the satisfactory rate and cycling performances as LIB full cells, RH-derived C/SiO_x was found to be a viable and sustainable anode active material for LIBs.

This study focused on the development of advanced LIBs using eco-friendly active materials. Knowledge was gained on the recycled cathode, recovered from the pyrolysis of LIB stacks, and on the RH-derived C/SiO_x composite anodes. The concept and industrial benefits of “green LIBs” were proposed in this dissertation. These advancements can contribute to sustainable LIB fabrication and ultimately support the realization of a carbon-neutral society.

摘要

Li 遷移金属酸化物正極と炭素質負極によって特徴付けられるリチウムイオン電池（LIB）は，重要なエネルギー貯蔵デバイスとして登場した。LIB は，ゼロエミッション車や再生可能エネルギーによる送電網などの分野において広範な用途で用いられ，カーボンニュートラルな社会の実現に貢献している。LIB とその構成材料の需要は今後 10 年間で飛躍的に増加すると予想されている。LIB の正極には，高い正極電位と十分なリチウム化比容量を得るために，レアメタルを豊富に含む Li 遷移金属酸化物が利用されてきた。特に，Li，Ni，Co および Mn から成る三元系 Li 遷移金属酸化物の正極活物質は車載用途で広く採用されている。しかしながら，これらレアメタルのサプライチェーンは，国際情勢によって大きな影響を受ける可能性がある。そのため，持続可能な LIB の生産システムを構築するため，これらの金属をリサイクルすることに関心が高まってきている。一方，LIB の負極は，その負極電位が低く安定していることから，1990 年代の LIB の実用化以来，黒鉛が LIB 負極の主な選択肢となっている。長い時間をかけて，LIB に黒鉛を使用するための技術的経験が蓄積されてきた。しかしながら，次世代 LIB には，より高いリチウム化比容量，優れたレートおよびサイクル性能，ならびに長寿命を有する負極材が要求される。このような技術的要求に応えるために，LIB 電極活物質の持続可能な製造方法についての詳細な調査が必要である。そこで，本学位論文では，農業廃棄物由来および使用済み LIB から回収したレアメタルに由来する環境に優しい活物質を用いた LIB の充放電性能に焦点を当てる。

Li，Ni，Co および Mn などのレアメタルは，LIB 正極活物質の重要な構成要素である。これら金属の不確実な将来のサプライチェーンに対処するため，LIB 廃棄物に関して信頼性が高くて効率的なリサイクル方法を確立することが重要である。使用済み LIB から Ni，Co および Mn の実用的な回収プロセスの 1 つは，大気暴露なしで電池スタック全体を熱分解することで，より安全で時間効率の良い前処理を確実とする。このプロセスでは，LIB スタックの熱分解残さである“ブラックマス”を精製し，不純物を含む Ni，Co および Mn の水酸化物へと変換する。これら金属水酸化物は炭酸リチウムと混合して空気中で焼成し，リサイクル $LiNi_{1/3}Co_{1/3}Mn_{1/3}O_2$ を生成する。過剰な Li および残留 F とともに，Al，Cu および Fe を合計で 4 質量%の金属不純物を含むリサイクル $LiNi_{1/3}Co_{1/3}Mn_{1/3}O_2$ を用いたその正極は，ハーフセルおよびフルセル構成のもと電気化学的に特性付けした。リサイクル $LiNi_{1/3}Co_{1/3}Mn_{1/3}O_2$ は，市販 LIB 正極活物質 $LiNi_{0.5}Co_{0.2}Mn_{0.3}O_2$ と比較して，リチウム化比容量はやや低かったが，非常に高い容量保持率（2 C で 1000 サイクル後に 91.2%）を示した。この結果は，リチウム化比容量がわずかに減少するものの，金属不純物の共存はその LIB 正極にわずかな悪影響しかもたらさないことを示している。これは，熱分解した LIB スタックから回収した $LiNi_{1/3}Co_{1/3}Mn_{1/3}O_2$ 正極活物質は LIB に有効に使用できることを示唆している。

複合材料は，LIB 負極として使用した場合，優れた電気化学的特性が得られることで知られている。本研究では，ハードカーボン（HC）とナノサイズシリコン（N-Si）を 8:2 の質量比で混合し，LIB 負極活物質として使用した。ハーフセル構成における定電流電気化学評価では，複合負極は 0.1 C で高容量（531 mAh g^{-1}）を示し，0.1 から 10 C までの電流密度の増加に対して優れた安定性を示した。実用的な LIB 負極性能を評価するため，$LiNi_{0.5}Co_{0.2}Mn_{0.3}O_2$｜8:2 HC/N-Si フルセルを用いた充放電サイクル試験を実施した。フルセルの組立て前，異なるカットオフ負極比容量（200–600 mAh g^{-1}）で複合負極をプレリチウム化した。LIB フルセルの複合負極における過剰プレリチウム化の影響について検討した。プレリチウム化工程でカットオフ負極比容量を 500 mAh g^{-1} 以上に設定することで，8:2 HC/N-Si 複合負極を用いたフルセルは，2 C で 200 サイクルを超えても最も高い容量保持率（>62%）を示した。これら成果は，複合 LIB 負極に対して適切なプレリチウム化レベルを選択することの重要性を強調している。

LIB 負極の持続可能で環境に優しい製造を実現するため，農業廃棄物であるもみ殻（RH）について検討した。RH は，年間，世界で約 1 億 5 千万トン排出されているが，現在の利用は一部の農業および家畜の分野に限られていた。日本では，排出された RH の約 30%が有効に利用されていない。RH 由来炭素（C）および酸化ケイ素（SiO_x）の複合材を作製し，LIB 負極としての電気化学的特性を評価した。C/SiO_x 複合材は，生の RH を不活性条件のもと 600 ° C で加熱することで生成し，その後，蒸留水での SiO_x の洗浄，もしくは NaOH 水溶液で部分的にあるいは完全に SiO_x を除去した。それらを次に 1000 °C で加熱し，45，24 および 5 質量%の SiO_x を含む 3 種類の C/SiO_x を製造した。これら複合材の LIB 負極性能をハーフセルおよびフルセル構成で評価し，C/SiO_x における SiO_x の役割を調査した。ハーフセル構成では，C および SiO_x 成分の比容量をそれぞれ 375 および 475 mAh g^{-1} に定めた。フルセル試験では，プレリチウム化を適用した C/SiO_x 複合材の安定した負極動作が示された。$LiNi_{0.5}Co_{0.2}Mn_{0.3}O_2$ 正極とプレリチウム化 C/SiO_x 負極から成る LIB フルセルは，高い初期クーロン効率（〜85%）を示した。充放電電流密度が増加するにつれて，容量保持率は SiO_x の含有量が高いほど改善した。サイクル試験では，最も高い SiO_x 含有量のフルセルがセル比容量の大幅な減少を示した。LIB フルセルにおいて，十分なレートおよびサイクル特性，ならびに SiO_x 含有量の違いを考慮しても，RH 由来 C/SiO_x は LIB に関して実行可能で持続可能な負極活物質であることが見出された。

本研究は，環境に優しい電極活物質を用いた次世代 LIB の開発に焦点を当てている。LIB スタックの熱分解残さから回収したリサイクル正極，および RH 由来 C/SiO_x 複合負極に関する知見が得られた。本論文では，“グリーン LIB”の概念および産業上の利点を提案した。これらの発展は，持続可能な LIB の製造に貢献でき，最終的にはカーボンニュートラルな社会の実現を支援できる。

Contents

Chapter 1

Preface

1. 1 Research Focus

This research focuses on electrode-active materials for Li-ion batteries (LIBs), which are energy storage devices with a high energy density of 120–200 Wh kg^{-1} and an average voltage of approximately 4 V during discharge [1, 2]. By connecting several LIB cells in series and parallel, LIB stacks can provide high capacity and voltage for electrical energy storage systems. Higher energy density and operating cell voltage for individual LIBs can reduce the number of electrode materials and cells required, leading to decreased weight and size for various applications. The charging and discharging performances of LIBs, such as energy density, power capability, operating cell voltage, and cycle life, are determined by the electrochemical properties of the active materials used in LIB electrodes [3–6]. Material costs and supply quantities also depend on the properties of the raw materials used for the active materials. Factors such as prime costs, resource reserves, and ready availability are essential for producing low-cost materials. Thus, intensive research on electrode-active materials for LIBs leads to improvements in performance and cost reduction for these batteries, ultimately contributing to the development of advanced electrical energy storage systems.

1. 2 Brief History

In the late 1990s, the demand for rechargeable batteries gradually increased along with the need for portable electronic devices. From the 1970s to the 1990s, researchers investigated and sought promising active materials for LIB electrodes, ultimately discovering outcomes associated with constituent materials and inner structures of the pristine LIBs. As a result, the well-known basic structure of LIBs, employing a Li transition metal oxide (LTMO) as a cathode and a carbonaceous material as an anode, was established as the existing cell structure [7–9]. By immersing both electrodes into organic solvents containing Li salts such as $LiBF_4$ and $LiPF_6$

in the LIB cells, Li ions can transfer between the cathode and anode during charging and discharging. This migration of Li ions enables the release and reception of electrons to/from external electrical circuits, allowing LIBs to function as rechargeable batteries. LIBs, which have higher energy density and acceptable power capability compared to other secondary batteries, have been mostly utilized as rechargeable batteries, surpassing nickel-cadmium, nickel-metal hydride, and lead-acid batteries [1]. In 1991, the first LIBs were commercialized by Sony. Since then, LIBs have dominated the market for energy storage devices, providing convenience and portability to numerous electronic devices. Recently, the usage of LIBs has expanded from small-scale applications (electronic devices, electrical power tools, and others) to large-scale applications (zero-emission vehicles and stationary energy storage systems) [10]. The invention and development of LIBs have made a significant contribution to human society's advancement. In recognition of their groundbreaking work on LIBs, J. B. Goodenough, M. S. Whittingham, and A. Yoshino were awarded the Nobel Prize in Chemistry in 2019. Currently, novel rechargeable batteries with higher energy density and excellent power capability are strongly desired to realize the electrification of transport machinery in automotive and transportation industries. However, practical use has not been realized due to challenges and difficulties in developing novel rechargeable batteries with stable operation, high performance, and high safety. Therefore, energy storage devices will continue to rely on existing LIBs until new rechargeable batteries are developed.

1. 3 Background and Objective

LIBs serve as a convenient and powerful power source for portable electronic devices, electrical power tools, zero-emission vehicles, and stationary energy storage systems. The demand for LIBs has clearly increased alongside the expansion of these applications. As a result, the production volume of LIBs has drastically increased in recent years, and massive amounts of electrode materials are needed for manufacturing LIB cells. Reducing production costs remains a critical challenge in order to provide low-cost LIB products, regardless of their applications, sizes, and storage capacities.

LTMOs are commonly used in LIB cathodes. These cathodes contain a significant amount of rare metals, which have high value and limited resource reserves. Consequently, the mass production of LIBs could be hindered by constraints in cathode preparation. In recent years, recycling rare metals from waste LIBs has gained significant attention as a way to efficiently utilize these valuable resources without additional mining. The circular provision of rare metals through recycling technologies enables sustainable production of LIBs and the establishment of new material suppliers in the home country. In contrast, LIB anodes often use materials like C, Si, and previously mentioned composite materials, regardless of their degree of crystallization. Graphite remains the main active material for LIB anodes, even though other carbon and Si-based materials are considered possible alternatives. This reliance on graphite makes the mass production of LIBs challenging due to the limited material options. Industrial and agricultural wastes are discharged in large quantities worldwide in proportion to increased production in specific fields. Agricultural waste, such as rice husk (RH), which consists of organic components and silica (SiO_x), is a promising precursor for active materials in LIB anodes. Using agricultural waste is an effective means of sourcing materials domestically to meet the mass production demands of LIBs. In particular, Japan can expect a stable supply of anode materials due to the active rice production in specific regions of the country.

My objective in this project is to utilize eco-friendly and cost-effective active materials, derived from recycled rare metals for the cathode, and RH for the anode in LIBs. The produced active materials were electrochemically evaluated using LIB testing cells (half- and full-cell configurations). Based on the obtained results, the physical and electrochemical properties, effectiveness, and feasibility of the active materials produced in this work were discussed in detail. Consequently, it was demonstrated that the advanced LIBs, also called “green LIBs,” utilizing eco-friendly and economically active materials exhibited superior charging and discharging performances compared to existing LIBs.

1. 4 Overview of the Following Chapters

Chapter 2 provides a comprehensive overview of the current status of LIBs and reviews previous works related to waste LIB recycling and RH applications. In Chapter 3, the electrochemical performance of the $LiNi_{1/3}Co_{1/3}Mn_{1/3}O_2$ (NCM111) cathode recovered from waste LIB stacks is presented. In this chapter, I evaluated the electrochemical performance of the recycled NCM111 derived from waste LIB stacks and discussed the feasibility of using the recycled NCM111 cathode in LIB systems. Chapter 4 presents the effects of excessive prelithiation on a hard carbon (HC)/nanosized-Si (N-Si) composite anode in LIB full cells, while Chapter 5 focuses on the application of RH as LIB anode active materials. Chapter 4 investigates the effects of excessive prelithiation on an HC/N-Si composite anode in depth and concludes that excessive prelithiation is effective for composite anodes containing HC and N-Si in LIBs. The knowledge obtained in Chapter 4 regarding prelithiation is applied in Chapter 5, where RHs, consisting of amorphous C and SiO_x, similar to the composition of HC/N-Si composite materials in Chapter 4, are successfully applied in LIB anodes due to the prelithiation of the anodes in advance. Based on the results, I assessed the feasibility of using RH-derived anodes in LIBs. Finally, the outcomes of this dissertation are summarized in the Conclusions in Chapter 6.

Reference

[1] C. Julien, A. Mauger, A. Vijh, K. Zaghib, *Lithium Batteries*, Switzerland, Springer International Publishing, 2016.

[2] O. Kazunori, *Lithium Ion Rechargeable Batteries*, Germany. Wiley-VCH, 2009.

[3] Y. Takahashi, S. Tobe, A. Kinoshita, H. Fujimoto, I. Nakane, S. Fujitani, Development of lithium-ion batteries with a $LiCoO_2$ cathode toward high capacity by elevating charging potential, *J. Electrochem. Soc.* 155(7) (2008) A537–A541.

[4] W. A. Appiah, J. Park, S. Song, S. Byun, M.-H. Ryou, Y. M. Lee, Design optimization of $LiNi_{0.6}Co_{0.2}Mn_{0.2}O_2$/graphite lithium-ion cells based on simulation and experimental data, *J. Power Sources* 319 (2016) 147–158.

[5] H. Zheng, J. Li, X. Song, G. Liu, V. S. Battaglia, A comprehensive understanding of electrode thick ness effects on the electrochemical performances of Li-ion battery cathodes, *Electrochim. Acta* 71 (2012) 258–265.

[6] H. Li, Practical evaluation of Li-ion batteries. *Joule* 3 (2019) 908–919.

[7] Y. Masaki, R. J. Brodd, *Lithium-Ion Batteries*, New York, Springer Science+ Business Media, 2009.

[8] B. Xu, D. Qian, Z. Wang, Y. S. Meng, Recent progress in cathode materials research for advanced lithium ion batteries, *Mater. Sci. Eng. R Rep.* 73 (2012) 51–65.

[9] M.-S. Balogun, W. Qiu, Y. Luo, H. Meng, W. Mai, A. Onasanya, T. K. Olaniyi, Y. Tong, A review of the development of full cell lithium-ion batteries: The impact of nanostructured anode materials, *Nano Res.* 9(10) (2016) 2823–2851.

[10] F. Li, L. Kong, Y. Sun, Y. Jin, P. Hou, Micron-sized monocrystalline $LiNi_{1/3}Co_{1/3}Mn_{1/3}O_2$ as high-volumetric-energy-density cathode for lithium-ion batteries, *J. Mater. Chem. A* 6 (2018) 12344–12352.

Chapter 2

Literature Review

2. 1 Current State of Research on Electrode Materials for LIBs

The depletion of resources, air pollution, and greenhouse warming are still critical environmental issues. To tackle these challenges, the automotive industry is actively developing electric and plug-in hybrid vehicles to minimize exhaust emissions and promote the use of clean energy sources [1–2]. Electric-powered vehicles require high-capacity and high-power energy storage devices like LIBs [3–4]. LIBs are also increasingly being installed as stationary energy storage systems in grid systems combined with renewable energy generation [5]. As large-scale applications for LIBs expand, their demand will undoubtedly increase, making it essential to ensure a stable supply of construction materials and the mass production of LIBs in the future.

Figure 1 illustrates the construction materials and charging-discharging mechanism of a LIB cell. One or more active materials are typically used in the cathode and anode, where oxidation and reduction reactions occur conversely during charging and discharging. By repeating the transfer of Li-ions between the cathode and anode, LIBs allow for repeatable charging–discharging with a high operating cell voltage and serve as an energy supplier for various applications. Generally, a combination of a LTMO cathode and a carbonaceous anode in LIB cells is often used to achieve stable and better battery performances (high cell voltage, high energy density, long cycle life, and low self-discharge) [6–7]. The electrolyte and separator individually play roles in Li-ion transport between both electrodes and preventing direct physical contact and electrical short circuits at the electrodes, respectively. In the cathodes, an LTMO contains a certain amount of rare metals (Li, Co, Ni, and Mn) [8]. These rare metals face critical problems such as limited producing countries, poor supply capability, and expensive sourcing costs. Therefore, supplying the rare metals necessary for LIB cathodes may become more challenging in the future.

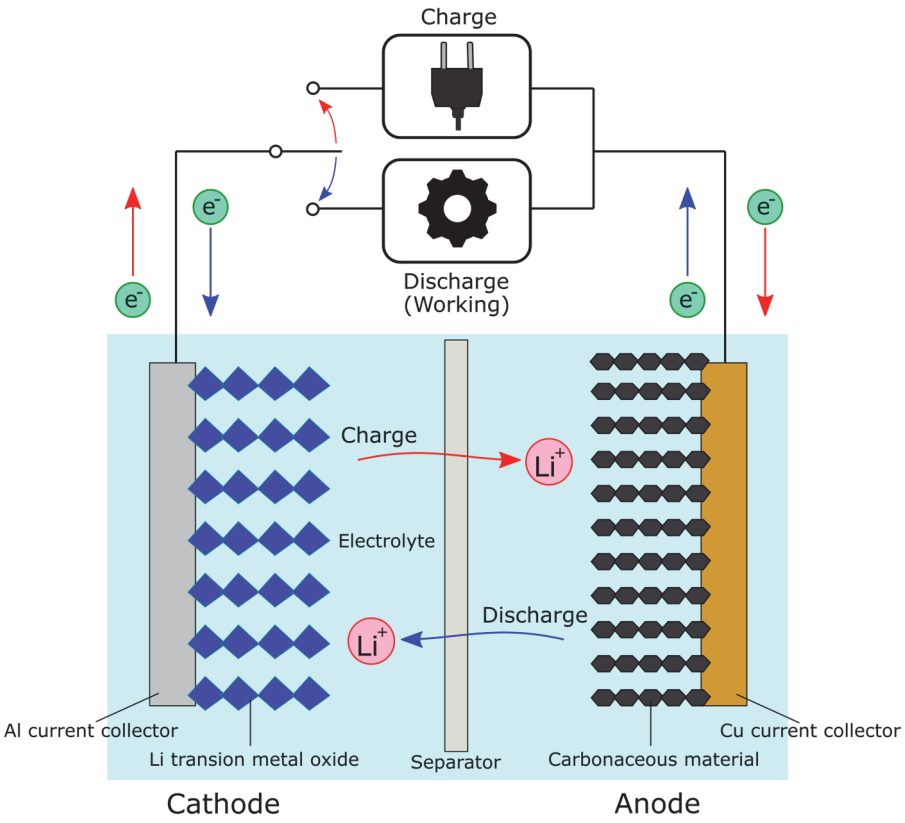

Figure 1 Construction materials and charging-discharging mechanism of a Li-ion battery (LIB) cell.

Recycling rare metals already used in cathodes of waste LIBs is garnering much attention for the effective reutilization of valuable resources. Common recycling processes typically involve mechanical, thermal, and chemical processing [9–10]. Through the recycling process, rare metals can be successfully extracted in the form of pure metals, metal salts, or metallic hydroxide, which are then used as a precursor for LTMOs. However, the aforementioned recycling processes have disadvantages, such as electrical shock hazards during pre-discharging, explosion accidents during disassembly, and low workability due to a reliance on manual operations [11–12]. In the coming decades, it is forecasted that a large number of waste LIBs (end-of-life and defective products) of various applications and sizes will be discharged. To manage the substantial amount of waste LIBs in the future, there is a strong need for

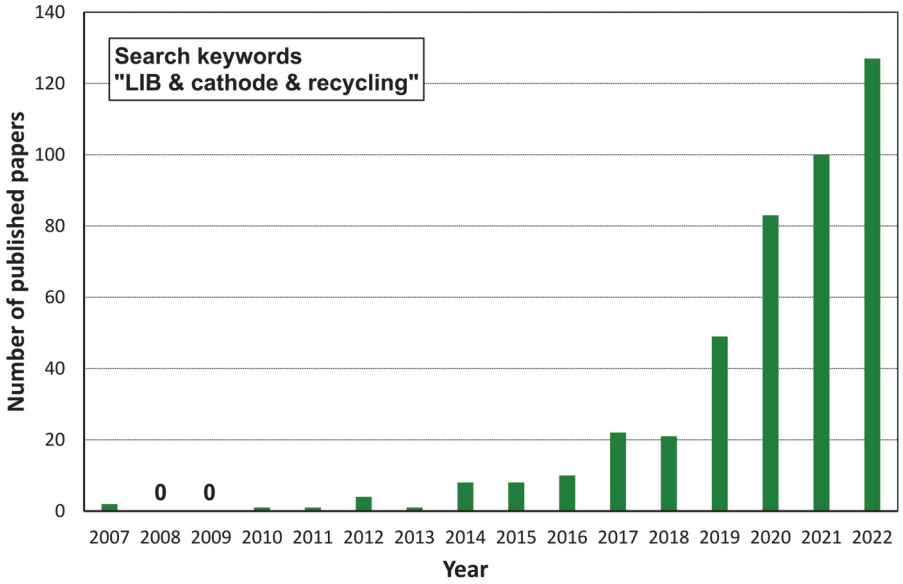

Figure 2 Number of published papers containing the keywords "LIB," "cathode," and "recycling."

technological innovation in recycling processes that prioritize process automation, high safety standards, superior recovery efficiency, and environmentally and economically sustainable methods. In recent years, research papers associated with recycling waste LIBs have drastically increased, according to a survey of paper counts in Scopus (Figure 2). Researchers' interests are driven by the development of functional and novel recycling processes and the characterization of cathode active materials resynthesized with recovered rare metals.

Anode active materials have been dependent on graphite since the early commercialization of LIBs. Graphite-based anodes offer high lithiation capacity (372 mAh g^{-1}), low working potential, and good cyclability in LIBs [13–15]. However, further improved anodic performances are needed to satisfy the requirements of high-performance LIBs applied in large-scale transportation and electric systems. Recently, amorphous C- or Si materials have been recognized as possible alternative anode active materials. These promising materials can be easily obtained as precursors, as they are generated as various agricultural wastes, industrial scraps, and others. Previous works have found that novel active materials produced from agricultural or industrial wastes exhibited better electrochemical performances in Li-ion storage applications [16–20]. Therefore, utilizing waste-derived precursors is a promising and valuable

approach to achieving a stable supply and mass production of electrode materials and LIB cells.

In this Chapter, I present economical and eco-friendly material preparations for LIB electrodes based on agricultural waste and industrial scraps. I focus on agricultural waste in the form of RH and spent LIBs used in vehicle applications. My aim is to review the effectiveness of using such wastes for LIB electrode materials, as well as the electrochemical performances of the prepared active materials in LIBs. Section 2.2 briefly presents current cathode/anode active materials and their electrochemical properties. Section 2.3 covers recycling processes for the recovery of remaining rare metals in waste LIBs, while Section 2.4 explores various processing techniques for RH suitable for LIB anodes. In these sections, the challenges of material preparation and usage with such wastes, as well as the electrochemical performances of the active materials prepared for LIB applications, are discussed. Section 2.5 summarizes the economical and eco-friendly active materials based on waste-type biomass and LIB products and presents future perspectives for LIB electrode materials.

2. 2 Active Materials for LIB Electrodes

2. 2. 1 *Cathodes*

A LIB cell has a predetermined Li storage capacity, which is constrained by the cathode chemistry of the cathode active material utilized in LIBs. This limitation arises from the fact that Li in the cathode active material corresponds to a finite Li source inside the LIB [21]. The choice of cathode active materials significantly impacts the working potential, current rate dependence (rate performance), and cyclability of the LIB cell [22–23]. Therefore, selecting the right cathode active material is critical for achieving superior charging and discharging performance in LIB cells [22–23]. Commonly, an LTMO is used as the cathode active material. Presently, materials are selected from various inorganic oxidized materials with distinct crystalline structures, including layered-type ($LiCoO_2$, $LiNiO_2$, and $LiNi_{1-x-y}Co_xMn_yO_2$ (NCM) [24–25]), spinel-type ($LiMn_2O_4$ and $LiNi_{0.5}Mn_{1.5}O_4$ [26–28]), and olivine-type ($LiFePO_4$ [29–30]) materials.

Among layered-type materials, LIBs that use NCM-based cathodes are preferred for use in vehicle applications [31–32]. The electrochemical performance of NCM is dependent on its chemical composition, particularly the proportions of Li, Ni, Co, and Mn, which affect the cathodic performance of the active materials. Li in the layered-type materials ($LiCoO_2$ and $LiNiO_2$) determines the Li storage capacity per unit mass (specific capacity), internal resistance, and electrochemical behavior during lithiation and delithiation [33]. Ni increases the specific capacity, Co provides improved electron conductivity, and Mn helps maintain the stable crystalline structure and strengthen cyclability [22, 25, 34]. By controlling the three transition metal compositions (Ni, Co, and Mn) to an equal ratio (x=y=~1/3), the NCM111 cathode exhibits good cyclability, high thermal stability, and a specific capacity of 150–160 mAh g^{-1} at a charge cutoff voltage of 4.3 V vs. Li/Li^+ [35]. NCM ($LiNi_{0.5}Co_{0.2}Mn_{0.3}O_2$ (NCM523) and $LiNi_{0.6}Co_{0.2}Mn_{0.2}O_2$ (NCM622)), with high Ni content of up to 0.5–0.6, offers a higher specific capacity than NCM111 [36–37]. Recent advances in cathode chemistry have been focusing on improving the specific capacity and specific energy in LIB cathodes.

Increasing the Ni content is an effective approach to achieving high capacity in NCM, resulting in highlighted specific energy at the electrode level. However, further increasing the Ni content (>0.8) causes poor cyclability, low thermal stability, and cation mixing of Li and Ni ions in the active materials, leading to problems [38]. To address these issues, many researchers have attempted material design (surface modification, cation doping, unique particle modification, etc.) and functional material use (electrolyte additive and binder) [39–41]. Through these strategies, the cathodic performances of $LiNi_{0.8}Co_{0.1}Mn_{0.1}O_2$ (NCM811) have been improved, but the commercialization of LIBs that use NCM811 cathodes is still expected to take some time. Thus, it is widely accepted that NCM cathodes with low-to-middle Ni content should be used in existing LIBs due to their acceptable cathodic performance and economical material cost compared to $LiCoO_2$ cathodes.

In addition to improving the performance of LIB cathodes, reducing material costs is another important issue. In the early commercialization of LIBs, $LiCoO_2$ was employed as the cathode material [42]. However, $LiCoO_2$ contains a rare and expensive metal, Co, which makes the cathode material two times more expensive than carbon- or Si-based anode materials, and contributes significantly to the overall cost of the LIB cell [43]. Furthermore, the limited production countries and yields of rare metal resources present serious supply issues. To address these cost and supply concerns, development of next-generation cathode active materials that contain low or no Co is being actively pursued. As described above, NCM is a promising choice for reducing material cost since Co can be replaced with other transition metals such as Ni and Mn. $LiFePO_4$ is also attractive for low-cost LIBs, despite having slightly lower working potential and energy density than layered-type materials [44–45]. However, due to its low electron conductivity resulting from the olivine structure and contained Fe, $LiFePO_4$ requires pre-processing with carbon coating, particle size reduction, and effective cation doping [46]. Pre-processed $LiFePO_4$ exhibits superior current rate dependence and time response, as well as acceptable specific capacity and excellent cyclability as the cathode material for LIBs. Moving forward, continuous exploration will be necessary to develop cathode active materials with high performance and low material cost.

2. 2. 2 *Anodes*

In 1991, Sony commercialized the first pristine LIB using a $LiCoO_2$ cathode and a non-graphitizable carbon anode. To improve charging and discharging performance, the non-graphitizable carbon was replaced with graphite, which has favorable anodic performance, including a lithiation specific capacity of 372 mAh g^{-1}, low working potential (approximately 0 V vs. Li/Li^+), acceptable cyclability, and abundant resources [47–48]. Today, the combination of a $LiCoO_2$ cathode and graphite anode is a well-known LIB cell design used in various electronic devices [42, 49]. Considering the dramatic increase in demand for LIBs, the material options for anode active materials are limited and inadequate, necessitating the exploration of alternative anode active materials to graphite. In recent years, composite anodes using graphite

and other carbon or Si-based materials have shown improved anodic performance in LIB applications [50–52]. These attempts have successfully reduced the graphite content in the anodes. However, the component ratio of graphite is still relatively high, and LIB anodes remain reliant on traditional graphite.

Anode active materials are typically classified based on their Li storage mechanism, including intercalation, alloying, and conversion reactions. Carbon materials store Li ions through Li-ion intercalation and deintercalation reactions. In the case of graphite, Li ions are inserted into the graphite, with one Li atom accommodated in the hexagonal geometry of six C atoms, and stored by forming graphite intercalation compounds (i.e., LiC_6). During lithiation and delithiation, the graphite anode operates with a low and flat potential curve close to 0 V vs. Li/Li^+. However, Li metal is likely to be deposited on the anode surface near 0 V vs. Li/Li^+, and Li-dendrites frequently cause unstable cell operation [53]. In particular, Li-dendrites can occur in graphite during fast charging and low-temperature conditions, reducing its durability in high-power or severe working conditions for electrical tools or vehicles. Non-graphitized carbons, such as HC, store Li ions similar to graphite, but also have additional storage sites in macro-/meso-pores and cluster regions formed with randomly arranged graphene sheets [54]. Previously published studies have shown that hard-carbon anodes exhibit higher specific capacity, better rate performance, excellent cyclability, and strong Li-dendrite durability [55]. Unlike graphite, HC shows a slope-like working potential above 0 V vs. Li/Li^+ during Li-ion intercalation-deintercalation, avoiding operation near the Li-dendrite potential and stabilizing anode operation without risk of Li-dendrite. Other carbon materials, such as graphene, carbon nanotubes, and porous carbon, are attractive anode active materials due to their low material cost, simple preparation, and multiple forms [56–57]. Currently, there is a drive to explore and develop novel carbon materials with exceptional anodic performance.

Si and its oxides have gained much attention as anode active materials due to their drastically high lithiation specific capacity at a full Li storage state. Si-based anodes have over 10 times

the specific capacity of graphite anodes (4200 mAh g^{-1} for pure Si vs. 372 mAh g^{-1} for graphite) [58]. Increasing specific capacity reduces the amount of electrode material needed for LIB production, allowing for size and weight reduction and enhancing energy and power density at the cell level. The Li storage mechanism of Si-based materials involves Li alloying, which results in huge volume expansion. In addition to Si, alloy materials, such as Sn, Pb, Al, Au, Pt, Zn, Cd, Ag, and Mg, can also serve as Li-ion receivers [59]. Li alloying in Si offers higher lithiation specific capacity and improved electron conductivity but also leads to large capacity fading and poor cyclability due to huge volume expansion, bad electrical contact, and electrode failure during Li alloying and dealloying. The huge volume expansion in Si particles causes the solid-electrolyte interface (SEI) film to repeatedly break and repair during lithiation and delithiation, leading to active Li loss within the LIB cells. Researchers have proposed successful approaches at the material and/or electrode levels to overcome these drawbacks [49, 60]. Reducing the particle size of Si anodes to the nano-scale and modifying their structure have resulted in favorable anodic performances, effectively mitigating the mechanical stress caused by volume expansion. Moreover, incorporating carbon mixing (e.g., HC, graphene, and carbon nanotubes), selecting appropriate binders, and adding electrolyte additives during cell assembly have proven beneficial for electrode fabrication and optimal LIB anode operation. Consequently, significant research efforts are being devoted to developing alloy-type materials as replacements for graphite.

Transition metal compounds, including oxides, sulfides, nitrides, fluorides, phosphides, and selenides, store Li ions through intercalation or conversion reactions. The corresponding metals are Fe, Co, Ni, Cu, and Zn [61]. Ti-based oxides such as TiO_2 and $Li_4Ti_5O_{12}$ store Li ions through Li-ion intercalation mechanisms [62–63]. Transition metal compounds have the advantage of avoiding Li-dendrites in the anode because they operate with electropositive potential against 0 V vs. Li/Li^+. Compared to graphite with Li-ion intercalation mechanism, transition metal compounds can serve as highly stable anodes in LIBs. Additionally, they offer higher lithiation specific capacity (700–1200 mAh g^{-1}) and excellent cycling performance [63].

Production costs for transition metal compounds are also lower than for alloying materials. However, practical use of transition metal compounds is hindered by several drawbacks, including particle pulverization caused by large volume expansion (<200%), large voltage hysteresis during lithiation and delithiation, and poor electron and ionic conductivity [61]. Researchers have improved the electrochemical properties through material design (layered nanostructure, hierarchical structure, etc.) and by combining transition metal compounds with carbon materials. Although there are many materials with different Li storage mechanisms, attaining superior electrochemical performances is still a challenging task. In the future, the anode active material options are likely to expand from a single candidate (graphite) to multiple materials.

2. 3 Reutilization of Rare Metals Used in Cathode Active Materials

2. 3. 1 *Overview*

In the future, there will be a significant increase in demand for LIBs across various sectors, including electronic devices, transportation, stationary energy storage, and others [64–65]. While the production and use of LIBs contribute to the effective utilization of renewable energy generation and the widespread adoption of zero-emission vehicles, a considerable amount of waste LIBs, referred to as end-of-life LIBs, are generated as hazardous and environmentally damaging scrap. Additionally, a significant number of defective products are produced during LIB production. However, these used and/or unwanted batteries still contain valuable metals, such as Li, Ni, and Co. Given that rare metal sourcing is highly competitive, developing recycling and recovery technologies is recognized as an important solution for an economical and circulative material supply [66–67]. Therefore, it is essential to effectively collect rare metals from waste LIBs and apply them in the next LIB production cycle. Recycling methods for cathode active materials used in waste LIBs are classified into two routes: i) pyrometallurgy and hydrometallurgy, and ii) direct recycling.

2. 3. 2 *Pyrometallurgy and Hydrometallurgy*

The characteristic procedure in pyrometallurgy involves roasting, calcination, and pyrolysis at higher temperatures to recycle waste LIBs [68]. This method generates intermediate products such as alloys, slags, and gases [9, 69]. Typically, the alloy contains Co, Cu, Ni, and Fe, while the slag contains Li, Al, Mn, Si, and Ca [69, 70]. Following the heat treatment, these products are further processed by hydrometallurgy to obtain desirable metals. Pyrometallurgy is a promising method with a huge disposal capacity and is favorably adopted by major companies in the recycling industry [71–72]. The temperature during the heat treatment is an important factor for removing impurities such as carbon black, polyvinylidene difluoride (PVDF) binder, electrolyte, and organic solvents, as well as ensuring efficient follow-up processing [68, 73–74]. The pyrometallurgy method demonstrates a high concentration of target metals by using suitable temperature conditions and separating materials using mechanical processes such as magnetic selection and gravimetry concentration. The separated materials, including the concentrated metals, can then be processed further.

The metals that are concentrated by preprocessing are commonly collected using the hydrometallurgical method and then synthesized as a precursor for LTMOs (cathode active materials). The preprocessing can be considered a part of the hydrometallurgy, which is a thermal treatment method. Hydrometallurgy is an effective method because it reduces hazardous gas emissions, enables secure recovery of specified metals, and has a high recovery efficiency [75–76]. In hydrometallurgy, the materials collected from the pretreatments undergo inorganic, organic, or bio-leaching to extract the metals as metallic ions into a solvent. The metallic ions in the solvent are then collected using solvent extraction, chemical precipitation, or electrolytic deposition, resulting in the solidification of metal compounds that are suitable for the next processing step. In hydrometallurgical processes, purification is also carried out to remove any metallic impurities that may be derived from the battery components. The purified metal compounds are then reused as a precursor for cathode active materials.

The precursor, obtained through pyrometallurgy, hydrometallurgy, or a combination of these methods, is processed by mixing a lithium source such as Li_2CO_3 or LiOH and sintering at high temperatures in air (reactivation). Upon completion of the reactivation steps, an LTMO can be synthesized as the cathode active material. Through the recycling process, various metals can be recovered from the damaged cathode material in waste LIBs and repurposed as fresh materials. However, contamination with impurities such as Cu, Fe, Al, Mg, P, and F cannot be avoided due to the recovery mechanism involving the starting materials of the compounds and the use of chemical solutions containing Na, Cl, and S. In recent studies, researchers have been extensively evaluating the electrochemical performance of cathode active materials containing specific amounts of impurities [70, 77–79].

Regardless of the recycling methods, waste LIBs generally undergo pre-discharging, dismounting, and mechanical separation to collect metal components with relatively high safety. Pre-discharging and mechanical disassembly processes may present risks of electrical shock hazards and heating accidents during preprocessing. These risks arise from the difficulty in disassembling commercial LIBs and the fact that the vast majority of procedures are performed manually. Pre-discharging of waste LIBs is typically achieved by immersion in a NaCl solution or high-speed shredding in cryogenic nitrogen, both of which are well-known methods for eliminating the residual capacity in LIBs [80–81]. In particular, high-speed shredding is an effective approach that bypasses the disassembly process and ensures safe operation, thanks to an inert atmosphere filled with N_2 gas and an automated process. After discharging, fully discharged LIBs undergo dismounting and separation processes. Dismounting requires considerable manual effort, while the separation process is either semi-automated or fully automated. For future recycling processes, there is a need for high-safety and simplified procedures that eliminate the reliance on manual labor and achieve high recovery rates for desired metals.

2. 3. 3 *Direct Recycling*

Direct recycling is another approach for utilizing valuable metals in waste LIBs [82–85]. This method involves the liberation and reactivation processes utilizing chemical, mechanical, or thermal treatments. The target material for a cathode active material is contained in a compound coated on an Al foil current collector. In the liberation process, the compounds must be separated from the Al foil and then freed from other electrode components such as conductive agents and polymer binders. Sintering under inert conditions or immersion in an organic solvent (e.g., N-methyl pyrrolidone, dimethylformamide, and dimethylethanamide) are typically employed to peel the compound from the Al foil [84–85]. After such processes, impurities from conductive agents, binders, and electrolyte residues are removed by additional thermal treatment. The reactivation process is carried out by adding any lithium sources or lithium-containing residues to the separated materials [82, 86]. This process involves the addition of lithium sources and solid-phase reactions, resulting in active lithium compensation in the damaged materials recovered from cathode components. Direct recycling offers advantages such as the ready availability of recycled materials, fewer processing steps, and lower environmental impact compared to hydrometallurgical methods, making it economically and environmentally friendly [87]. However, direct recycling may also result in contamination from residues, such as by-products produced during charging and discharging, and unreacted materials in the reactivation process. Therefore, it is crucial to conduct intensive investigations on the effects of these residues on the electrochemical performance of the obtained products.

2. 3. 4 *Electrochemical Performances on Recycled Cathode Active Materials*

In earlier studies, the focus of recycling processes for waste LIBs was on secure recovery and improving the recovery rate of rare metals. Recently, the physical and electrochemical properties of recycled cathode active materials in LIB cathodes have been characterized simultaneously after metal recovery and material preparation in the recycling process. Two research groups, Ma et al. and Beak et al., discovered that the nearly complete removal of impurities introduced by the recycling process led to a recovery of the specific capacity close

to the initial capacity achieved using fresh materials [88–89]. The effects of metallic or non-metallic impurities in certain amounts on the recycled cathode active materials in LIB cathodes remain an open question.

Inevitably, metallic and/or non-metallic impurities (e.g., Al, Cu, Fe, Mg, Na, F, S, Cl, etc.) are introduced into the reproduced cathode active materials during the recycling process. Table 1 summarizes the material specifications and electrochemical performances of the recycled cathode active materials intended for LIB cathodes. A small amount of Al-doping resulted in improvements in current rate capability and crystalline structure stabilization, as well as a decrease in maximum specific capacity [95–96]. Degradation of cycling performance was observed when Al was doped in excessive amounts in NCM materials [89]. Regardless of doping amounts, Al incorporation also acted as a structural modification additive, affecting secondary particle formation during the synthesis process [90, 91]. Moreover, the occurrence frequency of cation mixing in the crystalline structure was reduced in cathode active materials. The $LiCoO_2$-based cathodes containing Cu impurities demonstrated better rate and cycling performance, although the acquired specific capacity was slightly lower [92]. During material synthesis and cathodic operation, Cu contamination presented several disadvantages: Co coprecipitation in impurity removal, agglomerated particle formation, and dissolution and deposition of Cu alongside Mn at the anode surface during cell operation [92, 97]. Doping a small amount of Fe was effective in enhancing rate and cycling performance in NCM material-based cathodes, due to the improved crystalline structure resulting from Fe occupying Li sites [79, 98]. However, the electrochemical performance of NCM-based cathodes containing impurities deteriorated when excessive amounts of Fe, Cu and Al were present [96]. These impurities originate from cathode and anode current collectors, body frames, bus bars, and other sources. Perfect removal of impurities is not realistic in recycled products, even with extreme processing, considering the associated efforts, costs, and environmental impacts. Trace amounts of single or multiple impurities can maintain not only electrochemical performances but also provide positive effects on performance improvements.

Table 1 Material specification and electrochemical performances on the recycled cathode materials for Li-ion batteries (LIBs)

Material specification		Starting materials	Pretreatments and metal recovery methods	Performances			Ref.
Target chemical composition	Mainly included impurities			CAP_{MAX} * [mAh g^{-1}]	Current rate	Cycling	
$LiNi_{1/3}Co_{1/3}Mn_{1/3}O_2$	2.54 at.% Al, 0.16 at.% Cu, 4.21 at.% F, 2.11 at.% S	Spent LIBs used for laptop and EV applications	Mechanical pretreatment Acid leaching Precipitation	~136 @ 0.1 C	Improved	Deteriorated	89
$LiNi_{1/3}Co_{1/3}Mn_{1/3}O_2$	0.57 mass% Al	Spent NCM-based LIBs	Mechanical pretreatment Acid leaching Precipitation	~115 @ 1 C	Sustained	Deteriorated	90
$LiNi_{1/3}Co_{1/3}Mn_{1/3}O_2$	4 mol.% Al	Spent $LiCoO_2$-based LIBs	Mechanical pretreatment Acid leaching Sol-gel method	154 @ 0.2 C	Improved	Sustained	91
$LiCoO_2$	Specified few amounts of Cu	Spent LIBs used for portable applications	Mechanical pretreatment Acid leading Precipitation	128 @ 0.03 C	Improved	Improved	92
$LiNi_{1/3}Co_{1/3}Mn_{1/3}O_2$	0.05 mol.% Mg	Spent LIBs	Thermal and mechanical pretreatment Acid leaching Precipitation	~155 @ 0.5 C	-	Deteriorated	93
$LiNi_{1/3}Co_{1/3}Mn_{1/3}O_2$	Almost perfect removed	Spent LIBs	Mechanical pretreatment Acid leaching Precipitation	-	Improved	Improved	88
$LiNi_{1/3}Co_{1/3}Mn_{1/3}O_2$	1.3 mol.% Al, 1.7 mol.% Cu, 1.0 mol.% Fe	Spent LIBs used for PHEV applications	Thermal and mechanical pretreatment Acid leaching Precipitation	121 @ 0.1 C	Sustained	Deteriorated	94
$LiFePO_4$	Not analyzed (Possible contaminants: electrode-derived residues of PVDF and carbon black)	Scraps discarded by $LiFePO_4$ cathode production	Thermal and mechanical pretreatment	135 @ 0.1 C	Sustained	-	84
$LiFePO_4$	Not analyzed (Possible contaminants: $LiFePO_4$-derived decomposition products)	Spent $LiFePO_4$-based LIBs used for EV applications	Mechanical and chemical treatment Thermal treatment	~130 @ 0.2 C	Improved	Sustained	83
$LiNi_{1/3}Co_{1/3}Mn_{1/3}O_2$	0.003 at.% Al (Possible contaminants: electrode-derived residues of PVDF and carbon black)	Spent power-type LIBs with 2000 cycling	Mechanical and thermal pretreatment Mechanochemical treatment with Li additives Thermal treatment	165 @ 0.2 C	Improved	Sustained	82
$LiNi_{1/3}Co_{1/3}Mn_{1/3}O_2$	Not analyzed for metallic impurities (Possible contaminants: Al, Li-containing compounds (LiF and Li_2CO_3))	Spent NCM-based LIBs	Mechanical pretreatment Thermal treatment	170 @ 0.1 C	Improved	Improved	86

* Maximum specific capacity at delithiation during the initial cycle

Other impurities originating from metal recovery processes also impact material preparation and electrochemical performance of recycled cathode active materials [89, 99–100]. Sulfuric acid (H_2SO_4), commonly used in industrial applications, dissolves valuable metals in the leaching process, leaving sulfur residues in the final products. Sodium (Na) contamination often occurs through chemical precipitation with a NaOH solution, affecting electrochemical performance in LIB cathodes without inhibiting crystalline structure growth. It is essential to eliminate remaining electrolyte components and by-products, including fluorine (F), during the recycling process. If electrolyte component removal is insufficient, F and phosphorus (P) derived from lithium salts can become incorporated into the recycled cathode active materials. The impurities can cause particle modification, changes in the crystalline structure, and a decrease in the specific capacity. However, a slight amount of such impurities may have negligible effects on the electrochemical performance of LIB cathodes.

2. 4 Applications of Agricultural Waste on Anode Active Materials

2. 4. 1 *Overview*

Rice is considered one of the world's three most important grains and is predominantly produced in Asia, with China and India having particularly large yields [101]. During rice production, RHs are generated alongside bearing and thrashing paddy rice. Paddy rice mainly consists of rice kernel and husk, accounting for 77 and 23 wt%, respectively [102]. Approximately 150 million tons of RHs are produced annually, with a significant amount remaining as an underutilized resource in rice-producing countries [102–103]. Currently, RH utilization is limited to a few agricultural and industrial applications. In agriculture, RHs are used as soil fertilizer additives, mulching materials, and stockbreeding mats in livestock barns. In industry, they are used as biomass fuel and in the production of functional materials such as rice-husk-derived charcoal and activated char. RHs contain 20–30 wt% SiO_x in addition to organic components like lignin, cellulose, and hemicellulose [104–105]. By absorbing silicic acids ($Si(OH)_4$ or $Si(OH)_3O^-$) from soil, SiO_x accumulates in RHs and plays a crucial role in protecting against environmental and biological stresses, such as high temperature, drought,

buckling, pest insects, and plant diseases [19, 106]. Although RHs have various applications, their consumption is relatively small. In the energy sector, RH combustion allows for thermal energy acquisition, but also results in RH ash disposal and smoke emission [107]. Handling RHs in energy applications is challenging due to the difficult process of removing remaining ash. Consequently, SiO_x contamination in RHs hinders their widespread use. Therefore, it is crucial to explore additional applications for RHs beyond their current uses.

2. 4. 2 *Processing of RH Suited for LIB Anode Applications*

RHs have garnered attention as sustainable biomass sources for LIB anode active materials due to their composition of SiO_x and organic components. Through chemical and thermal treatments, RHs can be transformed into carbon- or silicon-intended materials (RH-C or RH-Si). Previous studies have reported that rice-husk-derived active materials with unique physical and electrochemical properties exhibit superior electrochemical performance in LIB anodes [108–112]. Strategies for producing these materials can be broadly categorized into two routes: i) reducing Si from SiO_x, and ii) carbonizing organic components with or without activation.

The goal of the first route is to produce high-purity RH-Si with an interesting nanostructure and drastically high lithiation specific capacity. In the SiO_x of paddy rice, the oxidation degree is indeterminable because it naturally accumulates during rice growth. Although SiO_x is of low quality, the specific capacity of SiO_2 is lower than that of pure Si (1965 mAh g^{-1} for SiO_2 vs. 4200 mAh g^{-1} for Si) [113]. When SiO_x is utilized as the primary active material, it can be transformed into high-purity Si through carbothermal or metallic reduction methods. Carbothermal reduction is commonly employed in industries using electric arc furnaces, where reduction reactions progress at approximately 2000 °C, consuming a significant amount of energy [114–116]. Metallic reduction is a more straightforward method for reducing SiO_x to Si, which can be demonstrated even at lab-scale facilities. Magnesiothermic reduction, involving mixing Mg powder and heating at low temperatures, is commonly chosen for Si reduction in rice-husk-derived SiO_x [111, 114–115]. The remaining RH components (organic materials) are

processed through thermal treatment under inert conditions and chemical modification, producing amorphous C that assists in Si alloying electrochemically. Alternatively, the organic components in the RH can be burned off in the air and evaporated as CO_2, CO, and other gases.

The other route involves carbonization with or without activation of RH-C derived from the organic parts of the RH. Heating under inert conditions transforms the RH into RH-C, providing Li storage capabilities. The crystalline structures of RH-C depend on the heating temperature during carbonization [110]. Before carbonization, the RH is washed with distilled water to remove impurity residues from its surface. To strongly remove impurity residues (mainly metallic oxides), a strong acid solution, such as HCl, is used for a prior purification step. SiO_x, alternatively referred to as ash, in heated products can be used as a Li-ion receiver or removed by a neutralization process using an alkaline solution, such as a NaOH solution. In cases where both C and SiO_x coexist, both materials serve as Li-ion storage materials in LIB anodes. When SiO_x is eliminated by NaOH immersion, the remaining RH-C stores Li ions exclusively. An additional activation process endows RH-C with higher specific surface area and developed pore structure. The improved physical properties due to activation result in superior electrochemical performance of RH-C in LIB anodes.

Regarding RHs, both types of processing can be employed to utilize them as anode active materials. However, rice-husk-derived anodes face a series of challenges related to electrochemical behaviors in the anodes, which hinder their applications in practical LIBs. In the following section, the electrochemical performance of the produced rice-husk-based active materials and the drawbacks in LIB anode operations are presented and discussed.

2. 4. 3 *Electrochemical Performance of the LIB Anodes*

Table 2 summarizes the electrochemical performance of RH-Si produced from RHs for LIB anodes. All the RH-Si anodes, with or without carbon components, exhibit low Coulombic efficiency (CE) in the first lithiation-delithiation cycle. In the first cycle, the electrolyte

decomposition, which involves the consumption of active Li ions, inevitably occurs at the anodes. As a result of the electrolyte decomposition, an electrochemically stable film at the interface between the active materials and electrolyte, often called the SEI film, forms in the anodes. During the Li alloying and dealloying process in each cycle, the expansion and contraction of RH-Si can cause the SEI film to break and repair continuously, leading to the ongoing consumption of Li ions within the LIB cells. Carbon remaining in the RH-Si can aid in acquiring capacity during Li-alloy reactions and mitigate the mechanical stress caused by Si expansion. In cases where carbon is absent in the RH-Si, applying suitable electrode design (incorporating conductive agents and binders with better buffer effects and strong bonding power) and adding electrolyte additives such as fluoroethylene carbonate can promote stable operation as LIB anodes.

After completing the irreversible side reactions in the first cycle, the RH-Si anodes exhibited higher reversible specific capacity compared to that of a graphite anode (approximately 350 mAh g^{-1}). Liu et al. and Jung et al. found that Si with high purity provided high CE in the first cycle and consistently high capacity [116–117]. Si combined with carbon produced from another carbon source (pyrrole) also granted the anode relatively high CE and reversible specific capacity [120]. On the other hand, the initial CE of the anodes comprising a combination of reduced Si and remaining C was inferior compared to those without a C component. However, the production mass yield from the starting material to the final products for the Si/C composites is considered to be high. Si-only materials had lower yields due to the elimination of remaining C in the RH-Si. Taking into account the increasing demand for LIB electrode materials in the future, an abundant and stable supply is essential for producing LIB cells and electrodes. Therefore, it is crucial to achieve high production mass yield and improved anodic performance using rice-husk-derived active materials.

Table 2 Electrochemical performances on RH-Si produced from rice husks for Li-ion battery (LIB) anodes

Material specification					Performances			
Produced material	Material notes	S_{BET} [m^2 g^{-1}]	W_{BJH} [nm]	Main processing methods	Y [%]	CE_{1st} [%]	Reversible specific capacity [mAh g^{-1}]	Ref.
Porous Si	Si with 99.6 % purity	54	>20	Acid leaching and burnoff in air Mg reduction Acid leaching	~5	~70	1750 @ 0.5 C	116
C-coated 3D porous Si	Si with 99.92 % purity and 3-10 nm C coating layer	87	~10–50	Acid leaching and burnoff in air Mg reduction and acid leaching Carbon coating	7.7	84.2	1615 @0.1 C	117
3D structured Si/C	3 D structure containing amorphous C matrix	199	6–9	Acid leaching Carbonization under Ar Mg reduction and acid leaching	-	49.2	536 @ 0.1 A g^{-1}	118
Si/C	Nanosized-Si distributed in amorphous C matrix	-	-	Acid leaching Carbonization under inert atmosphere Mg reduction and acid leaching	-	49	-	113
Si/C	18.3 wt% Si and the rest of C	-	-	Simultaneous process of Mg reduction and carbonization Acid leaching	-	61.9	650 @ 100 mA g^{-1}	119
3D porous Si/C	69.4 wt% C and the rest of Si	267.4	43.5	Acid leaching Hydrothermal treatment using an alkaline solution Mg reduction and acid leaching	~16.7	57.3	345 @ 50 mA g^{-1}	111
Si/pyrrole-derived-C	30 wt% C and the rest of Si with a slight amount of N The carbon with N-doping derive from pyrrole	27.5	~25	Acid leaching Carbonization in Air Mg reduction and acid leaching Adding and mixing C source, and carbonization under Ar	6	72.0	~950 @ 100 mA g^{-1}	120

S_{BET}: specific surface area by calculated with BET theory, W_{BJH}: main pore width revealed by the BHJ theory, Y: production mass yield from starting material to final product, CE_{1st} Coulombic efficiency in the first cycle

Carbonization with inert gases initiates the transformation from RH to RH-C, resulting in high production yields (~36 mass%) [121]. Similar to the electrochemical properties of RH-Si, low CE of RH-C was observed at the anodes [122–125]. This decrease in CE is due to the amorphous crystalline structure of the carbon components in the rice-husk-based active materials. In addition to Li storage in the carbon of RH-C, SiO_x also acts as a Li-ion receiver with Li alloying mechanisms. If necessary, SiO_x can be utilized as Li storage materials or removed by a neutralization process. In cases where SiO_x is removed, textural properties are typically developed to obtain activated and porous structures for RH-C. These unique properties are achieved by activation methods using various chemical solutions and gases as activating agents. The developed textural properties endow RH-C with superior electrochemical performance, such as maximum specific capacity and rate capability [123, 126]. In RH-C production, SiO_x removal and carbon activation are considered key approaches for achieving acceptable anodic performance in LIBs. In particular, the removal process for SiO_x is regarded as an essential treatment to determine the production mass yield of rice-husk-derived active materials.

Previous research on the application of rice-husk-derived active materials in LIB anodes has been largely limited to electrochemical characterization through half-cell testing (a setup involving a produced electrode and Li metal counter electrode). Half-cell evaluation effectively reveals individual electrochemical performance for test samples due to the Li metal counter electrode acting as an infinite Li source and compensating for Li loss. However, in actual LIBs, the loss of active Li cannot be compensated for, as the Li source in the cathode active materials is finite. Prelithiation is known to be an effective method for alleviating Li loss in anodes [127–128]. By applying prelithiation to the anodes beforehand, side reactions such as SEI film formation are mostly completed, allowing for stable operation during the initial cycle. Our research group and a few others have successfully demonstrated this through experiments where rice-husk-based anodes were evaluated by operating LIB full cells in combination with LTMO cathodes (full-cell testing) [121, 129, 130]. Moving forward, it is recommended that

full-cell testing be conducted to assess the electrochemical performance of produced rice-husk-based anodes as a means of determining their feasibility as advanced materials.

2. 5 Summary and Future Perspective

The popularization of portable and convenient devices, motorized transportation, and renewable energy generation has improved the quality of life for many people while also reducing environmental burden. This progress requires powerful and low-cost energy storage devices, with LIBs emerging as a leading candidate. As demand for LIBs is expected to increase drastically in the future, mass production and a consistent supply of related electrode materials are imperative. Manufacturing LIB cells and packs through the extensive consumption of raw materials collected from natural sources is not sustainable considering finite resources and geo-environmental impacts. Therefore, repurposing agricultural waste (waste-intended biomass) and LIB scraps (already used rare metal sources) is a promising, economically viable, and environmentally friendly approach to ensuring a consistent supply of raw materials without additional harvesting. The aforementioned approaches contribute to addressing critical challenges associated with material supply and cost in both LIB cathodes and anodes.

Existing cathode active materials in LIBs contain a significant amount of rare metals (Li, Co, and Ni), resulting in high material costs. Considering the highly competitive nature of procuring such precious resources, establishing alternative supply chains that do not rely on harvesting from the place of origin is essential for the mass production of LIB cells. Recycling technologies such as pyrometallurgy, hydrometallurgy, direct recycling, and combination methods can enable the effective utilization of rare metals in waste LIBs. Cathode active materials recovered from waste LIBs consist of indispensable components (LTMOs) as well as a certain amount of impurities. Previous research has shown that reducing the amount of impurities leads to higher specific capacity during lithiation and delithiation. Moreover, a slight amount of impurities can help stabilize the crystalline structure, resulting in superior electrochemical performance and stable operation in LIB cathodes. However, excessive impurities can cause unstable crystalline

structures and deteriorated electrochemical performance in synthesized products. This accumulated knowledge supports the popularization of cathode active materials recycled from waste LIBs, while emphasizing the importance of impurity removal processes for producing next-generation cathode active materials.

In LIB anodes, graphite is predominantly used as the primary anode active material. Composite anodes, which combine graphite with other carbon materials or Si-based materials, are also being considered as alternative anodes. However, anode active materials still heavily rely on traditional graphite. In the future, the demand for LIBs is predicted to increase drastically due to the popularization of zero-emission vehicles and stationary energy storage systems. As a result, the limited range of material options available for graphite raises significant concerns about future material supply and LIB production. Agricultural waste, such as RHs, has been gaining attention as a potential source for novel anode active materials because of its benefits in material availability, cost, and flexibility in processing into carbon- or Si-based materials. Following two different processing routes, RH-derived active materials can be successfully prepared and applied in LIB anodes. Although the CE of RH-derived anodes is low, prelithiation can enable the stable operation of LIBs using RH-based anodes. Moreover, the composition and textural properties of RH-derived active materials significantly influence their performance in LIBs. Consequently, RHs hold great potential as LIB anode active materials, and the development of new material supplies is highly likely in rice-producing countries.

Reference

[1] R. Schmuch, R. Wagner, G. Hörpel, T. Placke, M. Winter, Performance and cost of materials for lithium-based rechargeable automotive batteries, *Nat. Energy* 3 (2018) 267–278.

[2] Y. Miao, P. Hynan, A. von Jouanne, A. Yokochi, Current Li-ion battery technologies in electric vehicles and opportunities for advancements, *Energies* 12(6) (2019) 1074.

[3] J. Hu, S. Zhong, T. Yan, Using carbon black to facilitate fast charging in lithium-ion

batteries, *J. Power Sources* 508 (2021) 230342.

[4] S. Kim, D. Yang, K. Rhee, J. Sohn, Recycling process of spent battery modules in used hybrid electric vehicles using physical/chemical treatments, *Res. Chem. Intermed.* 40 (2014) 2447–2456.

[5] D. Y. Voropaeva, E. Y. Safronova, S. A. Novikova, A. B. Yaroslavtsev, Recent progress in lithium-ion and lithium metal batteries, *Mendeleev Commum.* 32(3) (2022) 287–297.

[6] P. Bernard, H. Martinez, C. Tessier, E. Garitte, S. Franger, R. Dedryvere, Role of negative electrode porosity in long-term aging of NCM//graphite Li-ion batteries, *J. Electrochem. Soc.* 162(13) (2015) A7096–A7103.

[7] J. Kasnatscheew, M. Evertz, B. Streipert, R. Wagner, R. Klöpsch, B. Vortmann, H. Hahn, S. Nowak, M. Amereller, A.-C. Gentschev, P. Lamp, M. Winter, The truth about the 1st cycle Coulombic efficiency of $LiNi_{1/3}Co_{1/3}Mn_{1/3}O_2$ (NCM) cathodes, *Phys. Chem. Chem. Phys.* 18 (2016) 3956–3965.

[8] E. Gratz, Q. Sa, D. Apelian, Y. Wang, A closed loop process for recycling spent lithium ion batteries, *J. Power Sources* 262 (2014) 255–262.

[9] S. Kim, J. Bang, J. Yoo, Y. Shin, J. Bae, J. Jeong, K. Kim, P. Dong, K. Kwon, A comprehensive review on the pretreatment process in lithium-ion battery recycling, *J. Clean. Prod.* 294 (2021) 126329.

[10] H. Bae, Y. Kim, Technologies of lithium recycling from waste lithium ion batteries: a review, *Mater. Adv.* 2 (2021) 3234.

[11] J. Li, G. Wang, Z. Xu, Generation and detection of metal ions and volatile organic compounds (VOCs) emissions from the pretreatment processes for recycling spent lithium-ion batteries, *Waste Manag.* 52 (2016) 221–227.

[12] T. Zhang, Y. He, L. Ge, R. Fu, X. Zhang, Y. Huang, Characteristics of wet and dry crushing methods in the recycling process of spent lithium-ion batteries, *J. Power Sources* 240 (2013) 766–771.

[13] A. Eftekhari, Low voltage anode materials for lithium-ion batteries, *Energy Storage Mater.* 7 (2017) 157–180.

[14] Y. Zheng, Y.-B. He, K. Qian, B. Li, X. Wang, J. Li, S. W. Chiang, C. Miao, F. Kang, J. Zhang, Deterioration of lithium iron phosphate/graphite power batteries under high-rate discharge cycling, *Electrochim. Acta* 176 (2015) 270–279.

[15] J. Hassoun, F. Bonaccorso, M. Agostini, M. Angelucci, M. G. Betti, R. Cingolani, M. Gemmi, C. Mariani, S. Panero, V. Pellegrini, B. Scrosati, An advanced lithium-ion battery based on a graphene anode and a lithium iron phosphate cathode, *Nano Lett.* 14 (2014) 4901–4906.

[16] C. Li, C. Liu, W. Wang, Z. Mutlu, J. Bell, K. Ahmed, R. Ye, M. Ozkan, C. S. Ozkan, Silicon derived from glass bottles as anode materials for lithium ion full cell batteries, *Sci. Rep.* 7 (2017) 917.

[17] J. Xiang, W. Lv, C. Mu, J. Zhao, B. Wang, Activated hard carbon from orange peel for lithium/sodium ion battery anode with long cycle life, *J. Alloys Compd.* 701 (2017) 870–874.

[18] J. Ajuria, E. Redondo, M. Arnaiz, R. Mysyk, T. Rojo, E. Goikolea, Lithium and sodium ion capacitors with high energy and power densities based on carbons from recycled olive pits, *J. Power Sources* 359 (2017) 17–26.

[19] L. Zhang, X. Liu, Q. Zhao, S. Dou, H. Liu, Y. Huang, X. Hu, Si-containing precursors for Si-based anode materials of Li-ion batteries: A review, *Energy Storage Mater.* 4 (2016) 92–102.

[20] S. E. Wang, I.-S. Jang, Y. C. Kang, J. Chun, D.-S. Jung, Residual silica removal and nanopore generation on industrial waste silicon using ammonium fluoride and its application to lithium-ion battery anodes, *Chem. Eng. J.* 419 (2021) 129389.

[21] J. Xu, R. D. Deshpande, J. Pan, Y.-T. Cheng, V. S. Battaglia, Electrode side reactions, capacity loss and mechanical degradation in lithium-ion batteries, *J. Electrochem. Soc.* 162(10) (2015) A2026–A2035.

[22] C. Lee, Y. Miyahara, T. Abe, K. Miyazaki, Electrochemical properties of Ni-rich $LiNi_xCo_yMn_zO_2$ materials for use in aqueous lithium-ion batteries: How do they differ from those in non-aqueous systems?, *J. Power Sources* 524 (2022) 231081.

[23] Y. Tian, Y. Liu, F. Li, Y. Sun, X. Wei, P. Hou, Realizing high energy-density lithium-ion batteries: High Ni-content or high cut-off voltage of single-crystal layered cathodes?, *J. Electroanal. Chem.* 924 (2022) 116847.

[24] J. W. Fergus, Recent developments in cathode materials for lithium ion batteries, *J. Power Sources* 195 (2010) 939–954.

[25] L. Cheng, B. Zhang, S.-L. Su, L. Ming, Y. Zhao, C.-H. Wang, X. Ou, Comparison of monocrystalline and secondary $LiNi_{0.5}Co_{0.2}Mn_{0.3}O_2$ cathode material for high-performance lithium-ion batteries, *J. Alloys Compd.* 845 (2020) 156202.

[26] B. T. Habte, F. Jiang, Microstructure reconstruction and impedance spectroscopy study of $LiCoO_2$, $LiMn_2O_4$ and $LiFePO_4$ Li-ion battery cathodes, *Microporous Mesoporous Mater.* 268 (2018) 69–76.

[27] H. Yu, X. Dong, Y. Pang, Y. Wang, Y. Xia, High power lithium-ion battery based on spinel cathode and hard carbon anode, *Electrochim. Acta* 228 (2017) 251–258.

[28] S. Lee, Y. Cho, H.-K. Song, K. T. Lee, J. Cho, Carbon-coated single-crystal $LiMn_2O_4$ nanoparticle clusters as cathode material for high-energy and high-power lithium-ion batteries, *Angew. Chem.* 124 (2012) 8878–8882.

[29] K. Zaghib, J. Dubé, A. Dallaire, K. Galoustov, A. Guerfi, M. Ramanathan, A. Benmayza, J. Prakash, A. Mauger, C. M. Julien, Enhanced thermal safety and high power performance of carbon-coated $LiFePO_4$ olivine cathode for Li-ion batteries, *J. Power Sources* 219 (2012) 36–44.

[30] Z. Zhang, T. Zeng, C. Qu, H. Lu, M. Jia, Y. Lai, J. Li, Cycle performance improvement of $LiFePO_4$ cathode with polyacrylic acid as binder, *Electrochim. Acta* 80 (2012) 440–444.

[31] B. A. Walker, C. O. Plaza-Rivera, S.-S. Sun, W. Lu, J. W. Connell, Y. Lin, Dry-pressed lithium nickel cobalt manganese oxide (NCM) cathodes enabled by holey graphene host, *Electrochim. Acta* 362 (2020) 137129.

[32] X. Yang, Z. Zuo, H. Wang, Q. Chen, H. Zhang, Z. Huang, B. Wu, H. Zhou, The contradiction between the half-cell and full-battery evaluations on the tungsten-coating

$LiNi_{0.5}Co_{0.2}Mn_{0.3}O_2$ cathode, *Electrochim. Acta* 180 (2015) 604–609.

[33] Y.-M. Choi, S.-I. Pyun, J.-S. Bae, S.-I. Moon, Effects of lithium content on the electrochemical lithium intercalation reaction into $LiNiO_2$ and $LiCoO_2$ electrodes, *J. Power Sources* 56 (1995) 25–30.

[34] H.-J. Noh, S. Youn, C. S. Yoon, Y.-K. Sun, Comparison of the structural and electrochemical properties of layered $Li[Ni_xCo_yMn_z]O_2$ (x = 1/3, 0.5, 0.6, 0.7, 0.8 and 0.85) cathode material for lithium-ion batteries, *J. Power Sources* 233 (2013) 121–130.

[35] S. Liu, L. Xiong, C. He, Long cycle life lithium ion battery with lithium nickel cobalt manganese oxide (NCM) cathode, *J. Power Sources* 261 (2014) 285–291.

[36] L. Jiao, Z. Liu, Z. Sun, T. Wu, Y. Gao, H. Li, F. Li, L. Niu, An advanced lithium ion battery based on a high quality graphitic graphene anode and a $Li[Ni_{0.6}Co_{0.2}Mn_{0.2}]O_2$ cathode, *Electrochim. Acta* 259 (2018) 48–55.

[37] Y. Abe, T. Saito, S. Kumagai, Effect of prelithiation process for hard carbon negative electrode on the rate and cycling behaviors of lithium-ion batteries, *Batteries* 4 (2018) 71.

[38] Y. Ding, R. Wang, L. Wang, K. Cheng, Z. Zhao, D. B. Mu, B. Wu, A short review on layered $LiNi_{0.8}Co_{0.1}Mn_{0.1}O_2$ positive electrode material for lithium-ion batteries, *Energy Procedia* 105 (2017) 2941–2952.

[39] P. Teichert, G. G. Eshetu, H. Jahnke, E. Figgemeier, Degradation and aging routes of Ni-rich cathode based Li-ion batteries, *Batteries* 6 (2020) 8.

[40] D. Becker, M. Börner, R. Nölle, M. Diehl, S. Klein, U. Rodehorst, R. Schmuch, M. Winter, T. Placke, Surface modification of Ni-rich $LiNi_{0.8}Co_{0.1}Mn_{0.1}O_2$ cathode material by tungsten oxide coating for improved electrochemical performance in lithium-ion batteries, *ACS Appl. Mater. Interfaces* 11(20) (2019) 18404–18414.

[41] L.-B. Tang, Y. Liu, H.-X. Wei, C. Yan, Z.-J. He, Y.-J. Li, J.-C. Zheng, Boosting cell performance of $LiNi_{0.8}Co_{0.1}Mn_{0.1}O_2$ cathode material via structure design, *J. Energy Chem.* 55 (2021) 114–123.

[42] B. Xu, D. Qian, Z. Wang, Y. S. Meng, Recent progress in cathode materials research for

advanced lithium ion batteries, *Mater. Sci. Eng. R Rep.* 73 (2012) 51–65.

[43] M. Kotal, S. Jakhar, S. Roy, H. K. Sharma, Cathode materials for rechargeable lithium batteries: Recent progress and future prospects, *J. Energy Storage* 47 (2022) 103534.

[44] Y. Yao, P. Qu, X. Gan, X. Huang, Q. Zhao, F. Liang, Preparation of porous-structured $LiFePO_4$/C composite by vacuum sintering for lithium-ion battery, *Ceram. Int.* 42 (2016) 18303–18311.

[45] J. Shim and K. A. Striebel, Cycling performance of low-cost lithium ion batteries with natural graphite and $LiFePO_4$, *J. Power Sources* 119–121 (2003) 955–958.

[46] Z. Huang, P. Luo, D. Wang, Preparation and characterization of core-shell structured $LiFePO_4$/C composite using a novel carbon source for lithium-ion battery cathode, *J. Phys. Chem. Solids* 102 (2017) 115–120.

[47] J.-H. Kim, M.-J. Jung, M.-J. Kim, Y.-S. Lee, Electrochemical performances of lithium and sodium ion batteries based on carbon materials, *J. Ind. Eng. Chem.* 61 (2018) 368–380.

[48] V. Agubra and J. Fergus, Lithium ion battery anode aging mechanisms, *Materials* 6 (2013) 1310–1325.

[49] M.-S. Balogun, W. Qiu, Y. Luo, H. Meng, W. Mai, A. Onasanya, T. K. Olaniyi, Y. Tong, A review of the development of full cell lithium-ion batteries: The impact of nanostructured anode materials, *Nano Res.* 9(10) (2016) 2823–2851.

[50] H. Park, N. Yoon, D. Kang, C. Young, J. K. Lee, Electrochemical characteristics and energy densities of lithium-ion batteries using mesoporous silicon and graphite as anodes, *Electrochim. Acta* 357 (2020) 136870.

[51] S. Jeong, X. Li, J. Zheng, P. Yan, R. Cao, H. J. Jung, C. Wang, J. Liu, J.-G. Zhang, Hard carbon coated nano-Si/graphite composite as a high performance anode for Li-ion batteries, *J. Power Sources* 329 (2016) 323−329.

[52] U. Farooq, J.-H. Choi, S. A. Pervez, A. Yaqub, D.-H. Kim, Y.-J. Lee, M. Saleem, C.-H. Doh, Effect of binder and composition ratio on electrochemical performance of silicon/graphite composite battery electrode, *Mater. Lett.* 136 (2014) 254–257.

[53] K.-H. Chen, V. Goel, M. J. Namkoong, M. Wied, S. Müller, V. Wood, J. Sakamoto, K. Thornton, N. P. Dasgupta, Enabling 6C fast charging of Li-ion batteries with graphite/hard carbon hybrid anodes, *Adv. Energy Mater.* 11 (2021) 2003336.

[54] H. Cheng, J. G. Shapter, Y. Li, G. Gao, Recent progress of advanced anode materials of lithium-ion batteries, *J. Energy Chem.* 57 (2021) 451–468.

[55] X. Zhang, C. Fan, S. Han, Improving the initial Coulombic efficiency of hard carbon-based anode for rechargeable batteries with high energy density, *J Mater. Sci.* 52 (2017) 10418–10430.

[56] Y. Ahmad, M. Colin, C. Gervillie-Mouravieff, M. Dubois, K. Guérin, Carbon in lithium-ion and post-lithium-ion batteries: Recent features, *Synth. Met.* 280 (2021) 116864.

[57] Y. Sun, G. Ning, C. Qi, J. Li, X. Ma, C. Xu, Y. Li, X. Zhang, J. Gao, An advanced lithium ion battery based on a sulfur-doped porous carbon anode and a lithium iron phosphate cathode, *Electrochem. Acta* 190 (2016) 141–149.

[58] V. G. Khomenko and V. Z. Barsukov, Characterization of silicon- and carbon-based composite anodes for lithium-ion batteries, *Electrochim. Acta* 52 (2007) 2829–2840.

[59] U. Kasavajjula, C. Wang, A. J. Appleby, Nano- and bulk-silicon-based insertion anodes for lithium-ion secondary cells, *J. Power Sources* 163 (2007) 1003–1039.

[60] M. A. Azam, N. E. Safie, A. S. Ahmad, N. A. Yuza, N. S. A. Zulkifli, Recent advances of silicon, carbon composites and tin oxide as new anode materials for lithium-ion battery: A comprehensive review, *J Energy Storage* 33 (2021) 102096.

[61] P. U. Nzereogu, A. D. Omah, F. I. Ezema, E. I. Iwuoha, A. C. Nwanya, Anode materials for lithium-ion batteries: A review, *Appl. Surf. Sci. Adv.* 9 (2022) 100233.

[62] C. Wang, S. Wang, L. Tang, Y.-B. He, L. Gan, J. Li, H. Du, B. Li, Z. Lin, F. Kang, A robust strategy for crafting monodisperse $Li_4Ti_5O_{12}$ nanospheres as superior rate anode for lithium ion batteries, *Nano Energy* 21 (2016) 133–144.

[63] J. Lu, Z. Chen, F. Pan, Y. Cui, K. Amine, High-performance anode materials for rechargeable lithium-ion batteries, *Electrochem. Energy Rev.* 1 (2018) 35–53.

[64] H. Ku, Y. Jung, M. Jo, S. Park, S. Kim, D. Yang, K. Rhee, E.-M. An, J. Sohn, K. Kwon,

Recycling of spent lithium-ion battery cathode materials by ammoniacal leaching, *J. Hazard. Mater.* 313 (2016) 138–146.

[65] J. Guan, Y. Li, Y. Guo, R. Su, G. Gao, H. Song, H. Yuan, B. Liang, Z. Guo, Mechanochemical process enhanced cobalt and lithium recycling from wasted lithium-ion batteries, *ACS Sustain. Chem. Eng.* 5 (2017) 1026–1032.

[66] Y. Zhou, Z. Hu, Y. Huang, Y. Wu, Z. Hong, Effect of solution wash on the electrochemical performance of $LiNi_{0.8}Co_{0.1}Mn_{0.1}O_2$ cathode materials, *J. Alloys Compd.* 888 (2021) 161584.

[67] L. Li, Y. Bian, X. Zhang, Y. Guan, E. Fan, F. Wu, R. Chen, Process for recycling mixed-cathode materials from spent lithium-ion batteries and kinetics of leaching, *Waste Manag.* 71 (2018) 362–371.

[68] F. Wang, T. Zhang, Y. He, Y. Zhao, S. Wang, G. Zhang, Y. Zhang, Y. Feng, Recovery of valuable materials from spent lithium-ion batteries by mechanical separation and thermal treatment, *J. Clean. Prod*. 185 (2018) 646–652.

[69] R. Zhan, T. Payne, T. Leftwich, K. Perrine, L. Pan, De-agglomeration of cathode composites for direct recycling of Li-ion batteries, *Waste Manag.* 105 (2020) 39–48.

[70] J. Diekmann, C. Hanisch, L. Froböse, G. Schälicke, T. Loellhoeffel, A.-S. Fölster, A. Kwade, Ecological recycling of lithium-ion batteries from electric vehicles with focus on mechanical processes, *J. Electrochem. Soc*. 164(1) (2017) A6184–A6191.

[71] Y. Shi, G. Chen, Z. Chen, Effective regeneration of $LiCoO_2$ from spent lithium-ion batteries: a direct approach towards high-performance active particles, *Green Chem.* 20 (2018) 851.

[72] Recycling of Li-ion and Li-solid state batteries: The role of hydrometallurgy, in: B. Davis et al. (eds.), *Extraction 2018*, Springer, Cham, 2018.

[73] D. Song, X. Wang, E. Zhou, P. Hou, F. Guo, L. Zhang, Recovery and heat treatment of the $Li(Ni_{1/3}Co_{1/3}Mn_{1/3})O_2$ cathode scrap material for lithium ion battery, *J. Power Sources* 232 (2013) 348–352.

[74] J. Wang, Z. Liang, Y. Zhao, J. Sheng, J. Ma, K. Jia, B. Li, G. Zhou, H.-M. Cheng, Direct

conversion of degraded $LiCoO_2$ cathode materials into high-performance $LiCoO_2$: A closed-loop green recycling strategy for spent lithium-ion batteries, *Energy Stor. Mater.* 45 (2022) 768–776.

[75] H. Wang, K. Huang, Y. Zhang, X. Chen, W. Jin, S. Zheng, Y. Zhang, P. Li, Recovery of lithium, nickel, and cobalt from spent lithium-ion battery powders by selective ammonia leaching and an adsorption separation system, *ACS Sustain. Chem. Eng.* 5 (2017) 11489–11495.

[76] Y. Yang, G. Huang, S. Xu, Y. He, X. Liu, Thermal treatment process for the recovery of valuable metals from spent lithium-ion batteries, *Hydrometallurgy* 165 (2016) 390–396.

[77] T. Wu, G. Wang, B. Liu, Q. Huang, Y. Su, F. Wu, R. M. Kelly, The role of Cu impurity on the structure and electrochemical performance of Ni-rich cathode material for lithium-ion batteries, *J. Power Sources* 494 (2021) 229774.

[78] S. Wang, J. Zhu, Y. Li, G. Cao, Y. Chen, D. Zhang, Z. Tan, J. Yang, J. Zheng, H. Li, Role of Al on the electrochemical performances of quaternary nickel-rich cathode $LiNi_{0.8}Co_{0.1}Mn_{0.1-x}Al_xO_2$ ($0 \leq x \leq 0.06$) for lithium-ion batteries, *J. Electroanal. Chem.* 888 (2021) 115200.

[79] S. Park, D. Kim, H. Ku, M. Jo, S. Kim, J. Song, J. Yu, K. Kwon, The effect of Fe as an impurity element for sustainable resynthesis of $Li[Ni_{1/3}Co_{1/3}Mn_{1/3}]O_2$ cathode material from spent lithium-ion batteries, *Electrochim. Acta* 296 (2019) 814–822.

[80] G. Mishra, R. Jha, A. Meshram, K. K. Singh, A review on recycling of lithium-ion batteries to recover critical metals, *J. Environ. Chem. Eng.* 10 (2022) 108534.

[81] A. Mayyas, D. Steward, M. Mann, The case for recycling: Overview and challenges in the material supply chain for automotive Li-ion batteries, *Sustainable Mater. Technol.* 19 (2018) e00087.

[82] X. Meng, J. Hao, H. Cao, X. Lin, P. Ning, X. Zheng, J. Chang, X. Zhang, B. Wang, Z. Sun, Recycling of $LiNi_{1/3}Co_{1/3}Mn_{1/3}O_2$ cathode materials from spent lithium-ion batteries using mechanochemical activation and solid-state sintering, *Waste Manag.* 84 (2019) 54–63.

[83] J. Chen, Q. Li, J. Song, D. Song, L. Zhang, X. Shi, Environmentally friendly recycling and effective repairing of cathode powders from spent $LiFePO_4$ batteries, *Green Chem.* 18 (2016) 2500–2506.

[84] H. S. Kim and E. J. Shin, Re-synthesis and electrochemical characteristics of $LiFePO_4$ cathode materials recycled from scrap electrodes, *Bull. Korean Chem. Soc.* 34(3) (2013) 851–855.

[85] Y.-J. Liu, Q.-Y. Hu, X.-H. Li, Z.-X. Wang, H.-J. Guo, Recycle and synthesis of $LiCoO_2$ from incisors bound of Li-ion batteries, *Trans. Nonferrous Met. Soc. China* 16 (2006) 956–959.

[86] Z. Chi, J. Li, L. Wang, T. Li, Y. Wang, Y. Zhang, S. Tao, M. Zhang, Y. Xiao, Y. Chen, Direct regeneration method of spent $LiNi_{1/3}Co_{1/3}Mn_{1/3}O_2$ cathode materials via surface lithium residues, *Green Chem.* 23 (2021) 9099–9108.

[87] J. Park, S. Park, M. Beak, S. Jeong, K. Kwon, Impacts of residual electrolyte components of spent lithium-ion batteries on the physical/electrochemical properties of resynthesized cathode active materials, *J. Clean. Prod.* 379 (2022) 134570.

[88] X. Ma, M. Chen, Z. Zheng, D. Bullen, J. Wang, C. Harrison, E. Gratz, Y. Lin, Z. Yang, Y. Zhang, F. Wang, D. Robertson, S.-B. Son, I. Bloom, J. Wen, M. Ge, X. Xiao, W.-K. Lee, M. Tang, Q. Wang, J. Fu, Y. Zhang, B. C. Sousa, R. Arsenault, P. Karlson, N. Simon, Y. Wang, Recycled cathode materials enabled superior performance for lithium-ion batteries, *Joule* 5 (2021) 2955–2970.

[89] M. Beak, J. Park, S. Park, S. Jeong, J. Kang, W. Choi, W.-S. Yoon, K. Kwon, Understanding the effect of nonmetallic impurities in regenerated cathode materials for lithium-ion battery recycling by tracking down impurity elements, *J. Hazard. Mater.* 425 (2022) 127907.

[90] S. Krüger, C. Hanisch, A. Kwade, M. Winter, S. Nowak, Effect of impurities caused by a recycling process on the electrochemical performance of $Li[Ni_{0.33}Co_{0.33}Mn_{0.33}]O_2$, *J Electroanal. Chem.* 726 (2014) 91–96.

[91] Z. Zhang, M. Yu, B. Yang, C. Jin, G. Guo, J. Qiu, Regeneration of Al-doped

$LiNi_{1/3}Co_{1/3}Mn_{1/3}O_2$ cathode material via a sustainable method from spent Li-ion batteries, *Mater. Res. Bull.* 126 (2020) 110855.

[92] C. Peng, K. Lahtinen, E. Medina, P. Kauranen, M. Karppinen, T. Kallio, B. P. Wilson, M. Lundström, Role of impurity copper in Li-ion battery recycling to $LiCoO_2$ cathode materials, *J. Power Sources* 450 (2020) 227630.

[93] Y. Weng, S. Xu, G. Huang, C. Jiang, Synthesis and performance of $Li[(Ni_{1/3}Co_{1/3}Mn_{1/3})_{1-x}Mg_x]O_2$ prepared from spent lithium ion batteries, *J. Hazard. Mater.* 246–247 (2013) 163–172.

[94] Y. Abe, K. Sawa, M. Tomioka, R. Watanabe, T. Yodose, S. Kumagai, Electrochemical performance of $LiNi_{1/3}Co_{1/3}Mn_{1/3}O_2$ cathode recovered from pyrolysis residue of waste Li-ion batteries, *J. Electroanal. Chem.* 922 (2022) 116761.

[95] S. Kim, S. Park, M. Jo, M. Beak, J. Park, G. Jeong, J.-S. Yu, K. Kwon, Electrochemical effects of residual Al in the resynthesis of $Li[Ni_{1/3}Mn_{1/3}Co_{1/3}]O_2$ cathode materials, *J Alloys Compd.* 857 (2021) 157581.

[96] S. Jeong, S. Park, M. Beak, J. Park, J.-S. Sohn, K. Kwon, Effect of residual trace amounts of Fe and Al in $Li[Ni_{1/3}Mn_{1/3}Co_{1/3}]O_2$ cathode active material for the sustainable recycling of lithium-ion batteries, *Materials* 14 (2021) 2464.

[97] M. Jo, S. Park, J. Song, K. Kwon, Incorporation of Cu into $Li[Ni_{1/3}Co_{1/3}Mn_{1/3}]O_2$ cathode: Elucidating its electrochemical properties and stability, *J. Alloys Compd.* 764 (2018) 112–121.

[98] S. Park, C. Jo, H. J. Kim, S. Kim, S.-T. Myung, H.-K. Kang, H. Kim, J. Song, J. Yu, K. Kwon, Understanding the role of trace amount of Fe incorporated in Ni-rich $Li[Ni_{1-x-y}Co_xMn_y]O_2$ cathode material, *J. Alloys Compd.* 835 (2020) 155342.

[99] M. Beak, S. Park, S. Kim, J. Park, S. Jeong, B. Thirumalraj, G. Jeong, T. Kim, K. Kwon, Effect of Na from the leachate of spent Li-ion batteries on the properties of resynthesized Li-ion battery cathodes, *J. Alloys Compd.* 873 (2021) 159808.

[100] W. Hua, J. Zhang, Z. Zheng, W. Liu, X. Peng, X.-D. Guo, B. Zhong, Y.-J. Wang, X. Wang, Na-doped Ni-rich $LiNi_{0.5}Co_{0.2}Mn_{0.3}O_2$ cathode material with both high rate

capability and high tap density for lithium ion batteries, *Dalton Trans.* 43 (2014) 14824–14832.

[101] SK S. Hossain, L. Mathur, P. K. Roy, Rice husk/rice husk ash as an alternative source of silica in ceramics: A review, *J. Asian Ceram. Soc.* 6 (2018) 299–313.

[102] R. Chen, S. S. C. Congress, G. Cai, W. Duan, S. Liu, Sustainable utilization of biomass waste-rice husk ash as a new solidified material of soil in geotechnical engineering: A review, *Constr. Build. Mater.* 292 (2021) 123219.

[103] C. Chaikawang, R. Hongthong, S. Kaewmala, S. Pongha, Y. Kanapana, N. Meethong, Surface modification of rice husk ash as anodes for lithium ion batteries, *Materials Today Proceedings* 5(6) (2018) 13989–13994.

[104] L. Wang, J. Xue, B. Gao, P. Gao, C. Mou, J. Li, Rice husk derived carbon-silica composites as anodes for lithium ion batteries, *RSC Adv.* 4 (2014) 64744–64746.

[105] G. T.-K. Feya and C.-L. Chen, High-capacity carbons for lithium-ion batteries prepared from rice husk, *J. Power Sources* 97–98 (2001) 47–51.

[106] Y. Feng, X. Liu, L. Liu, Z. Zhang, Y. Teng, D. Yu, J. Sui, X. Wang, SiO_2/C composite derived from rice husks with enhanced capacity as anodes for lithium-ion batteries, *Energy Technol. Environ. Sci.* 3 (2018) 10338–10344.

[107] K. Kaviyarasu, E. Manikandan, J. Kennedy, M. Jayachandran, M. Maaza, Rice husks as a sustainable source of high quality nanostructured silica for high performance Li-ion battery requital by sol-gel method – a review, *Adv. Mater. Lett.* 7(9) (2016) 684–696.

[108] J. Hou, X. Mao, J. Wang, C. Liang, J. Liang, Preparation of rice husk-derived porous hard carbon: A self-template method for biomass anode material used for high-performance lithium-ion battery, *Chem. Phys.* 551 (2021) 111352.

[109] Q. Ma, Y. Dai, H. Wang, G. Ma, H. Guo, X. Zeng, N. Tu, X. Wu, M. Xiao, Directly conversion the biomass-waste to Si/C composite anode materials for advanced lithium ion batteries, *Chin. Chem. Lett.* 32 (2021) 5–8.

[110] Y. Guo, X. Chen, W. Liu, X. Wang, Y. Feng, Y. Li, L. Ma, B. Di, Y. Tian, Preparation of rice husk-based C/SiO_2 composites and their performance as anode materials in lithium

ion batteries, *J. Electron. Mater.* 49(2) (2020) 1081–1089.

[111] X. Fan, B. Yin, T. Wu, M. Feng, G. C. Zhang, S. Li, S. Tang, J. Gu, B. Wen, L. Lu, Rice husk-based 3D porous silicon/carbon nanocomposites as anode for lithium-ion batteries, *Energy Technol.* 7 (2019) 1800787.

[112] I. J. Fernandes, D. Calheiro, F. A. L. Sánchez, A. L. D. Camacho, T. L. A. de Compos Rocha, C. A. M. Moraes, V. C. de Sousa, Characterization of silica produced from rice husk ash: Comparison of purification and processing methods, *Mater. Res.* 20 (2017) 512–518.

[113] T. Autthawong, O. Namsar, A. Yu, T. Sarakonsri, Cost-effective production of SiO_2/C and Si/C composites derived from rice husk for advanced lithium-ion battery anodes, *J. Mater. Sci. Mater. Electron.* 31 (2020) 9126–9132.

[114] A. Daulay, Andriayani, Marpongahtun, S. Gea, Synthesis and application of silicon nanoparticles prepared from rice husk for lithium-ion batteries, *Case Stud. Chem. Environ. Eng.* 6 (2022) 100256.

[115] Y. Shen, Rice husk silica derived nanomaterials for sustainable applications, *Renewable Sustainable Energy Rev.* 80 (2017) 453–466.

[116] N. Liu, K. Huo, M. T. McDowell, J. Zhao, Y. Cui, Rice husks as a sustainable source of nanostructured silicon for high performance Li-ion battery anodes, *Sci. Rep.* 3 (2013) 1919.

[117] D. S. Jung, M.-H. Ryou, Y. J. Sung, S. B. Park, J. W. Choi, Recycling rice husks for high-capacity lithium battery anodes, *Proc. Natl. Acad. Sci. U. S. A.* 110 (2013) 12229–12234.

[118] K. Yu, H. Zhang, H. Qi, X. Gao, J. Liang, C. Liang, Rice husk as the source of silicon/carbon anode material and stable electrochemical performance, *Inorg. Chem.* 3 (2018) 5439–5444.

[119] H. Chu, Q. Wu, J. Huang, Rice husk derived silicon/carbon and silica/carbon nanocomposites as anodic materials for lithium-ion batteries, *Colloids Surf. A* 558 (2018) 495–503.

[120] L. Liao, T. Ma, Y. Xiao, M. Wang, Y. Gao, T. Fang, Enhanced reversibility and cyclic stability of biomass-derived silicon/carbon anode material for lithium-ion battery, *J. Alloys Compd.* 873 (2021) 159700.

[121] Y. Abe, M. Tomioka, M. Kabir, S. Kumagai, Role of SiO_x in rice-husk-derived anodes for Li-ion batteries, *Sci. Rep.* 12 (2022) 975.

[122] K. Yu, Y. Wang, X. Wang, W. Liu, J. Liang, C. Liang, Preparation of porous carbon anode materials for lithium-ion battery from rice husk, *Mater. Lett.* 253 (2019) 405–408.

[123] K. Yu, J. Li, H. Qi, C. Liang, High-capacity activated carbon anode material for lithium-ion batteries prepared from rice husk by a facile method, *Diamond Relat. Mater.* 86 (2018) 139–145.

[124] Y. Ju, J. A. Tang, K. Zhu, Y. Meng, C. Wang, G. Chen, Y. Wei, Y. Gao, SiO_x/C composite from rice husks as an anode material for lithium-ion batteries, *Electrochim. Acta* 191 (2016) 411–416.

[125] L. Wang, Z. Schnepp, M. M. Titirici, Rice husk-derived carbon anodes for lithium ion batteries, *J. Mater. Chem. A* 1 (2013) 5269–5273.

[126] J. Cui, F. Cheng, J. Lin, J. Yang, K. Jiang, Z. Wen, J. Sun, High surface area C/SiO_2 composites from rice husks as a high-performance anode for lithium ion batteries, *Powder Technol.* 311 (2017) 1–8.

[127] B. F. Song, A. Dhanabalan, S. L. Biswal, Evaluating the capacity ratio and prelithiation strategies for extending cyclability in porous silicon composite anodes and lithium iron phosphate cathodes for high capacity lithium-ion batteries, *J. Energy Storage* 28 (2020) 101268.

[128] X. Li, X. Sun, X. Hu, F. Fan, S. Cai, C. Zheng, G. D. Stucky, Review on comprehending and enhancing the initial Coulombic efficiency of anode materials in lithium-ion/sodium-ion batteries, *Nano Energy* 77 (2020) 105143.

[129] X. Fan, S. Li, Y. Cui, L. Lu, C. Zhou, Z. Liu, Fe_3O_4/rice husk-based maco-/mesoporous carbon bone nanocomposite as superior high-rate anode for lithium ion battery, *J. Solid State Electrochem.* 21 (2017) 27–34.

[130] J. Cui, H. Zhang, Y. Liu, S. Li, W. He, J. Hu, J. Sun, Facile, economical and environment-friendly synthesis process of porous N-doped carbon/SiO_x composite from rice husks as high-property anode for Li-ion batteries, *Electrochim. Acta* 334 (2020) 135619.

Chapter 3

Electrochemical Performance of $LiNi_{1/3}Co_{1/3}Mn_{1/3}O_2$ Cathode Recovered from Pyrolysis Residue of Waste LIBs

3. 1 Introduction

LIBs have been widely used as indispensable power sources in various applications, such as mobile electronics, automobiles, and industrial robots. In the automotive industry, battery electric vehicles (BEVs) and plug-in hybrid electric vehicles (PHEVs) require high-performance LIBs with high energy density, excellent power capability, long cycle life, and reliable safety [1–4]. Commercial LIB cells are generally composed of LTMO cathodes, graphitic anodes, separators, and non-aqueous electrolytes. In any LIB cell, the cathode active material plays an important role as a finite Li source, thereby significantly influencing the cell performance.

The LTMOs have been extensively used as active cathode materials [5–7]. The $LiCoO_2$ exhibits a sufficiently positive electrode potential, good electrical conductivity, and comparatively high specific capacity (~140 mAh g^{-1}). Therefore, it has been used in the cathode materials of high-quality LIBs, particularly in mobile electronics such as smartphones, tablets, and laptop computers [6, 7]. However, Co is an expensive rare metal because of its uneven distribution worldwide. Over the past decade, the application of LIB cells in BEVs and PHEVs has rapidly progressed, which enabled the reduction of CO_2 emissions from the transportation sector. Ternary LTMOs ($LiNi_{1-x-y}Co_xMn_yO_2$) in which Co is partially replaced by Ni and Mn have been extensively investigated for automotive applications that require large-scale, low-cost, and continuous fabrication of LIB cells [8–16]. Among them, NCM111, which has an equivalent Ni, Co, and Mn content (x=y=1/3) showed good Li-ion extraction/insertion properties when used as a LIB cathode and is widely used in automotive applications [12]. Therefore, the incorporation of Ni in ternary LTMOs is required to offer a high specific capacity upon slow Li-ion extraction/insertion, that is, under a low charge–discharge current density for the cells

[10, 17]. NCM523, NCM622, and NCM811 have been recognized as promising active cathode materials for automotive LIBs.

Since LIB cells were first commercialized, the utilization or recycling of waste (end-of-life) cells has attracted much attention, regardless of size and applied fields. When BEVs that utilize metric tons of LIB cells become mainstream automobiles in the future, the effective reutilization of rare metals, such as Li, Ni, Co, and Mn in the cathode with cost-effectiveness and in industrial processes is essential for the sustainable fabrication of LIB cells. A significant interest in the recycling of key materials used in waste cells has been undertaken by academia and the industrial sector, and significant research results on LIB cell recycling have been reported [18–28].

Hydrometallurgy has commonly been used to produce a precursor of the cathode active material recovered from spent LIBs [18, 22, 29]. This procedure includes five steps: (1) cell discharging (electrical neutralization); (2) cell disassembly; (3) mechanical-, thermal-, solvent-peeling, or a combination of the three types of peeling from the current collectors; (4) grinding; and (5) chemical refining and recovery. The LIB cells intended for automotive applications need to be robustly packaged to withstand strong mechanical shock, penetration of any type of liquid, fire, and high temperatures. Waste LIB stacks are usually disassembled into inner parts (cathode, anode, and separator) and outer covers. However, direct cell disassembly requires safety measures against electrocution, fire, and exposure to chemicals. Moreover, robust packaging complicates the mechanical extraction of cathode active materials from cells. Thus, the direct cell disassembly procedure described above is ineffective for recycling cathode active materials from a large quantity of LIB cells removed from discarded BEVs. A countermeasure to automatically and safely extract the cathode active materials from waste LIB stacks in a timely manner without the complex disassembly process is pyrolysis under inert conditions, which enables us to readily collect the pyrolysis residue of the cathodes and render it electrically harmless and safe against fire. It is possible to increase the Ni, Co, and Mn contents in the

pyrolysis residue by selecting the appropriate pyrolysis temperature, and mechanically and magnetically collecting the cathode active materials from the pyrolyzed LIB stacks. The refined pyrolysis residue was converted into a mixture of hydroxides of Ni, Co, and Mn (the precursors of the cathode active material). However, it is difficult to avoid the contamination of cell-derived metals, which are mainly Al from cathode current collectors, Cu from anode current collectors and cell wire-conductors, and Fe from cell packaging and fixtures.

In the field of recycling or recovery of cathode active materials from LIB cells, the effect of metallic impurities, such as Al, Cu, and Fe, in ternary LTMOs on their electrochemical performance has attracted much attention. A small percentage of Al, Cu, or Fe at equivalent ratios to the sum of Ni, Co, and Mn contents has been demonstrated to be harmless to the electrochemical performance of ternary LTMO cathodes [30–32]. Based on the performance retention in the presence of metallic impurities, their incorporation into cathodes has become more acceptable to improve the sustainable fabrication of LIB cells.

This study aims to provide new knowledge regarding the recycling of waste LIB cells that meets the new era of acceptable incorporation of metallic impurities in cathode materials. A waste LIB stack that was used in a PHEV was prepared and pyrolyzed under air-free conditions, and it required no complex or harmful processes. Subsequently, grinding, classification (sieving), and hydrometallurgy processes were performed for the pyrolyzed stack, thus producing the precursor of the cathode active material in the state of Ni, Co, and Mn hydroxides in the presence of Al, Cu, and Fe. By mixing the synthesized precursor and Li_2CO_3 and then heating the mixture in air at 800 °C, the waste-LIB-derived cathode active material of $LiNi_{1/3}Co_{1/3}Mn_{1/3}O_2$ (W-NCM) with Al, Cu, and Fe impurities at a total of 4.0 mass% was achieved. Commercial NCM523 was also evaluated in a similar manner to verify the validity of the evaluation procedure and compared with W-NCM as a commercial cathode material for BEV applications. Herein, the effect of high-level multi-impurities on the electrochemical performance of waste-LIB-derived cathodes was evaluated.

3. 2 Experimental

3. 2. 1 *Material Preparation and Characterization*

The cathode active material was recovered from a waste LIB stack (~75 kg) that was used in a Japanese PHEV. The process flow from the stack pyrolysis to the preparation of the cathode active material precursor is shown in Figure 1. First, the waste LIB stack was pyrolyzed in a closed chamber at 800 °C for 2 h and then cooled down to room temperature, with limiting inflow of air. At temperatures higher than 700 °C, the reactions of Li metal oxides with C, which can be supplied from the anode active material and the cathode conductive agent can occur so as to form pure metals, metal oxides, LiO_2, Li_2CO_3, O_2, CO, CO_2, etc. [29, 32, 33]. The pyrolyzed stack was then fractured using a hammer crusher at a constant circumferential speed of 38 m s^{-1}. The fractured stack was sieved into grains with sizes <1.2 mm, and the sieved grains were dispersed in water at a grain-to-water mass ratio of 10. The slurry was supplied at 100 mL min^{-1} for magnetic separation at a magnetic flux density of 0.15 T and a dram rotation speed of 45 min^{-1}. The magnetized grains in the wet state were dried and processed by hydrometallurgy.

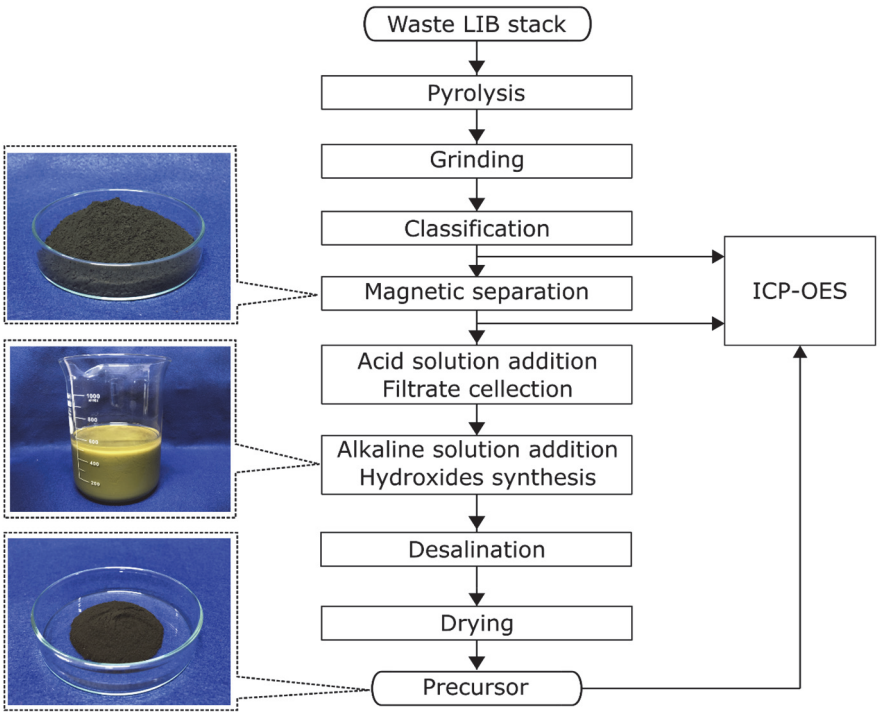

Figure 1. Processing flow from waste LIB stack to the cathode active material precursor.

The refined grains (5 g) were mixed with 100 mL of HCl solution (12 mol L^{-1}), and the solution was maintained at 70−100 °C for 1 h. Then, 100 mL of deionized water and 100 mL of HNO_3 solution (14 mol L^{-1}) were added to the above solution. The resulting solution was heated at 160 °C for 1 h and then naturally cooled to room temperature. The insoluble substances therein were removed by filtration using a filter paper. A NaOH solution (2 mol L^{-1}) was poured into the filtered solution to maintain a pH of 11−12, which allowed precipitation of the metallic hydroxides. The precipitated hydroxides were collected from the solution by filtration (using filter paper) and dried at 105 °C in air. The dried hydroxides were pulverized using a mortar and pestle. The pulverized samples were desalinated by immersion and stirred in deionized water. Subsequently, the desalinated samples were filtered and dried at 105 °C in air, which yielded the precursor of the cathode active material.

The precursor was mixed with Li_2CO_3 at a mass ratio of 2.5 and milled using a disk mill. The mixture was sintered in air in a two-step heating procedure at 600 °C for 1 h, followed by heating at 800 °C for 4 h, and then naturally cooled to room temperature. The final product of the waste-LIB-derived ternary LTMO cathode active material was designated as W-NCM. The metallic composition of the W-NCM was determined by dissolution in an acidic solution and further analysis was performed using inductively coupled plasma optical emission spectrometry (ICP-OES, iCAP 6300 Duo, Thermo Fisher Scientific K.K., Japan). The ICP-OES was also applied to the intermediate materials produced during the recovery of cathode active materials (the sieved grains, the magnetically separated grains and the precursor), providing their compositions. The metal content of the oxides in W-NCM was analyzed using an X-ray fluorescence (XRF) analyzer (ZSX Primus II, Rigaku Corp., Japan). The microscopic morphology of the prepared W-NCM particles was analyzed by scanning electron microscopy (SEM, VE-8800, Keyence Corp., Japan). Energy dispersive X-ray spectroscopy (EDX) was performed for the W-NCM particles using an EDX system (INCA Energy 250, Oxford Instruments, UK) attached to the SEM equipment in order to determine the particle elemental mapping and composition including the non-metallic elements of C, O, and F. For the

determination of particle composition, the average atomic concentration of three individual particles was calculated by narrowing the analysis region to within the particle surface.

3. 2. 2 *Electrode Fabrication*

To evaluate the electrochemical performance of W-NCM in both half- and full-cell configurations, the electrodes were fabricated by coating them onto an Al foil as the current collector. Commercial ternary LTMO ($LiNi_{0.5}Co_{0.2}Mn_{0.3}O_2$ (NCM523), Beijing Easpring Material Technology Co., Ltd., China) was also prepared for comparison and is termed as NCM in this study. For cathode fabrication, a slurry was prepared by mixing 80 mass% of cathode active material, 10 mass% of acetylene black (Denka Co., Ltd., Japan), and 10 mass% of PVDF (KF polymer F #9130, Kureha Corp., Japan), all of which were then added to N-methylpyrrolidone (Tokyo Chemical Industry Co., Ltd., Japan). The prepared slurry was coated on an Al foil (no surface treatment, *t*20 μm, Hohsen Corp., Japan), and the coated Al foil was dried in air at 100 °C for 6 h. The loading masses of W-NCM and NCM were 1.5–2.5 and 2.3–3.0 mg cm^{-2}, respectively. The coating thicknesses of the cathodes were 30–59 and ~35 μm for W-NCM and NCM, respectively. The anode was prepared using graphite (CGB-10, Nippon Graphite Co., Ltd., Japan), acetylene black, styrene-butadiene rubber (TRD2001, JSR Corp., Japan), and sodium carboxymethyl cellulose (Cellogen 7A, DSK Co., Ltd., Japan) with a mass ratio of 90:5:2.5:2.5. Subsequently, they were added to distilled water and stirred using a planetary centrifugal mixer. The resultant slurry was coated on a Cu foil (no surface treatment, *t*20 μm, Hohsen Corp., Japan). The graphite anodes had loading masses of 1.2–1.4 mg cm^{-2} and electrode coating thicknesses of 14–21 μm.

3. 2. 3 *Cell Assembly and Electrochemical Measurement*

The dried cathode and anode sheets were punched into ϕ15 mm disks. The disks were dried at 140 °C for >5 h under vacuum and then used for the cell assembly. CR2032 coin-type half- and full-cells were used. For the assembly of the half-cell, W-NCM or NCM cathode, a Li metal foil (ϕ15 mm, *t*0.2 mm, Honjo Metal Co., Ltd., Japan), polypropylene separator (2500, Celgard

LLC, USA), and non-aqueous electrolyte (1 mol L^{-1} $LiPF_6$ in a mixture of ethylene carbonate and diethyl carbonate with 1:1 vol.%, Kishida Chemical Co., Ltd., Japan) were used. The full-cell was assembled using a cathode (W-NCM or NCM), graphite anode, polypropylene separator, and non-aqueous electrolyte. All the cell assembly processes were conducted in an argon-filled glove box with the dew point maintained at below −40 °C. The prepared cell assemblies were aged at 70 °C for 4 h outside the glove box and naturally cooled to room temperature for the enhancement of electrolyte penetration into the electrodes.

Using a battery charge–discharge system (HJ1020mSD8, Hokuto Denko Corp., Japan), the electrochemical performances of the W-NCM and NCM active materials were evaluated in both half- and full-cell configurations. The cathodes in the half-cells were operated in the potential range of 3.0–4.2 V vs. Li/Li^+. To evaluate the current dependence (rate performance) of the Li-ion extraction/insertion properties of the active materials, the current density was increased in a step-wise manner from 15 to 30, 75, 150, 300, 750, and 1500 mA g^{-1} and then decreased to the lowest level of 15 mA g^{-1}. Here, the current density in mA g^{-1} is the actual current level divided by the mass of the active material. The specific capacity of the active material was defined as the charge quantity (time integral of the current) divided by the mass of the active material. The CE was also defined as the ratio of Li-ion insertion to Li-ion extraction specific capacity. The Li-ion extraction/insertion cycles were repeated five times for each current density. Assuming the specific capacity of NCM111 to be 150 mAh g^{-1} [22, 32], the lowest and highest current densities of 15 and 1500 mA g^{-1} correspond to the C-rates of 0.1 and 10 C, respectively. The range of current density at 0.1−10 C during the half-cell rate test was determined in accordance with that of the full-cell rate test that is discussed in the subsequent sections. Following the rate performance evaluation, 500 cycles were performed to evaluate the cyclic stability of W-NCM and NCM under an increased current density of 300 mA g^{-1}.

The apparent specific capacities of W-NCM and NCM were precisely determined based on the half-cell results. The anode specific capacity of graphite was determined to be 340 mAh g^{-1}, as

described in our previous study [3]. For the full-cell assembly, a capacity ratio of anode to cathode of 1.2 was designed to prevent the formation of lithium dendrites on the anode surface [3]. The full-cells were charged and discharged in the cell voltage range of 2.5–4.2 V. The rate performance of the cathode active material was evaluated at 0.1–10 C, during which the charge–discharge process was repeated five times at each C-rate. The C-rate used for the full-cells was based on the apparent specific capacity of the active cathode material. The full-cells were then repeatedly charged and discharged 1000 times at 2 C to evaluate their cycling performance.

According to the rate performances before and after the cycling test, a relationship between the specific energy and specific power, referred to as the Ragone plot was also produced for the characterization of full-cells. The specific energy and specific power of the full-cell, which are both based on the total mass of the cathode and anode active materials were calculated using the following equations:

$$E_{\mathrm{FC}} = \frac{W_{\mathrm{D}}}{AM_{\mathrm{total}}} \ [\mathrm{Wh\ kg_{FC}^{-1}}] \quad , \quad (3.1)$$

$$P_{\mathrm{FC}} = \frac{V_{\mathrm{Dave}} \times I_{\mathrm{D}}}{AM_{\mathrm{total}}} \ [\mathrm{W\ kg_{FC}^{-1}}] \quad , \quad (3.2)$$

where E_{FC} is the specific energy; W_{D} is the energy released during the discharge process; AM_{total} is the total mass of the cathode and anode active materials; P_{FC} is the specific power; V_{Dave} is the average voltage during the discharge process, and I_{D} is the discharge current. Data from the third cycle at each C-rate during the rate tests were selected to produce Ragone plots. All the electrochemical measurements were performed at 25 °C.

3. 3 Results and Discussion

3. 3. 1 *Material Characterization*

Table 1. ICP-OES compositions of products generated during the recovery process of cathode active material, from the grains of pyrolysis residue to the recovered $LiNi_{1/3}Co_{1/3}Mn_{1/3}O_2$ (W-NCM).

Sample	Ni	Co	Mn	Li	Al	Cu	Fe	Others (by diff.)
Sieved grains (<1.2 mm)	14.1	10.9	10.2	3.2	6.0	1.6	0.7	53.3
Magnetically separated grains	22.3	23.3	21.1	1.1	2.3	2.8	1.4	25.7
Precursor	16.6	15.5	17.4	0	1.8	2.0	1.2	45.5
W-NCM	13.4	12.3	13.4	9.3	1.3	1.7	1.0	47.6

Unit: mass%

The composition of products generated during the recovery process of cathode active material from the waste LIB stack (sieved grains of pyrolysis residue, magnetically separated grains, precursor, and finally recovered product of W-NCM) were analyzed using ICP-OES; the results are provided in Table 1. The Ni, Co, Mn, and Li, which are the elements of $LiNi_{1/3}Co_{1/3}Mn_{1/3}O_2$ (38.4 mass% in total), and the metallic impurities of Al, Cu, and Fe (8.3 mass% in total) were detected in the sieved grains. Al, which is used as the current collector, exhibited the highest content (6.0 mass%) among the metal impurities. The remaining (53.3 mass%) composition is likely to be include O in the form of metal oxides, along with C and F which could not be dissolved in the acidic solution for ICP-OES. The use of wet magnetic separation increased and equalized the compositions of Ni, Co, and Mn, while the composition of others decreased to half (25.7 mass%) approximately. The Al content also decreased, demonstrating the effectiveness of wet magnetic separation in the cathode recovery process. The decrease in Li content was attributed to the water added for wet magnetic separation.

The W-NCM precursor, which is a dried precipitate obtained due to the formation of Ni, Co, Mn, Al, Cu, and Fe hydroxides, followed by desalination, exhibited similar contents of Ni, Co, and Mn (49.5 mass% in total) and a low amount of metallic impurities (4.0 mass% in total). The amount of other precursors (45.5 mass%) was significantly higher than that for the magnetically separated grains (25.7 mass%). The other precursors mostly contained H and O

due to the formation of hydroxide. The comparatively low level of other magnetically sieved grains indicated that the oxides of Ni, Co, and Mn allowed a partial reduction (stripping of O) and partial metallization due to the ambient carbon-containing materials such as electrolyte, separator, and resin-based outer package. In the final product of W-NCM, similar contents of Ni, Co, and Mn were confirmed, and a total of 4.0 mass% of metallic impurities (Al, Cu, and Fe) were detected. The stoichiometric Li content required to attain the composition of $LiNi_{1/3}Co_{1/3}Mn_{1/3}O_2$ is ~5 mass% under the above-mentioned composition of Ni, Co, and Mn, indicating that an excess Li content of ~4 mass% exists in W-NCM. Excess Li can take the form of Li_2CO_3, lithiated oxides of Al, Cu, and Fe, and/or other compounds such as Li_2O and Li(OH). XRF analysis revealed that the total oxide content of Ni, Co, and Mn was 86.0 mass%, and the contents of oxides of Al, Cu, and Fe were 3.6, 3.7, and 2.5 mass%, respectively.

The above results demonstrated that using the sieved grains of pyrolysis residue of the LIB stack inertly heated to 800 °C, the cathode active material could be recovered via wet magnetic separation, acid leaching, hydroxide synthesis, and sintering with the addition of Li_2CO_3. The wet magnetic separation process prior to the acid leaching was beneficial for reducing Al impurity used as the cathode current collector and non-metallic residues such as carbonaceous materials.

Figure 2 shows the SEM and elemental mapping images of the W-NCM particles. The overview image indicates that the size of the W-NCM particles ranged from 10 to 50 μm, which is larger than that of the commonly used micron-sized LTMO cathode active materials [34, 35]. In contrast, the particle size of NCM was 12 μm, which has been reported in literature [17]. Elemental mapping of specific particles suggested that all metallic elements were uniformly distributed on the particle surface. The EDX composition of the surface of the W-NCM particles is listed in Table 2. Significant quantities of C and F were detected, indicating the existence of excessive and residual Li_2CO_3, as well as residual fluoride-containing substances, which resulted from the PVDF binder used in the cathode of the brand-new LIB cell and electrolyte-

derived $LiPF_6$ salt. Based on the fact that W-NCM was sintered in air at 800 °C for 4 h, thermally stable metallic fluorides or LiF may have been produced in the W-NCM particles.

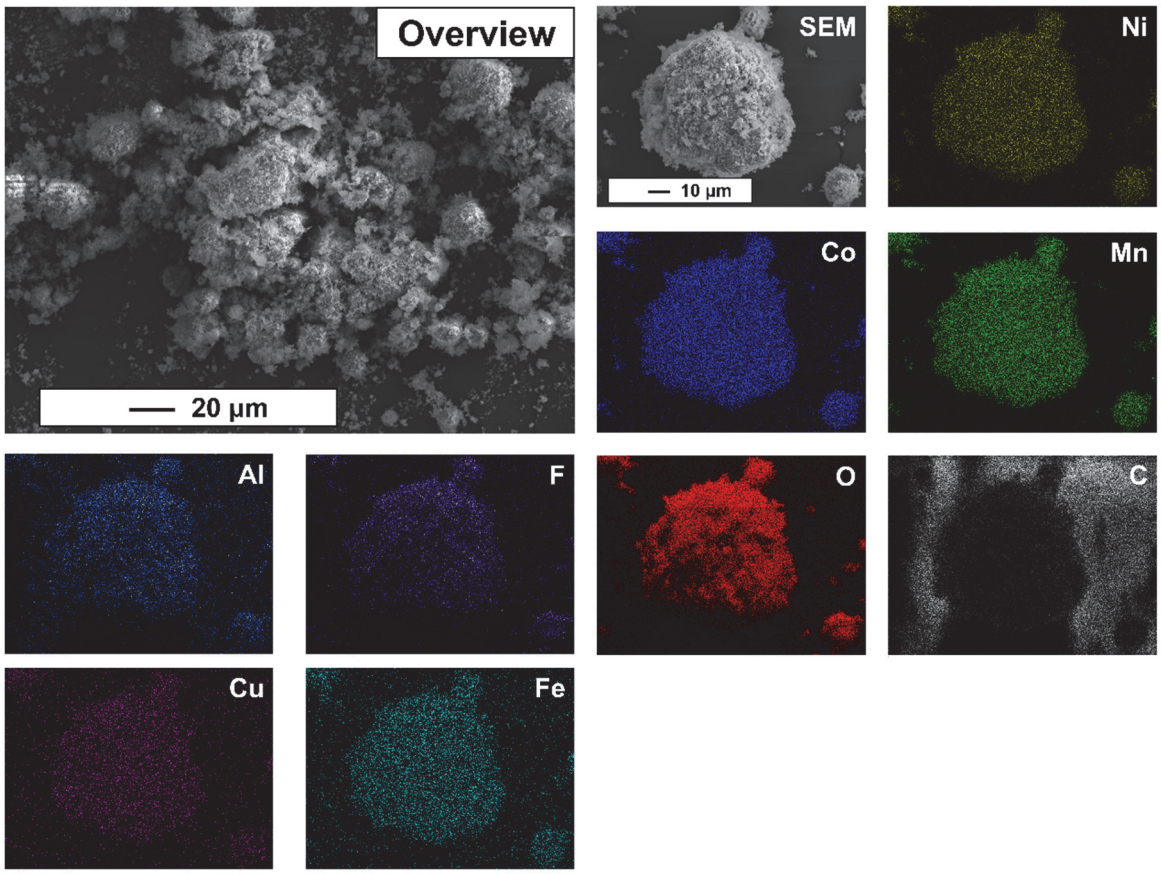

Figure 2. Microscopic overview of W-NCM particles and elemental mapping of the representative particles. The particles were fixed on a conductive carbon tape. In the mapping image of C, the white signals detected outside the particles were caused by the carbon tape.

Table 2. Surface composition of W-NCM particles obtained by EDX.

Element	Ni	Co	Mn	O	Al	Cu	Fe	C	F	Total
mass%	18.2	16.5	18.5	33.2	1.7	2.1	1.7	4.7	3.4	100

3. 3. 2 *Electrochemical Performances of W-NCM and NCM in Half-Cells*

The Li-ion extraction and insertion properties of the W-NCM and NCM cathode active materials in half-cells were evaluated, and the results are shown in Figure 3. The potential-specific capacity profiles for the initial five cycles at the lowest current density of 15 mA g^{-1} indicated that the specific capacities of W-NCM at the first Li-ion extraction and insertion

processes were 146 and 121 mAh g^{-1}, respectively, and the CE was 82.9%. Those of NCM were 174 and 153 mAh g^{-1}, respectively, and the CE was 87.7%. W-NCM and NCM exhibited similar potential-specific capacity profiles. A minor difference was observed in the potential reduction

at a higher specific capacity during Li-ion insertion. W-NCM showed a gradual decrease (at >100 mAh g^{-1}), while NCM exhibited a rapid decline. With increasing current density, the Li-

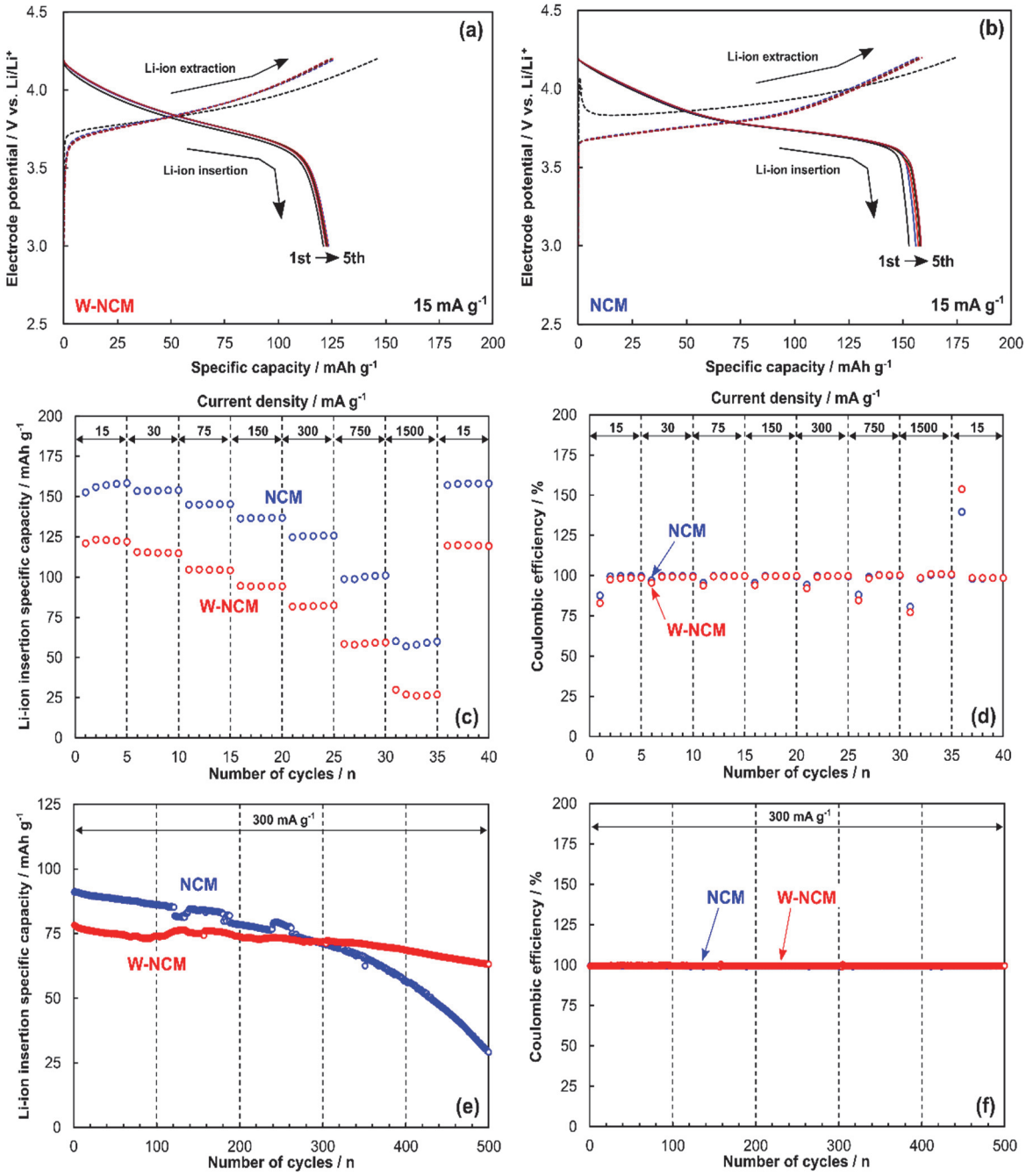

Figure 3. Electrochemical performances of the cathode active materials under half-cell configuration. Potential-specific capacity profiles of (a) W-NCM and (b) NCM at 15 mA g^{-1}. (c) Specific capacity of Li-ion insertion and (d) Coulombic efficiency at different current densities. (e) Specific capacity of Li-ion insertion and (f) Coulombic efficiency during the cycling test at 300 mA g^{-1}.

ion insertion-specific capacity of W-NCM and NCM decreased. NCM maintained a higher specific capacity than W-NCM throughout the rate test. The CEs of both the cathode active materials were nearly 100% after excluding the first cycles at each current density, thus allowing a hysteretic influence of the previous cycle. In the last five cycles, when the current density was reduced to 15 mA g^{-1}, the Li-ion insertion specific capacities of W-NCM and NCM were converted to 120 and 155 mAh g^{-1}, respectively. These values were used as the apparent specific capacities of the cathode active materials.

In the cycling test performed at 300 mA g^{-1}, the Li-ion insertion specific capacity of W-NCM is lower than that of NCM at the beginning of the test. However, W-NCM sufficiently maintained the specific capacity even after 500 cycles, showing an excellent capacity retention (80.7%, based on the results of the 5th and 500th cycles), whereas NCM suffered from a large capacity decline (33.6%). The reduced specific capacity of Li-ion extraction/insertion during the rate test and enhanced capacity retention during the cycling test were observed for W-NCM, which was likely related to the existence of metallic impurities and/or excess Li.

3. 3. 3 *Electrochemical Performances of W-NCM and NCM in Full-Cells*

The full-cell, wherein the W-NCM or NCM cathode and graphite anode were installed, was evaluated in the rate test using a cell voltage range of 2.5–4.2 V. The C-rate was used to express the current density, which was based on the determined apparent specific capacities. Thus, the 1 C values for W-NCM and NCM were 120 and 155 mA g^{-1}, respectively. Figure 4 shows the electrochemical performances of W-NCM and NCM in full-cells at different C-rates. Prior to the first charging process, the voltage of the full-cells was ~0 V. In the first charging process at 0.1 C, both the cell voltages steeply increased to 3.9 V, corresponding to a specific capacity of ~40 mAh g^{-1}. Then, the cell voltage gradually increased to 4.2 V, thereby reaching Li-ion extraction specific capacities of 122 and 159 mAh g^{-1} for W-NCM and W-NCM, respectively. These values were approximately equal to the specific capacities recorded in the half-cell rate test. In the first discharging process, the specific capacities of 82 and 116 mAh g^{-1} were

observed for W-NCM and NCM, respectively, at a cell voltage of 2.5 V. The CE values at the first cycle were 67.4% for W-NCM and 73.1% for NCM. The lower specific capacities and CEs when compared with the results of the half-cell tests were attributed to the loss of Li-ions that

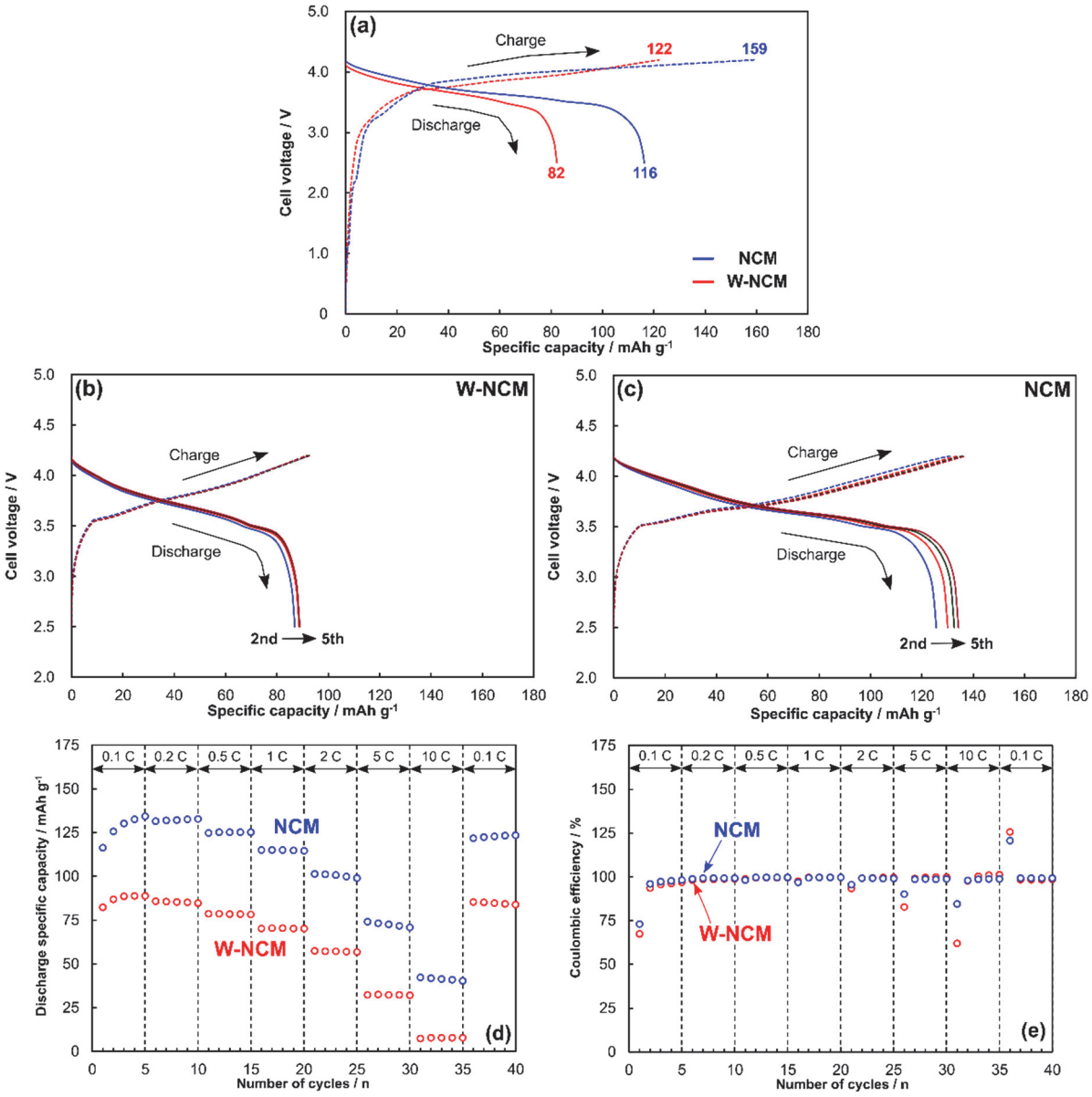

Figure 4. Rate performances of W-NCM and NCM cathode active materials in full-cells using graphite anodes. (a) Cell voltage-specific capacity profiles at the first cycle for W-NCM and NCM at a current density of 0.1 C (12.0 mA g^{-1} for W-NCM and 15.5 mA g^{-1} for NCM), (b) profiles from the 2nd to 5th cycle for W-NCM at 0.1 C, (c) those for NCM, (d) discharge specific capacities, and (e) Coulombic efficiencies of W-NCM and NCM at different C-rates.

resulted in the formation of SEI layers on the graphite anode surface [3]. The charge and discharge specific capacities of both the cathode active materials gradually increased from the 2nd to the 5th cycle, which was related to the stable formation of the SEI film [3]. The W-NCM exhibited a lower discharge specific capacity at all C-rates, and particularly at higher C-rates (>2 C). From the 2nd to the 5th cycle, both the CEs increased to a high value (>93%). However, the CE of W-NCM was lower than that of NCM. In the subsequent cycles, both the CEs were retained at ~100%. When the C-rate was subsequently lowered to 0.1 C (from the 36th to the 40th cycle), stable discharge specific capacities were observed for both W-NCM and NCM full-cells, which were 82 and 120 mAh g^{-1}, respectively. The use of a similar anode material and similar capacity ratio of the anode to cathode verified that W-NCM was inferior to NCM in terms of rate performance in a full-cell configuration, which agreed with the half-cell test results.

The cycling performances of W-NCM and NCM in a full-cell configuration with a graphite anode at 2 C are shown in Figure 5. The cell voltage-specific capacity profiles of W-NCM showed a minor change after 1000 charge-discharge cycles. With an increase in the number of cycles, the NCM exhibited steep cell voltage increases and decreases in the specific capacity. Both cathode active materials exhibited an insignificant increase in internal resistance, which could be observed at the beginning of the charge or discharge process (at ~0 mAh g^{-1}). An increase in the internal resistance may be associated with the growth of SEI films on the cathode and anode, electrolyte decomposition, and/or structural degradation of the active materials [17, 36]. Thus, the aging of NCM induced by charge–discharge cycling was attributed to the inactivation of Li ions in the cathode or anode. The discharge specific capacities of W-NCM and NCM during the cycling test indicated that W-NCM could nearly maintain its full specific capacity, whereas NCM exhibited a considerable decrease within ~400 cycles. The discharge specific capacity of W-NCM exceeds that of NCM at the ~160th cycle. The capacity retentions of W-NCM and NCM at the end of the cycling test were 91.2 and 33.7%, respectively, which were calculated based on the discharge specific capacities after the 5th and 1000th cycles. W-

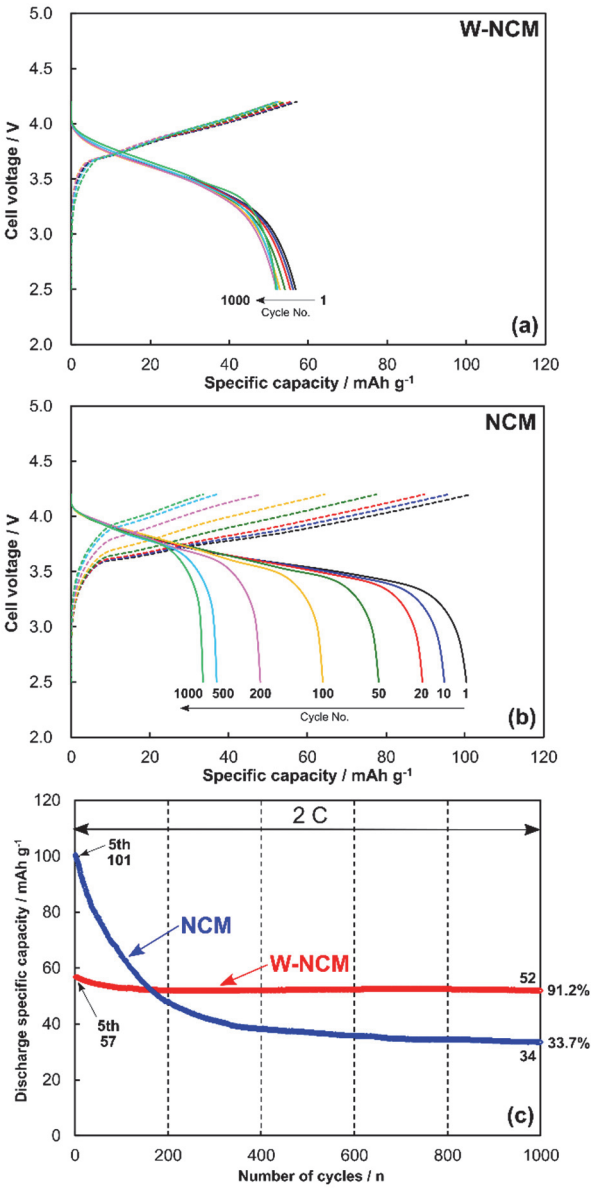

Figure 5. Cycling performances of W-NCM and NCM in full-cells using graphite anodes at a current density of 2 C. Cell voltage-specific capacity profiles for (a) W-NCM and (b) NCM at different numbers of cycles. (c) Discharge specific capacities of W-NCM and NCM throughout the cycling test.

NCM in the full-cell configuration was barely degraded by repeating the charge–discharge cycles at 2 C.

3. 3. 4 *Energy and Power Densities of Full-Cells*

Using the rate performance results of full-cells including W-NCM and NCM before and after the cycling tests, the relationship between the gravimetric energy and power densities of full-

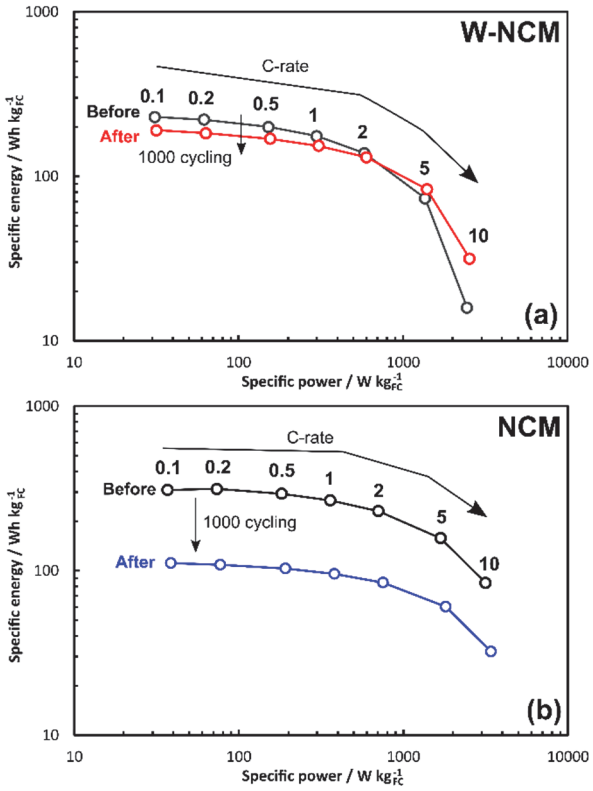

Figure 6. Ragone plots of full-cells using W-NCM and NCM cathodes, before and after the 1000 charge–discharge cycles. The specific energy and power were based on the total mass of the cathode and anode active materials. (a) W-NCM full-cell and (b) NCM full-cell.

cells was evaluated. Figure 6 shows Ragone plots of the full-cells based on the total mass of the cathode and anode active materials. Before the cycling test, the highest specific energies of the W-NCM and NCM full-cells were 229 and 308 Wh kg_{FC}^{-1}, respectively. Before the cycling test, the W-NCM full-cell maintained a specific energy of 200 Wh kg_{FC}^{-1} at a limited specific power of <150 W kg_{FC}^{-1}, whereas the NCM full-cell maintained that level of specific energy at a specific power of <1000 W kg_{FC}^{-1}. After being subjected to 1000 charge–discharge cycles at a current density of 2 C, the W-NCM full-cell exhibited a marginal decrease in the specific power at <500 W kg_{FC}^{-1}. The specific energy at a higher specific power (>1000 W kg_{FC}^{-1}) increased, and a specific energy of 32 Wh kg_{FC}^{-1} was attained even at a high specific power of ~2500 W kg_{FC}^{-1}, indicating that the rate performance of the W-NCM full-cell was nearly maintained after the charge–discharge cycling. The highest specific energy of the NCM full-cell subjected to 1000 cycles decreased to 111 Wh kg_{FC}^{-1}, and the specific energy decreased over the entire range

of specific power. These results suggest that the energy and power densities of the LIB full-cell using W-NCM as the cathode active material could be highly retained even when subjected to charge–discharge cycling.

3. 3. 5 *Electrochemical Performance of W-NCM Cathode Active Material*

The stable specific capacities of NCM ($LiNi_{0.5}Co_{0.2}Mn_{0.3}O_2$) in the half- and full-cells during Li-ion insertion were measured to be 155 and 120 mAh g^{-1}, respectively, which confirmed the performance evaluation validity of the ternary LTMO active materials. The W-NCM exhibited stable specific capacities of 120 and 82 mAh g^{-1} in the half- and full-cell configurations, respectively. The Li-ion insertion specific capacity of W-NCM in the half-cell was lower than that of fresh $LiNi_{1/3}Co_{1/3}Mn_{1/3}O_2$ (150−160 mAh g^{-1} in the potential range of 3.0−4.2 V vs. Li/Li^+), as previously confirmed [37–41]. The lower specific capacity of W-NCM is attributed to the presence of metallic and non-metallic impurities. The ICP-OES analysis indicated that W-NCM contained a total of 4.0 mass% Al, Cu, and Fe. To date, the behavior of metallic impurities in LTMO cathodes has been investigated. Krüger et al. reported the effect of Al impurities on the electrochemical performance of $LiNi_{1/3}Co_{1/3}Mn_{1/3}O_2$ in a half-cell configuration. At an Al content of 1.2 mass%, ~15 mAh g^{-1} decrease in the specific capacity of Li-ion insertion was observed in the potential range of 3.0–4.2 V vs. Li/Li^+ and current density of 1 C [42]. However, the specific capacity during the cycling test at 1 C was retained, independent of the presence of Al. Wang et al. also reported the role of Al in the electrochemical performance of $LiNi_{0.8}Co_{0.1}Mn_{0.1-x}Al_xO_2$ ($0 \leq x \leq 0.06$) in a half-cell configuration. A relatively low Al content of $x = 0.02$ (2 at%) had negligible effects on the Li-ion insertion specific capacity, rate capability, and cycling stability. An Al content of 4 and 6 at% decreased the Li-insertion specific capacity from 225 to 200 and 188 mAh g^{-1}, respectively, at 3.0–4.4 V vs. Li/Li^+ and 0.1 C. However, the addition 4.0 at% of Al enhanced both the rate and cycling performances [30]. Chen et al. investigated the specific capacity and cycling stability of $LiCoO_2$ with impurities of Al at 0–1.2 mass% or Cu at 0–3.0 mass% in a half-cell configuration operated at 3.0–4.3 V vs. Li/Li^+ and 0.1 C [43]. An Al content of 0.6 mass% marginally reduced the Li-ion

insertion specific capacity, while an Al content of 1.2 mass% considerably reduced it from 150 to 125 mAh g^{-1}. The addition of Cu at 0.03, 0.18, and 0.6 mass% exhibited an inverse effect on the specific capacity. A Cu content of 1.8 and 3.0 mass% decreased the specific capacity from 150 to 140 and 130 mAh g^{-1}, respectively. The specific capacity of the above $LiCoO_2$ including Al or Cu was sufficiently maintained during the cycling test at 0.1 C. Wu et al. also explored the role of $Li(Ni_{0.8}Co_{0.1}Mn_{0.1})_{1-x}Cu_xO_2$ ($0 \leq x \leq 0.02$) in a half-cell configuration operated at 2.8–4.3 V vs. Li/Li^+ and 0.1 C [31]. The addition of Cu at 1 and 2 at% increased the Li-ion insertion specific capacity from 190, to 226 and 214 mAh g^{-1}, respectively. The increased specific capacity was successfully retained during both the rate test at 0.1–5 C and cycling test at 1 C. The effect of Fe as an impurity on the electrochemical performance of $LiNi_{1/3}Co_{1/3}Mn_{1/3}O_2$ was investigated by Park et al. using a half-cell configuration operated at 3.0–4.3 V vs. Li/Li^+ and 0.1 C [32]. The addition of Fe to the 0.25 at% barely decreased the Li-ion insertion specific capacity, while the 1.0 at% Fe addition reduced it from 162 to 157 mAh g^{-1}. The rate capability at 0.1–10 C and cycling stability at 1 C were nearly retained with Fe impurities up to 1.0 at%. The content of Al, Cu, and Fe in W-NCM was 1.3, 1.7, and 1.0 mass%, respectively. Based on the above literature survey, the lowered specific capacity of W-NCM seems to be related to the presence of metallic impurities. When the above-mentioned LTMO cathodes accept a metallic impurity at low concentrations, no/minor degradation of the rate and cycling performance was observed. Thus, the reduced specific capacity for Li-ion insertion (120 mAh g^{-1} in a half-cell) and very high retention (91.2%) in the full-cell cycling test is attributed to the high-level of metallic impurities, such as Al, Cu, and Fe. However, the effect of the coexistence of Al, Cu, and Fe on the electrochemical performance of ternary LTMO cathodes is still unclear. The relationship between the content of each metal impurity in the recovered ternary LTMO cathode active materials and their electrochemical performance needs to be further evaluated.

The EDX results revealed that significant quantities of C (4.7 mass%) and F (3.4 mass%) were detected at the particle surface of W-NCM. In addition, ~4 mass% of Li was stoichiometrically

overloaded in the bulk of the W-NCM particles. During the pyrolysis process of the waste LIB stack, it was heated at 800 °C without exposure to air. The decomposition of the PVDF binder used to adhere $LiNi_{1/3}Co_{1/3}Mn_{1/3}O_2$ particles to the Al-foil current collector becomes active at >350 °C [44] and produces HF, which can reduce $LiNi_{1/3}Co_{1/3}Mn_{1/3}O_2$ and thus form LiF [45]. During stack pyrolysis, the residual $LiPF_6$ in the electrolyte can directly produce HF. Inside the sealed cell body, the reaction of the generated HF and direct reactions of PVDF and $LiPF_6$ with the cathode and anode can produce various metal fluorides and metal oxide fluorides. Residual F in these forms could not be filtered during the hydrometallurgical process, and hence, they remained in the W-NCM. Owing to the final sintering at 800 °C in air for the fabrication of W-NCM, the residual F can exist in the form of metal fluorides, metal oxide fluorides, and LiF. These products are resistant to the transportation of Li ions and barely contribute to the cycling of Li-ion uptake and release in the cathode. However, the protective effects of metal fluorides, such as AlF_3, formed on the surfaces of ternary LTMOs have been reported to enhance the cycling performance [46]. The contribution of the residual F to the electrochemical performance of W-NCM is not negligible. For the present cathode recovery system achieved by pyrolysis of a bare LIB stack under inert conditions, PVDF and $LiPF_6$–derived F can cause undesired side reactions at elevated temperatures. Further investigation of the residual mechanism of F in recovered LTMOs is of great importance.

The compositional analysis indicated that W-NCM contained excess Li in the form of Li_2CO_3. Li overloading was intended to compensate for the Li spent by the reduction of oxides of metallic impurities (Al_2O_3, CuO, and Fe_2O_3) during cyclic Li-ion extraction/insertion, with the formation of irreversible side products. Metallic oxides can react with Li ions to form metals and Li_2O, which is a reversible conversion reaction. Conversion reactions typically occur at 1.2–3.0 V vs. Li/Li^+ [47, 48]. However, the resultant Li_2O can react with $LiPF_6$ to form the irreversible byproduct of LiF [46], thereby reducing active Li ions. Therefore, W-NCM used in the cathode was operated at 3.0–4.2 V vs. Li/Li^+ in the half-cell, and >3.0 V vs. Li/Li^+ in the full-cell, referring to the potential-specific capacity profile of the used graphite, which was

reported in literature [3]. Thus, the Li-ion uptake and release capacities resulting from the conversion reactions of Al_2O_3, CuO, and Fe_2O_3 were minor. Therefore, the effect of residual Li_2CO_3 on the electrochemical performance of the ternary LTMOs should be considered. The excess Li_2CO_3 used in the synthesis of ternary LTMO has been revealed to be responsible for active CO, CO_2, and O_2 gas release at a potential >4.5 V vs. Li/Li^+, and these gas formations can be alleviated by cycles of aqueous washing and calcination [49]. In this study, the potential of W-NCM did not reach >4.5 V vs. Li/Li^+. Notably, the overloading of Li_2CO_3 onto renovated $LiCoO_2$ has been applied to achieve Li/Co = 1.0, 1.2, and 1.5 [43]. Similar specific capacities (150 mAh g^{-1}) and cycling performances were observed at Li/Co of 1.0 and 1.2. Li/Co of 1.5 resulted in a reduced specific capacity (140 mAh g^{-1}) and marginally degraded cycling performance. Based on the negative effects of excess Li_2CO_3, a lower content of Li_2CO_3 addition during the synthesis of W-NCM should have been selected. The specific capacity of W-NCM can be improved by adjusting the amount of Li_2CO_3 added during synthesis.

The SEM revealed that the aggregate (secondary) particles of the W-NCM ranged from 10 to 50 μm. The size distribution of primary and secondary particles of LTMO active materials can be tailored by varying the synthesis parameters, such as the aging time of hydroxide precipitation, calcination temperature, and time, which influences their electrochemical performance (specific capacity of Li-ion extraction/insertion, initial CE, rate capability, cycling stability, etc.) [41, 50–52]. The synthetic procedure for W-NCM will be optimized to reduce the aggregate particles to <~10 μm, thereby enhancing their electrochemical performance.

For the existing technology, the cathode components extracted from electrically neutralized and mechanically disassembled LIBs were heated to decompose the PVDF binder, and thus the cathode active material powder was stripped-off from the Al current collector [53]. The proposed recovery system can circumvent the existing complex and hazardous manual cell disassembly process and can be applied to the automatic fluidized bed refining process using the pyrolysis residue of LIB stacks which were entirely heated in an inert condition, and thereby

could be scrapped readily. Based on the acceptable specific capacity and excellent cycling performance of W-NCM in the presence of metallic impurities of Al, Cu, and Fe, as well as excessive Li and residual F, it is beneficial for the battery community to further explore the acceptability of certain levels of impurities in LIB cathode active materials from an economic, social, and environmental perspective.

3. 4 Summary

A ternary LTMO cathode active material was recovered from the residue of a waste automotive LIB stack pyrolyzed at 800 °C, without exposure to air. Its precursor was prepared via a sequential processes of cell pyrolysis, residue grinding, classification (sieving), wet magnetic separation, acid leaching, hydroxide precipitation, desalination, and drying. The W-NCM (a waste LIB-derived ternary LTMO) was synthesized by sintering the precursor that was stoichiometrically overloaded with Li_2CO_3 in air at 800 °C. The W-NCM has a composition of $LiNi_{1/3}Co_{1/3}Mn_{1/3}O_2$ with metallic impurities of Al, Cu, and Fe at a total of 4 mass%, as well as excess Li and residual F. The electrochemical performance of W-NCM was evaluated both in half- and full-cells, in comparison with a commercial LIB cathode active material NCM ($LiNi_{0.5}Co_{0.2}Mn_{0.3}O_2$) intended for automobile applications. A lower discharge specific capacity was observed for W-NCM during the performance evaluations, independent of the cell configuration. The W-NCM in the half-cell configuration exhibited a Li-ion extraction/insertion specific capacity of 120 mAh g^{-1} (70.4% of NCM). The specific capacity of W-NCM in a full-cell configuration was 85 mAh g^{-1} (69.1% of NCM). A much higher capacity retention (91.7%) was observed for W-NCM after 1000 charge–discharge cycles, while the capacity retention of NCM was 34.0%. Ragone plots for the W-NCM and NCM full-cell configurations before and after the cycling test indicated that the W-NCM full-cell configuration exhibited 200 Wh kg_{FC}^{-1} at a specific power of <150 W kg_{FC}^{-1}. After 1000 charge–discharge cycles, the W-NCM full-cell configuration exhibited a marginal decrease in the specific energy over the entire power density range investigated in this study.

It was revealed that W-NCM operated sufficiently as the cathode active material of the LIB full-cell regardless of the presence of certain metallic and non-metallic impurities. The content of Al, Cu, and Fe in W-NCM was determined to be 1.3, 1.7, and 1.0 mass%, respectively, using ICP-OES. The results of EDX analysis revealed a 3.4 mass% of F on the particle surface of W-NCM. Based on previous studies, the presence of impurities such as Al, Cu, and Fe in the form of oxides, F in the form of metal fluorides and metal oxide fluorides, and excessive Li_2CO_3 had a detrimental effect by reducing the Li-ion extraction/insertion specific capacity. The excellent cycling performance of W-NCM was presumably due to the coexistence of metallic impurities of Al, Cu, and Fe. In the proposed cathode recovery system via direct air-free pyrolysis of bare LIB stacks, the side reactions of PVDF and $LiPF_6$ in an enclosed cell may lead to F-contamination in the recycled cathode active material.

Although the developed methodology requires further improvements to reduce the impurities and optimize the loading level of Li, it is promising for large-scale and automatic recycling of waste LIBs, which will be enormously exhausted from BEVs and PHEVs. In the future, the effect of each metallic impurity (Al, Cu, or Fe) and their cooperative effect on the electrochemical performance (specific capacity, CE, rate capability, and cycling stability) of waste-LIB-derived ternary LTMO cathodes will be evaluated by optimizing the cathode particle morphology.

Reference

[1] J. Hu, S. Zhong, T. Yan, Using carbon black to facilitate fast charging in lithium-ion batteries, *J. Power Sources* 508 (2021) 230342.

[2] H. Park, N. Yoon, D. H. Kang, C. Young, J. K. Lee, Electrochemical characteristics and energy densities of lithium-ion batteries using mesoporous silicon and graphite as anodes, *Electrochim. Acta* 357 (2020) 136870.

[3] Y. Abe, S. Kumagai, Effect of negative/positive capacity ratio on the rate and cycling performance of $LiFePO_4$/graphite lithium-ion batteries, *J. Energy Storage* 19 (2018) 96–

102.

[4] I. H. Son, J. H. Park, S. Park, K. Park, S. Han, J. Shin, S. G. Doo, Y. Hwang, H. Chang, J. W. Choi, Graphene balls for lithium rechargeable batteries with fast charging and high volumetric energy densities, *Nat. Commun.* 8 (1) (2017) 1561.

[5] J. P. Pender, G. Jha, D. H. Youn, J. M. Ziegler, I. Andoni, E. J. Choi, A. Heller, B. S. Dunn, P. S. Weiss, R. M. Penner, C. B. Mullins, Electrode degradation in lithium-ion batteries, *ACS Nano* 14 (2) (2020) 1243–1295.

[6] R. Tang, Q. Yun, W. Lv, Y.-B. He, C. You, F. Su, L. Ke, B. Li, F. Kang, Q.-H. Yang, How a very trace amount of graphene additive works for constructing an efficient conductive network in $LiCoO_2$-based lithium-ion batteries, *Carbon* 103 (2016) 356–362.

[7] S. S. Zhang, K. Xu, T. R. Jow, Study of the charging process of a $LiCoO_2$-based Li-ion battery, *J. Power Sources* 160 (2) (2006) 1349–1354.

[8] M. Zhang, J. Shen, J. Li, D. Zhang, Y. Yan, Y. Huang, Z. Li, Effect of micron sized particle on the electrochemical properties of nickel-rich $LiNi_{0.8}Co_{0.1}Mn_{0.1}O_2$ cathode materials, *Ceram. Int.* 46 (4) (2020) 4643–4651.

[9] L. Cheng, B. Zhang, S.-L. Su, L. Ming, Y. Zhao, C.-H. Wang, X. Ou, Comparison of monocrystalline and secondary $LiNi_{0.5}Co_{0.2}Mn_{0.3}O_2$ cathode material for high-performance lithium-ion batteries, *J. Alloys Compd.* 845 (2020) 156202.

[10] L. Jiao, Z. Liu, Z. Sun, T. Wu, Y. Gao, H. Li, F. Li, L. Niu, An advanced lithium ion battery based on a high quality graphitic graphene anode and a $Li[Ni_{0.6}Co_{0.2}Mn_{0.2}]O_2$ cathode, *Electrochim. Acta* 259 (2018) 48–55.

[11] P.-E. Cabelguen, D. Peralta, M. Cugnet, P. Maillet, Impact of morphological changes of $LiNi_{1/3}Mn_{1/3}Co_{1/3}O_2$ on lithium-ion cathode performances, *J. Power Sources* 346 (2017) 13–23.

[12] X. Yang, Z. Zuo, H. Wang, Q. Chen, H. Zhang, Z. Huang, B. Wu, H. Zhou, The contradiction between the half-cell and full-battery evaluations on the tungsten-coating $LiNi_{0.5}Co_{0.2}Mn_{0.3}O_2$ cathode, *Electrochim. Acta* 180 (2015) 604–609.

[13] S. Liu, L. Xiong, C. He, Long cycle life lithium ion battery with lithium nickel cobalt

manganese oxide (NCM) cathode, *J. Power Sources* 261 (2014) 285–291.

[14] N. Loeffler, J. V. von Zamory, N. Laszczynski, I. Doberdo, G.-T. Kim, S. Passerini, Performance of $LiNi_{1/3}Mn_{1/3}Co_{1/3}O_2$/graphite batteries based on aqueous binder, *J. Power Sources* 248 (2014) 915–922.

[15] J. Ni, Y. Huang, L. Gao, A high-performance hard carbon for Li-ion batteries and supercapacitors application, *J. Power Sources* 223 (2013) 306–311.

[16] Y. Fujii, H. Miura, N. Suzuki, T. Shoji, N. Nakayama, Structural and electrochemical properties of $LiNi_{1/3}Co_{1/3}Mn_{1/3}O_2$: Calcination temperature dependence, *J. Power Sources* 171 (2) (2007) 894–903.

[17] Y. Abe, T. Saito, S. Kumagai, Effect of prelithiation process for hard carbon negative electrode on the rate and cycling behaviors of lithium-ion batteries, *Batteries* 4 (4) (2018) 71.

[18] S. Refly, O. Floweri, T. R. Mayangsari, A. H. Aimon, F. Iskandar, Green recycle processing of cathode active material from $LiNi_{1/3}Co_{1/3}Mn_{1/3}O_2$ (NCM111) battery waste through citric acid leaching and oxalate co-precipitation process, *Mater. Today Proc.* 44 (2021) 3378–3380.

[19] Y. Zhou, Z. Hu, Y. Huang, Y. Wu, Z. Hong, Effect of solution wash on the electrochemical performance of $LiNi_{0.8}Co_{0.1}Mn_{0.1}O_2$ cathode materials, *J. Alloys Compd.* 888 (2021) 161584.

[20] A. Islam, S. Roy, M. A. Khan, P. Mondal, S. H. Teo, Y. H. Taufiq-Yap, M. T. Ahmed, T. R. Choudhury, G. Abdulkreem-Alsultan, S. Khandaker, M. R. Awual, Improving valuable metal ions capturing from spent Li-ion batteries with novel materials and approaches, *J. Mol. Liq.* 338 (2021) 116703.

[21] S. E. Sloop, L. Crandon, M. Allen, M. M. Lerner, H. Zhang, W. Sirisaksoontorn, L. Gaines, J. Kim, M. Lee, Cathode healing methods for recycling of lithium-ion batteries, *Mater. Tech.* 22 (2019) e00113.

[22] L. Li, Y. Bian, X. Zhang, Y. Guan, E. Fan, F. Wu, R. Chen, Process for recycling mixed-cathode materials from spent lithium-ion batteries and kinetics of leaching, *Waste Manag.*

71 (2018) 362–371.

[23] L. Li, L. Zhai, X. Zhang, J. Lu, R. Chen, F. Wu, K. Amine, Recovery of valuable metals from spent lithium-ion batteries by ultrasonic-assisted leaching process, *J. Power Sources* 262 (2014) 380–385.

[24] P. Meshram, B. D. Pandey, T. R. Mankhand, Recovery of valuable metals from cathodic active material of spent lithium ion batteries: Leaching and kinetic aspects, *Waste Manag.* 45 (2015) 306–313.

[25] L. P. He, S. Y. Sun, X. F. Song, J. G. Yu, Recovery of cathode materials and Al from spent lithium-ion batteries by ultrasonic cleaning, *Waste Manag.* 46 (2015) 523–528.

[26] Y. Yang, G. Huang, S. Xu, Y. He, X. Liu, Thermal treatment process for the recovery of valuable metals from spent lithium-ion batteries, *Hydrometallurgy* 165 (2016) 390–396.

[27] H. Ku, Y. Jung, M. Jo, S. Park, S. Kim, D. Yang, K. Rhee, E. M. An, J. Sohn, K. Kwon, Recycling of spent lithium-ion battery cathode materials by ammoniacal leaching, *J. Hazard. Mater.* 313 (2016) 138–146.

[28] J. Wang, Z. Liang, Y. Zhao, J. Sheng, J. Ma, K. Jia, B. Li, G. Zhou, H.-M. Cheng, Direct conversion of degraded $LiCoO_2$ cathode materials into high-performance $LiCoO_2$: A closed-loop green recycling strategy for spent lithium-ion batteries, *Energy Storage Mater.* 45 (2022) 768–776.

[29] H. Bae, Y. Kim, Technologies of lithium recycling from waste lithium ion batteries: A review, *Mater. Adv.* 2 (10) (2021) 3234–3250.

[30] S. Wang, J. Zhu, Y. Li, G. Cao, Y. Chen, D. Zhang, Z. Tan, J. Yang, J. Zheng, H. Li, Role of Al on the electrochemical performances of quaternary nickel-rich cathode $LiNi_{0.8}Co_{0.1}Mn_{0.1-x}Al_xO_2$ ($0 < x < 0.06$) for lithium-ion batteries, *J. Electroanal. Chem.* 888 (2021) 115200.

[31] T. Wu, G. Wang, B. Liu, Q. Huang, Y. Su, F. Wu, R. M. Kelly, The role of Cu impurity on the structure and electrochemical performance of Ni-rich cathode material for lithium-ion batteries, *J. Power Sources* 494 (2021) 229774.

[32] S. Park, D. Kim, H. Ku, M. Jo, S. Kim, J. Song, J. Yu, K. Kwon, The effect of Fe as an

impurity element for sustainable resynthesis of $Li[Ni_{1/3}Co_{1/3}Mn_{1/3}]O_2$ cathode material from spent lithium-ion batteries, *Electrochim. Acta* 296 (2019) 814–822.

[33] J. Li, G. Wang, Z. Xu, Environmentally friendly oxygen-free roasting/wet magnetic separation technology for in situ recycling cobalt, lithium carbonate and graphite from spent $LiCoO_2$/graphite lithium batteries, *J. Hazard. Mater.* 302 (2016) 97–104.

[34] H. Yu, X. Dong, Y. Pang, Y. Wang, Y. Xia, High power lithium-ion battery based on spinel cathode and hard carbon anode, *Electrochim. Acta* 228 (2017) 251–258.

[35] J. W. Fergus, Recent developments in cathode materials for lithium ion batteries, *J. Power Sources* 195 (4) (2010) 939–954.

[36] Y. Abe, N. Hori, S. Kumagai, Electrochemical impedance spectroscopy on the performance degradation of $LiFePO_4$/graphite lithium-ion battery due to charge-discharge cycling under different C-rates, *Energies* 12 (23) (2019) 4507.

[37] Y. Wang, J. Jiang, J. R. Dahn, The reactivity of delithiated $Li(Ni_{1/3}Co_{1/3}Mn_{1/3})O_2$, $Li(Ni_{0.8}Co_{0.15}Al_{0.05})O_2$ or $LiCoO_2$ with non-aqueous electrolyte, *Electrochem. Commun.* 9 (10) (2007) 2534–2540.

[38] H.-J. Noh, S. Youn, C. S. Yoon, Y.-K. Sun, Comparison of the structural and electrochemical properties of layered $Li[Ni_xCo_yMn_z]O_2$ (x= 1/3, 0.5, 0.6, 0.7, 0.8 and 0.85) cathode material for lithium-ion batteries, *J. Power Sources* 233 (2013) 121–130.

[39] R. Jung, M. Metzger, F. Maglia, C. Stinner, H. A. Gasteiger, Oxygen release and its effect on the cycling stability of $LiNi_xMn_yCo_zO_2$ (NMC) cathode materials for Li-ion batteries, *J. Electrochem. Soc.* 164 (7) (2017) A1361–A1377.

[40] R. Jung, R. Morasch, P. Karayaylali, K. Phillips, F. Maglia, C. Stinner, Y. Shao-Horn, H. A. Gasteiger, Effect of ambient storage on the degradation of Ni-rich positive electrode materials (NCM811) for Li-ion batteries, *J. Electrochem. Soc.* 165 (2) (2018) A132–A141.

[41] D. Peralta, J. Salomon, J.-F. Colin, A. Boulineau, F. Fabre, C. Bourbon, B. Amestoy, E. Gutel, D. Bloch, S. Patoux, Submicronic $LiNi_{1/3}Mn_{1/3}Co_{1/3}O_2$ synthesized by co-precipitation for lithium ion batteries – Tailoring a classic process for enhanced energy and power density, *J. Power Sources* 396 (2018) 527–532.

[42] S. Krüger, C. Hanisch, A. Kwade, M. Winter, S. Nowak, Effect of impurities caused by a recycling process on the electrochemical performance of $Li[Ni_{0.33}Co_{0.33}Mn_{0.33}]O_2$, *J. Electroanal. Chem.* 726 (2014) 91–96.

[43] S. Chen, T. He, Y. Lu, Y. Su, J. Tian, N. Li, G. Chen, L. Bao, F. Wu, Renovation of $LiCoO_2$ with outstanding cycling stability by thermal treatment with Li_2CO_3 from spent Li-ion batteries, *J. Energy Storage* 8 (2016) 262–273.

[44] C. Hanisch, T. Loellhoeffel, J. Diekmann, K. J. Markley, W. Haselrieder, A. Kwade, Recycling of lithium-ion batteries: A novel method to separate coating and foil of electrodes, *J. Clean. Prod.* 108 (2015) 301–311.

[45] D. Song, X. Wang, E. Zhou, P. Hou, F. Guo, L. Zhang, Recovery and heat treatment of the $Li(Ni_{1/3}Co_{1/3}Mn_{1/3})O_2$ cathode scrap material for lithium ion battery, *J. Power Sources* 232 (2013) 348–352.

[46] A. Butt, G. Ali, K. T. Kubra, R. Sharif, A. Salman, M. Bashir, S. Jamil, Recent advances in enhanced performance of Ni-rich cathode materials for Li-ion batteries: A review, *Energy Technol.* (2022) 2100775.

[47] Y. Sun, H.-W. Lee, Z. W. Seh, N. Liu, J. Sun, Y. Li, Y. Cui, High-capacity battery cathode prelithiation to offset initial lithium loss, *Nat. Energy* 1 (1) (2016) 15008.

[48] M. Trukawka, K. Wenelska, L. Singer, R. Klingeler, X. Chen, E. Mijowska, Hollow carbon spheres loaded with uniform dispersion of copper oxide nanoparticles for anode in lithium-ion batteries, *J. Alloys Compd.* 853 (2021) 156700.

[49] S. E. Renfrew, B. D. McCloskey, Residual lithium carbonate predominantly accounts for first cycle CO_2 and CO outgassing of Li-stoichiometric and Li-rich layered transition-metal oxides, *J. Am. Chem. Soc.* 139 (49) (2017) 17853–17860.

[50] E. Antolini, $LiCoO_2$: Formation, structure, lithium and oxygen nonstoichiometry, electrochemical behavior and transport properties, *Solid State Ionics* 170 (3–4) (2004) 159–171.

[51] A. C. Wagner, N. Bohn, H. Geßwein, M. Neumann, M. Osenberg, A. Hilger, I. Manke, V. Schmidt, J. R. Binder, Hierarchical structuring of NMC111-cathode materials in lithium-

ion batteries: An in-depth study on the influence of primary and secondary particle sizes on electrochemical performance, *ACS Appl. Energy Mater.* 3 (12) (2020) 12565–12574.

[52] P. Teichert, G. G. Eshetu, H. Jahnke, E. Figgemeier, Degradation and aging routes of Ni-rich cathode based Li-ion batteries, *Batteries* 6 (1) (2020) 8.

[53] X. Meng, J. Hao, H. Cao, X. Lin, P. Ning, X. Zheng, J. Chang, X. Zhang, B. Wang, Z. Sun, Recycling of $LiNi_{1/3}Co_{1/3}Mn_{1/3}O_2$ cathode materials from spent lithium-ion batteries using mechanochemical activation and solid-state sintering, *Waste Manag.* 84 (2019) 54–63.

Chapter 4

Effects of Excessive Prelithiation on Full-Cell Performance of LIBs with a Hard-Carbon/Nanosized-Si Composite Anode

4. 1 Introduction

LIBs with high energy and/or power densities are desired for a wide variety of applications, such as portable electronic devices, electric vehicles, and grid storage systems [1–3]. Generally, electric-powered devices require optimal LIB systems with a specified voltage and electrical capacity; these are constructed using parallel/serial-connected LIB cells. Increasing the energy and power densities of each LIB cell allows these LIB systems to achieve miniaturization, weight and cost reduction, as well as economical consumption of battery materials. Graphite—a popular anode-active material—is primarily used in LIB anodes owing to its low working potential (~0 V vs. Li/Li^+), relatively high lithiation capacity (~350 mAh g^{-1}), and low cost [4–6]. Moreover, composite anodes comprising multiple anode-active materials are frequently used as LIB anodes. Simply mixing two types of active materials is a promising approach for achieving enhanced performance in terms of parameters such as capacity, current rate dependence, and cycle life [7–21]. Composite anodes are typically fabricated using graphite, other carbon materials such as HC, carbon black, graphene, and carbon nanotubes, as well as Si or Si oxides at specific mass ratios. Kierzek and Machnikowski discussed the practical aspects of Si/graphite composite anodes in a full-cell configuration [12]. Ge et al. synthesized composite anodes using two types of carbon materials (HC and graphite) and highlighted the importance of the HC loading on the composite anodes [13]. Hu et al. examined the effects of prelithiating a polyacrylic acid (PAA) binder on the operation of a Si/graphite composite anode in full cells [15]. Kim et al. fabricated graphite/Si composite anodes and evaluated their performance in half- and full-cell configurations [18]. In their study, graphite was used as the main active material for the composite anodes at considerably high mass ratios (>65 mass%). This indicates that composite anodes continue to be dependent on graphite.

HC, which is an alternative anode-active material to graphite, is an amorphous carbon with a disordered structure containing randomly arranged single graphene sheets [22]. The structure of HC facilitates its high lithiation capacity and buffer effect during lithiation and delithiation [23, 24]. Although HC has a few drawbacks (high irreversible capacity, low CE, and low tap density), its use can assist in alleviating the mechanical stress in the anode, thereby enabling a longer cycle life and improved power capability suited for power-type LIBs. Si has also garnered significant attention as a substitute anode-active material for graphite. Each Si atom electrochemically alloys with 4.4 Li atoms to form $Li_{4.4}Si$, which exhibits a remarkably high specific capacity at full Li-alloying (4200 mAh g^{-1}) [25, 26]. However, the Si particles cause a volume expansion of approximately 400 vol.% during lithiation, leading to cracks on the surface of the electrode or in its interior and the pulverization of Si, thereby degrading the anode performance [14, 17]. Furthermore, the electrical conductivity of Si is not as high as that of carbon materials. In recent studies, N-Si particles have been found to exhibit superior anode performance compared to that of conventional Si-based anodes, in addition to having less mechanical stress without critical performance degradation [5, 7, 9, 27–29]. Particle size reduction is effective for overcoming the aforementioned disadvantages of Si-based anodes. Attempts can also be made to increase the electrical conductivity by adding carbon materials, such as HC and carbon black, and exploiting the buffer effect to mitigate the volume expansion/contraction during lithiation and delithiation.

Composite anodes containing C, Si, and/or Si oxides are typically paired with a LTMO cathode in full-cell configurations. To achieve charge–discharge stability and safety, longer cycle life, and to prevent Li deposition on the anode, the capacity design for the anode and cathode must be performed in a balanced manner, which depends on their respective active materials [30–33]. The capacities of the cathode and anode are determined by the specific capacity and loading of the active material coated on the current collector. In general, the specific capacity of cathodes such as ternary LTMOs is limited to ~200 mAh g^{-1}. However, the theoretical specific capacity of pure Si is 4200 mAh g^{-1}, which is 21 times higher than that of the cathode. The anode/cathode

capacity ratio is tuned to be greater than 1.0 (anode-capacity-rich design) to prevent Li-dendrite formation on the anode surface [34, 35]. However, adjusting this capacity ratio is difficult for Si-based full-cell LIBs owing to the significant difference in the capacity between their cathode and anode. To overcome these problems, anodes with unique shapes such as ultrathin films and those with a considerably low loading have been fabricated using special processing techniques. However, these electrode fabrication processes are fairly complex and time- and cost-intensive. Thus, the Si-based composite anode with a low Si mass ratio is a realistic option for electrode fabrication and capacity design for LIB full cells. Additionally, a mixture of Si and carbon materials could improve the electrical conductivity, lithiation capacity, power capability, and cycle life and alleviate the mechanical stress.

Si- or HC-based anodes exhibit high irreversible capacities and low CEs in the initial cycle; the high irreversible capacities are due to electrolyte decomposition on the anode side, Li traps in the macro-/nanopores in the HC, and passivation of Si during Li alloying [22, 36]. The prelithiation of anodes is known to be essential for reducing the irreversible capacity and enhancing CE [24, 37–39]. Prelithiation is achieved using various mechanical or electrochemical methods [18, 28, 40], such as through (i) the direct contact of the anode with Li metal in the electrolyte, (ii) the addition of stabilized Li metal powder during the anode fabrication, and (iii) the electrochemical Li doping of the anode in a half-cell configuration (anode/Li cell). Among these methods, electrochemical Li doping can accurately control the amount of the Li dopant. Doping Li ions into the anode and assembling a full cell can lead to an excess of Li in the cell, which can unfortunately influence the operation and safety of the full-cell and degrade its performance. Accurately controlled prelithiation can help prevent Li-dendrite formation on the anode surface, permit safe full-cell operation, and suppress the performance degradation of LIB full-cells. Moreover, adding HC that exhibits a decent buffer effect to the anode can establish good electrical contact with the anode and enhance its robustness. Although the effects of the performance of prelithiated sole HC anodes have been extensively examined to date, the performance of prelithiated Si/HC composite anodes has

hardly been examined. Furthermore, the impact of the amount of Li compensated through prelithiation on the HC/Si composite anode performance in a full-cell configuration is unknown.

Therefore, composite anodes were fabricated in this study by simply mixing N-Si and HC. The HC/N-Si mass ratio was varied (9:1 and 8:2) during the anode fabrication. The performance of the prepared anodes was evaluated by conducting galvanostatic measurements to evaluate lithiation and delithiation at a low current density as well as the current rate dependence. Instead of the HC- and graphite-only anodes, a promising composite anode was selected, prelithiated, and then incorporated into full-cells with an NCM523 cathode. The composite anodes were prelithiated in a decomposable test cell with a Li metal foil; the cell was operated in constant-current mode until the predefined cutoff anodic specific capacities (200, 300, 400, 500, and 600 mAh g^{-1}) were achieved. Subsequently, the effects of the prelithiation on the HC/N-Si composite anode performance in full-cells were investigated and comprehensively analyzed.

4. 2 Experimental

4. 2. 1 *Electrode Fabrication*

All the active materials were used without further treatment. Three types of anode-active materials were purchased: N-Si (<100 nm, verified by transmission electron microscopy; 633097-10G, Sigma-Aldrich Co., LLC, St. Louis, MO, USA), graphite (CGB-10, spherical natural graphite, Nippon Graphite Co., Ltd., Otsu, Japan), and HC (LBV-1001, Sumitomo Bakelite Co., Ltd., Tokyo, Japan). Anode slurries were prepared by mixing one or two active materials (graphite, HC, HC/N-Si), a conductive agent, and a binder at a mass ratio of 80:10:10 in distilled water. The HC/N-Si mass ratios of 9:1 and 8:2 were investigated for the composite anode fabrication; these samples are denoted as HC9/N-Si1 and HC8/N-Si2, respectively. Acetylene black (Denka Co., Ltd., Tokyo, Japan) and a PAA binder were used as the conductive agent and binder, respectively. The prepared slurry was coated onto a 20 μm thick Cu foil current collector (Hohsen Corp., Osaka, Japan) and dried in an oven at 100 °C for >6 h. The dried anode sheet was cut into ϕ15 mm circles, and the circular electrodes were dried at 140 °C

for >3 h in a vacuum. The physical properties and performance of these anodes were then characterized. A cathode was fabricated in a manner similar to that for anode fabrication. NCM523 (NCM-523-ME5E12D, Beijing Easpring Material Technology Co., Ltd., Beijing, China) was used as the cathode-active material. The conductive agent used for the cathode was similar to that of the anode. PVDF (KF Polymer F #9130, Kureha Corp., Tokyo, Japan) and N-methyl-2-pyrrolidone (Tokyo Chemical Industry Co., Ltd., Tokyo, Japan) were used as the cathode binder and dispersing solvent, respectively. A 20 μm thick Al foil current collector (Hohsen Corp., Osaka, Japan) was used for fabricating the cathode. The cathode specification was the same as that of our previous work, and the NCM523 cathode had an initial CE of 86.3% [41].

4. 2. 2 *Physical Characterization*

The anode-active material was physically characterized in a powder form using a laser-diffraction particle-size-measurement system (SALD-200V; Shimadzu Corp., Kyoto, Japan) and surface-area-measuring instrument (Autosorb-3B, Quantachrome Instruments Inc., Boynton Beach, Florida, USA); the particle size distribution was estimated using the former by measuring the particles in distilled water containing a surface-acting agent, whereas the Brunauer–Emmett–Teller (BET) specific surface areas were determined using the latter by acquiring nitrogen adsorption–desorption isotherms at −196 °C and using the BET theory. SEM (VE-8800, Keyence Corp., Osaka, Japan) was performed to investigate the morphology of the particles on the active materials and the coating layer on the anodes at an acceleration voltage of 20 kV. Additionally, EDX was conducted using an INCA Energy 250 system (Oxford Instruments, Abingdon, Oxon, UK) mounted on the SEM body. The distributions of the C, O, and Si elements on the coating layer were surveyed by the EDX analysis of the anode cross-section as well as by detecting similar elements as the particle on the active materials.

4. 2. 3 *Electrochemical Measurements*

A CR2032-type coin cell was assembled with the prepared anode, 0.2 mm thick Li metal foil

(*ϕ*15 mm; Honjo Metal Co., Ltd., Osaka, Japan), propylene separator (*ϕ*18 mm, Celgard 2500; Celgard LLC, Charlotte, NC, USA), and organic electrolyte (1 M $LiPF_6$ in a 1:1 (*v*/*v*) mixture of ethylene carbonate and diethyl carbonate, Kishida Chemical Co., Ltd., Osaka, Japan). The cell was assembled in an argon-filled glove box at a dew point less than −80 °C. The active material loadings for the graphite and HC anodes were ~2.3 and ~2.3 mg cm^{-2}, respectively. The graphite and HC anodes exhibited electrode densities of 0.63 and 0.34 g cm^{-3}, respectively. In terms of specification of the composite anodes, the active material loading and electrode density were ~2.3 mg cm^{-2} and ~0.33 g cm^{-3}, respectively. The galvanostatic measurements of the assembled cells were performed using a battery charge–discharge system (HJ1020mSD8; Hokuto Denko Ltd., Co., Tokyo, Japan). The operating potential range was set to 0–2.5 V vs. Li/Li^+ for all the galvanostatic measurement in the half-cell configuration. First, Li-ion insertion–extraction was performed at a low current density of 20 mA g_A^{-1}, which corresponds to 0.1 C; the g_A unit represents the mass of the anode-active material used. Then, the current density was increased from 0.1 C to 0.2, 0.5, 1, 2, 5, and 10 C. Each C-rate experiment was repeated five times. In all the galvanostatic measurements, the current density is expressed as the C-rate. For example, 1 C indicates a current at which the cell capacity is perfectly discharged in 1 h. The applied current density was determined based on the specific capacity of the active materials (200 and 350 mAh g_A^{-1} for HC and graphite, respectively); that for the composite anode was assumed to be 250 mA g_A^{-1}.

4. 2. 4 *Design, Assembly, and Performance Evaluation of Full Cell*

The prepared NCM523 material was used as the cathode in full-cells. The HC8/N-Si2 composite anode, which exhibited superior performance in the aforementioned galvanostatic tests, was used on the counter electrode. Prior to full-cell assembly, the anode was prelithiated using a battery charge–discharge system and a decomposable test cell with a Li metal foil, a separator, and an organic electrolyte; these constituent materials are similar to those of the CR2032-type coin cell. After the prelithiation, the test cell was disassembled in a glove box, and the anode was carefully extracted. Then, the anode was retrofitted to a CR2032-type coin

cell, which was subsequently sealed using a swaging machine. Finally, aging treatment (preservation in atmosphere at 70 °C for ~3 h) was applied to the prepared cells. The cell comprised the NCM523 cathode, the HC8/N-Si2 composite anode, a propylene separator, and an organic electrolyte. The separator and electrolyte were similar to those used in the prelithiation system.

The galvanostatic charge–discharge tests were performed on the assembled full-cells. The full-cells were operated in the voltage range of 2.5–4.2 V. First, the rate performance of the full-cell was evaluated by increasing the C-rate from 0.1 to 10 C, with 1 C corresponding to 150 mA g^{-1}, which was based on the cathode specific capacity of NCM523 (150 mAh g_C^{-1}); the g_C unit represents the mass of the cathode-active material. Each C-rate experiment was repeated five times. Then, the full-cell was subjected to 200 charge–discharge cycles at 2 C to investigate the cycling stability and capacity retention during high-rate cycling. In the rate performance tests, the charge–discharge characteristics of the first cycle were targeted to evaluate the first CE, initial charge–discharge operation, and stability. The specific energy (E) and specific power (P) were calculated as follows using the third-cycle data at each C-rate in the rate performance tests:

$$E = \frac{Q_D \times V_D}{m_{C+A}} [\text{Wh kg}_{C+A}^{-1}], \quad (4.1)$$

$$P = \frac{I_D \times V_D}{m_{C+A}} [\text{W kg}_{C+A}^{-1}], \quad (4.2)$$

where Q_D is the discharge capacity, V_D is the average discharge voltage, m_{C+A} is the total mass of the cathode- and anode-active materials, and I_D is the discharge current. All the electrochemical measurements were carried out at 25 °C.

4. 3 Results and Discussion

4. 3. 1 *Half-Cell Evaluation*

Figure 1 shows the anode performance of the half-cell configuration. A graphite anode was used for comparison. The lithiation and delithiation specific capacities were clearly enhanced at the higher N-Si mass ratio. In the first cycle, the delithiation-specific capacity was lower than that of lithiation. This was due to electrolyte decomposition at the anode–electrolyte interface, where active Li ions were consumed by the electrolyte to form a stable and passive film, which is often called a SEI film. The CE in the first cycle determines the degree of consumption of active Li ions inside the cell. The graphite anode had a high CE of 84.5%, as well as a plateaued, low-potential curve. However, the HC, which exhibited a slope-like potential curve, showed a low CE of 68.9%. Moreover, blending the HC and N-Si improved the CE compared to that of sole HC, yielding values of 74.6% for HC9/N-Si1 and 73.3% for HC8/N-Si2. As the anodes were composed of HC and N-Si, the shapes of the potential curves of the blended active materials did not show significant changes compared with that of the HC.

By achieving first-cycle lithiation and delithiation after cell assembly, the anode was activated to store full Li ions in the active material. In the third cycle, all the anodes exhibited a stable specific capacity, with sole graphite and HC showing values of 311 and 188 mAh g_A^{-1}, respectively, during the delithiation. The combination of HC and N-Si in the anode enhanced the specific capacity; in particular, HC8/N-Si2 exhibited the maximum delithiation-specific capacity among the anodes (531 mAh g_A^{-1}). As the C-rate was increased from 0.1 to 10 C (Figure 1d), the blended active materials exhibited higher specific capacities. Even at 2 and 5 C, their delithiation-specific capacities were higher than those of the sole active materials. The maximum specific capacity of HC9/N-Si1 was similar to that of graphite at <0.5 C but increased thereafter. A comparison between graphite and HC9/N-Si1 suggests that the current rate dependence of the former was inferior to that of the latter [6, 9, 16].

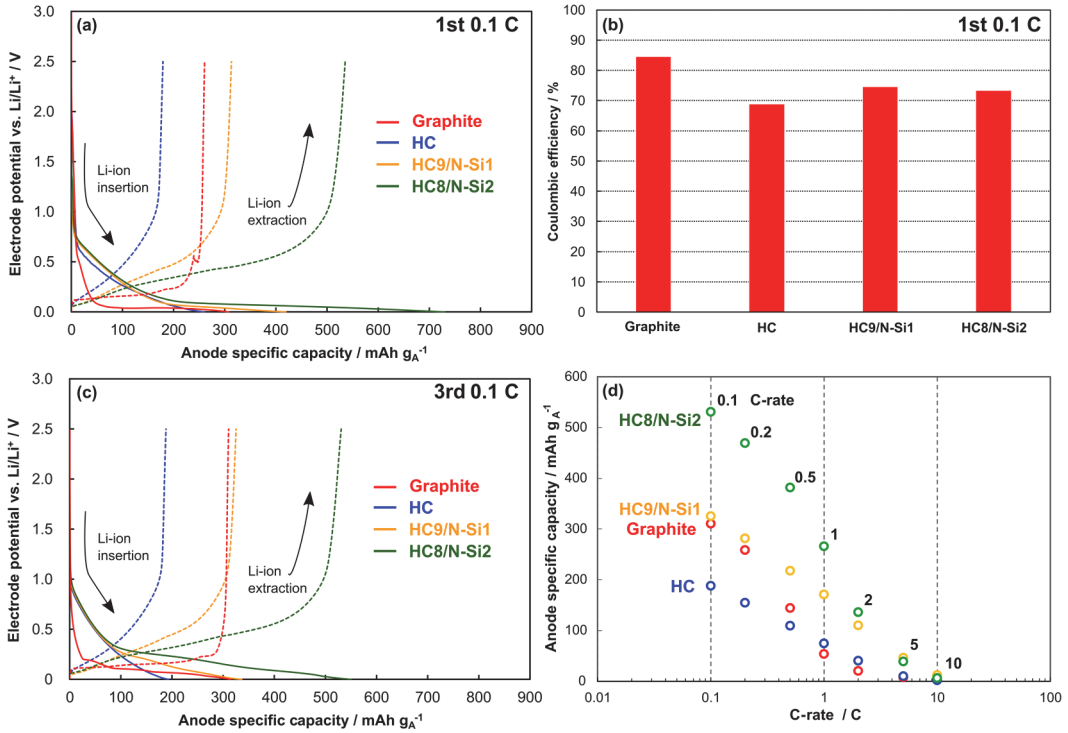

Figure 1. Performance of anode-active materials in the half-cell configuration. (a, c) Electrode potential as a function of anode specific capacity at 0.1 C in the (a) first and (c) third cycles. (b) Coulombic efficiencies (CEs) in the first cycle. (d) Rate performance at 0.1–10 C. The data of the third cycle for each C-rate are shown.

4. 3. 2 *Physical Characterization of Materials and Electrodes*

The physical properties of the active materials used to fabricate the anodes are summarized in Table 1. Graphite and HC had micron-sized particles (10–16 μm) and lower BET-specific surface areas (<8.2 m^2 g^{-1}) than that of N-Si (35.2 m^2 g^{-1}). However, the evaluation of the particle size of N-Si by laser-diffraction particle size measurement using a wet method was difficult because the nanosized particles readily agglomerated in the solution. The measured value (1.1 μm) corresponded to the agglomerated N-Si particles; therefore, the true particle size was determined to be 0.1 μm using specification-related data [42].

Table 1. Physical properties of the active materials used for anode fabrication.

	Graphite	HC	N-Si
D_m* (μm)	16	10	0.1 [42]
S_{BET}** (m^2 g^{-1})	8.0	8.2	35.2

* Medium diameter, ** BET specific surface area

The morphology, particle size, and elemental distributions for HC and N-Si particles were analyzed using SEM and EDX elemental maps (Figure 2a). Although the N-Si was agglomerated with several particles, the particle size was determined to be ~0.1 μm with spherical shape. The particle size of HC was ~10-μm with angulated outlines. The elemental mappings of C or Si, and O revealed the elemental distribution at the particle surface. In addition to the main component of C or Si, a small amount of O was observed in the particles; other elements were not detected in the EDX elemental maps. The HC8/N-Si2 composite anode, which showed optimal anode performance among the investigated anodes, was analyzed by SEM and EDX (Figure 2b–f). HC particles as large as 10 μm were observed on the anode surface. A sponge-like substance containing the conductive agent and PAA binder was firmly attached to the HC particles. Moreover, a few voids were observed in the anode (red dotted lines in Figure 2b), implying the creation of a void structure inside the coating layer of the anode. In the cross-sectional analysis (Figures 2d–f), the distributions of C, O, and Si were surveyed along the depth direction. Interestingly, C and Si mapping revealed that N-Si occupied the space between the large HC particles. O was detected in the anode because of the oxidation of the HC and/or N-Si particles.

4. 3. 3 *Specific Capacity of HC8/N-Si2 Anode*

Figure 3 shows the acquired delithiation curves for the HC and HC8/N-Si2 anodes as well as the specific capacity assignment of the HC and N-Si components of HC8/N-Si2. A half-cell evaluation at 0.1 C in the third cycle yielded an effective specific capacity of 531 mAh g_A^{-1} for the composite, with the HC-only anode showing a lower value of 188 mAh g_A^{-1}. The HC accounted for approximately 80 mass% of the active material in HC8/N-Si2. Therefore, HC contributed 80% of 188 mAh g_A^{-1} as the partial specific capacity to the blended active material, with the rest being supplied by N-Si (381 mAh g_A^{-1}). The apparent specific capacity of N-Si at full Li alloying was calculated to be 1905 mAh g_A^{-1}, which is approximately half the theoretical

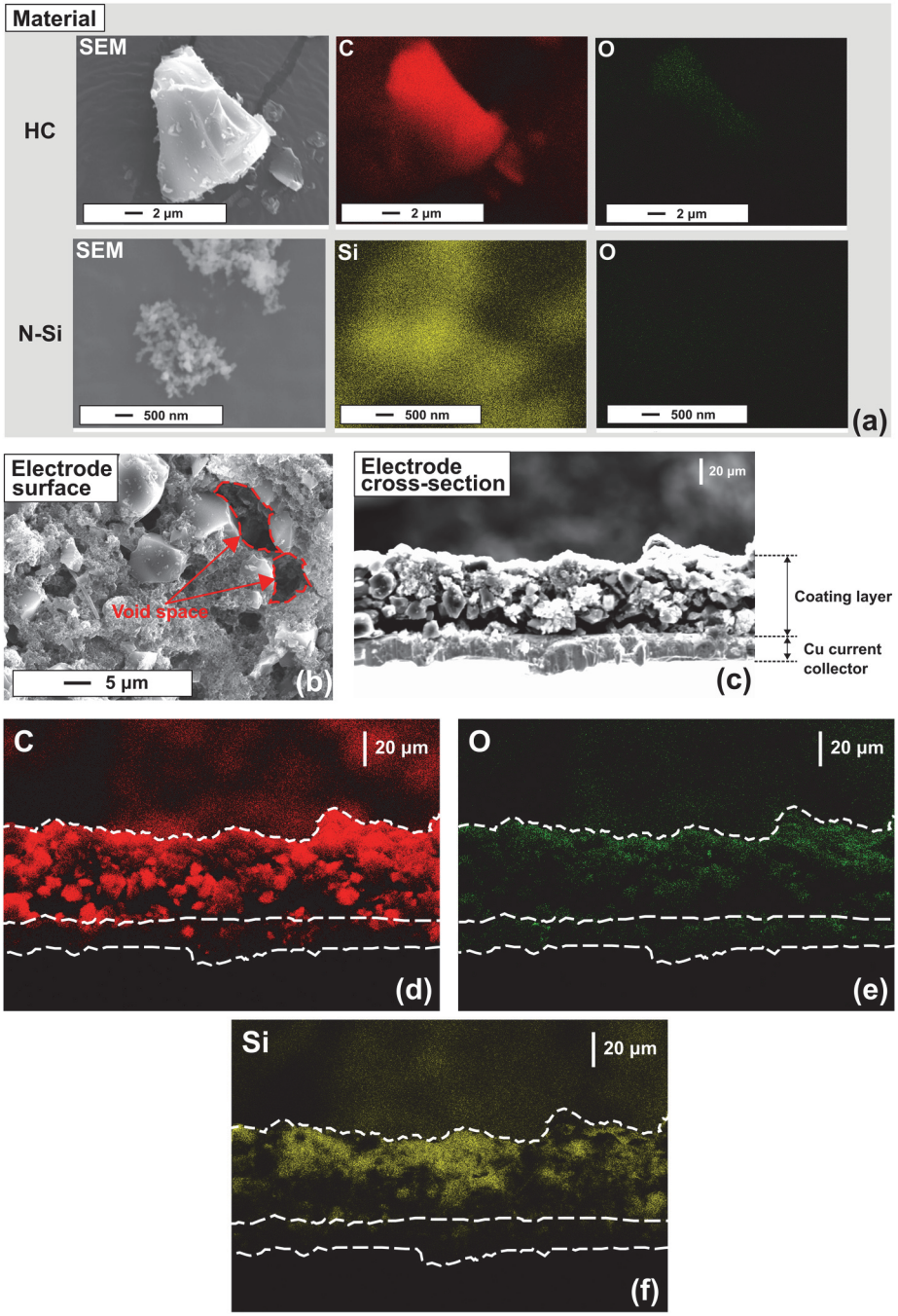

Figure 2. (a) SEM image and elemental mappings of HC and N-Si. SEM images of the (b) surface and (c) cross-section of the HC8/N-Si2 composite anode, and elemental maps of (d) C, (e) O, and (f) Si in the anode cross-section.

specific capacity of pure Si (4200 mAh g_A^{-1}). This was presumably related to the degree of oxidation and morphology of Si, as well as electrode design aspects, such as the component ratio of active and inactive materials and types of conductive agent and binder materials [28, 43, 44]. Therefore, the HC8/N-Si2 anode was estimated to have a specific capacity of 530 mAh

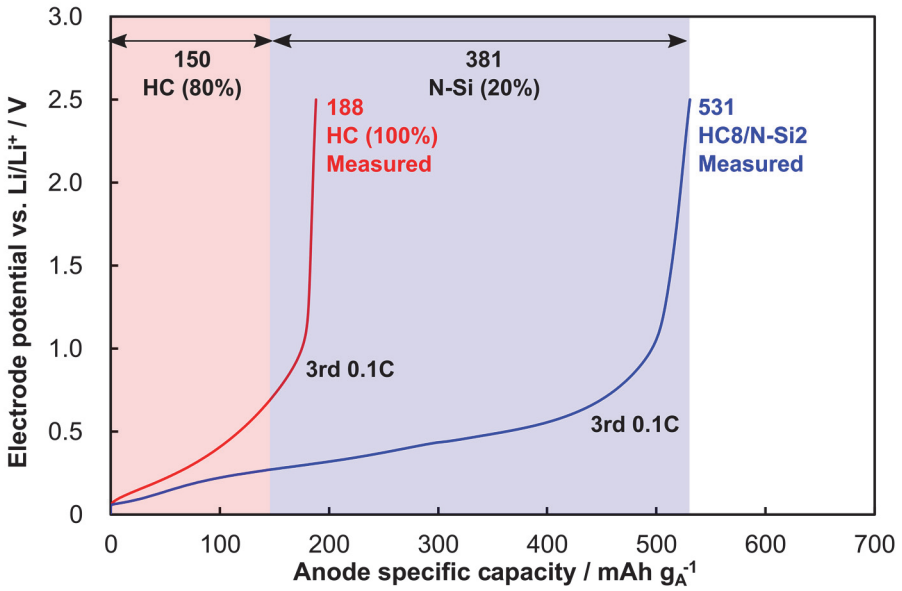

Figure 3. Delithiation curves for the HC and HC8/N-Si2 anodes, and the specific capacity assignment of HC and N-Si to that of the HC8/N-Si2 composite.

g_A^{-1}.

4. 3. 4 *Anode Prelithiation and Full-Cell Assembly*

Figure 4 shows a schematic of the prelithiation process and the corresponding results obtained using the HC8/N-Si2 composite anode in a full-cell configuration. Prelithiation was realized by operating a decomposable test cell with a Li metal foil and the HC8/N-Si2 anode (prelithiation cell) electrochemically doped with certain Li ions. Subsequently, the anode was incorporated into a full-cell with an NCM523 cathode (Figure 4a). The prelithiation capacity was controlled by setting a cutoff anodic specific capacity (200, 300, 400, 500, or 600 mAh g_A^{-1}). The prelithiation rate (R_L) was calculated as follows:

$$R_L = \frac{C_L}{C_A} \tag{4.3}$$

where C_L is the measured prelithiation capacity, and C_A is the anode capacity calculated using

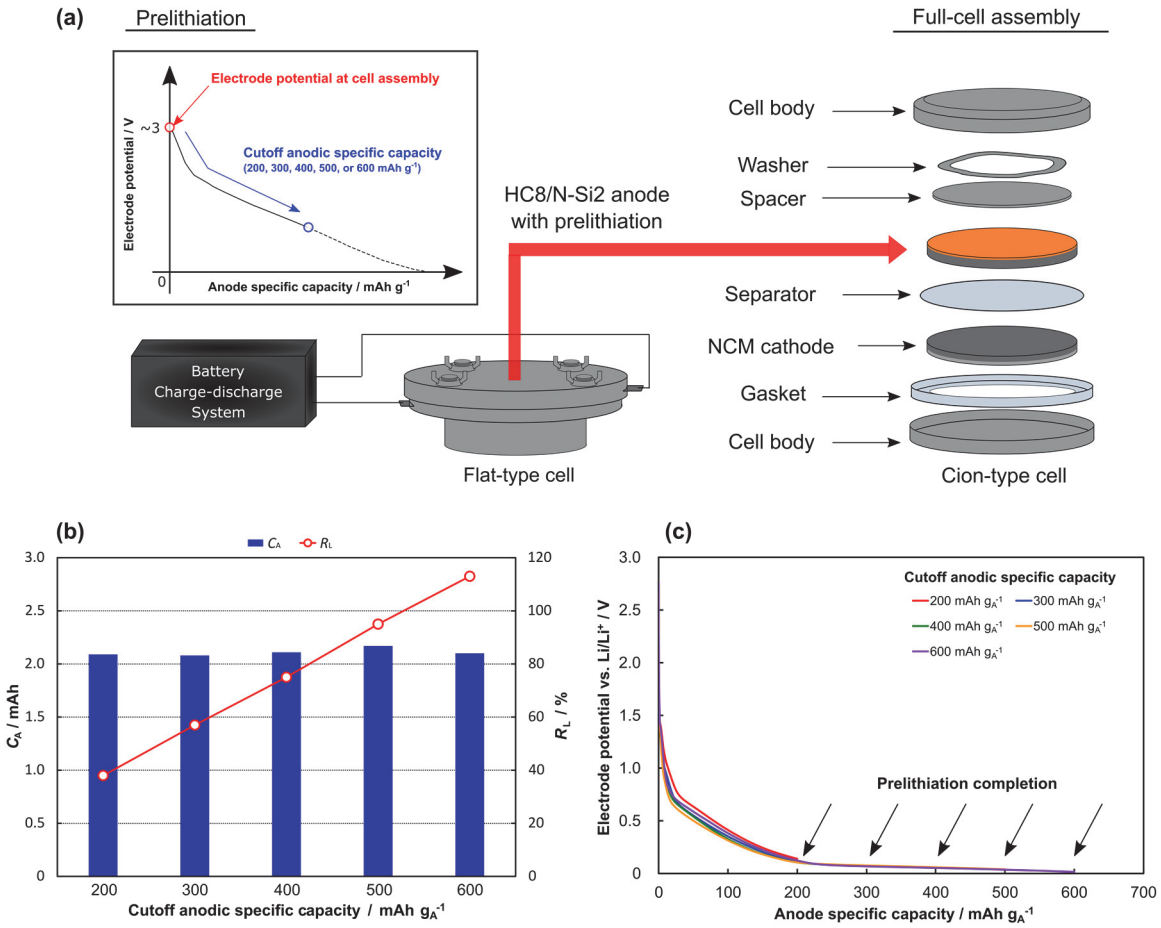

Figure 4. Prelithiation of the HC8/N-Si2 composite anode used in a full-cell configuration. (a) Illustrations of the prelithiation strategy and full-cell assembly. (b) Anode capacity (C_A) and prelithiation rate (R_L) corresponding to various cutoff anodic specific capacities. (c) Electrode potential as a function of anode specific capacity during the prelithiation at different cutoff anodic specific capacities.

the estimated specific capacity (530 mAh g_A^{-1}) and mass of the anode-active material. All the prelithiation cells showed similar C_A values of ~2.0 mAh. R_L increased proportionally with increasing cutoff anodic specific capacity from 200 to 500 mAh g_A^{-1}, and showed the highest value (113%) at a cutoff anodic specific capacity of 600 mAh g_A^{-1}. At the electrode level, the prelithiation process corresponding to 113% R_L allowed an excess of Li ions into the HC8/N-Si2 composite anode.

The open-circuit voltage (electrode potential vs. Li/Li^+) was measured to be ~3 V for all the prelithiated cells using a digital tester immediately after cell assembly. During the prelithiation process, the voltage decreased until the cutoff anodic specific capacity was achieved. Similar

potential profiles were exhibited by all the prelithiated cells; however, the electrode potential at completion of the prelithiation was different. A reductive reaction associated with SEI formation is known to occur between 0.4 and 1.0 V vs. Li/Li^+ for C, Si, and their composites [19, 39, 45–48]. During prelithiation, the electrode potential decreased to 0.14, 0.07, 0.06, 0.04, and 0.02 V vs. Li/Li^+ for the prelithiated cells with cutoff anodic specific capacities of 200, 300, 400, 500, and 600 mAh g_A^{-1}, respectively. These electrode potential at the end of prelithiation indicate that SEI film formation was almost complete on the anode. Immediately after the SEI film formation, the HC and N-Si likely stored residual Li ions that hardly reacted during the film formation. The HC, which exhibited a slope-like potential below 1.5 V vs. Li/Li^+ during Li-ion intercalation and de-intercalation, stored Li ions at the interlayer of randomly arranged graphene sheets (high-potential region) and in micro-/nanopores (low-potential region) [22, 49]. The alloying reaction of Si typically occurs at <0.3 V, and the potential is higher than that of Li-ion intercalation in graphite [44, 46, 47]. Thus, the unconsumed Li ions were mainly stored in the interlayer of the graphene sheets in the HC and Si particles. Furthermore, the different cutoff anodic specific capacities used for the prelithiation provided the HC with a varying number of Li ions to store in its graphene sheets.

Table 2 lists the design parameters for full-cells constructed using an NCM523 cathode and an HC8/N-Si2 composite anode with or without prelithiation (NCM523|HC8/N-Si2 cells). In these experiments, the HC8/N-Si2 composite anode was paired with an NCM523 cathode with an anode/cathode capacity ratio ($R_{A/C}$) of ~2.0. The cathode capacity (C_C) and C_A values were calculated using the mass and specific capacity of the active materials (150 mAh g_C^{-1} for NCM523 and 530 mAh g_A^{-1} for HC8/N-Si2). The active material loadings for the cathode (L_C) and anode (L_A) were 3.9–4.0 and 2.2–2.3 mg cm^{-2}, respectively. The thicknesses of the cathode (t_C) and anode (t_A) without the current collector were 38–60 and 70–88 μm, respectively. R_L and C_L increased with an increase in the cutoff anodic specific capacity from 200 to 600 mAh

Table 2. Design parameters for NCM|HC8/N-Si2 cells.

Cell parameter	NCM523|HC8/N-Si2 cell					
	RL0	RL38	RL57	RL75	RL95	RL113
C_C [mAh]	1.03	1.05	1.03	1.04	1.04	1.04
C_A [mAh]	2.13	2.09	2.08	2.11	2.17	2.10
$R_{A/C}$	2.07	1.99	2.02	2.03	2.09	2.02
L_C [mg cm^{-2}]	3.90	3.95	3.90	3.90	3.91	3.92
L_A [mg cm^{-2}]	2.27	2.24	2.22	2.25	2.32	2.25
t_C [μm]	40	38	41	40	38	60
t_A [μm]	75	70	70	72	72	88
C_{Li} [mAh]	-	0.79	1.18	1.59	2.05	2.38
R_L	0	0.38	0.57	0.75	0.95	1.13
*Max*_C_{Li} [mAh]	2.91	2.11	1.71	1.34	0.96	0.54

g_A^{-1}. The NCM523|HC8/N-Si2 cells are denoted as RL*x*, where *x* represents the prelithiation rate (R_L).

In order to evaluate the prelithiation and its effect on the HC8/N-Si2 anode, the margin capacity of the anode before the first lithiation (*Max*_C_{Li}) was calculated based on following equation:

$$Max\_C_{Li} = \frac{C_A}{CE_{HC8/N-Si2}} - C_{Li}[\text{mAh}], \tag{4.4}$$

where $CE_{HC8/N-Si2}$ is the CE (73.3%) of HC8/N-Si2 anode at the first cycle in the half-cell configuration. Until R_L exceeded 0.95, the prelithiated cells had a margin of *Max*_C_{Li} to C_C, and their anodes were not overcharged beyond the *Max*_C_{Li}. The *Max*_C_{Li} of RL95 slightly exceeded the C_C, whereas RL113 showed a C_C, which was approximately two-fold more than *Max*_C_{Li}. In these anodes, the overcharge was considered during the first charge.

4. 3. 5 *Full-Cell Evaluation*

Figure 5 shows the full-cell performance of the NCM523|HC8/N-Si2 cells with different R_L values. In the first cycle, the cell voltage of RL0 increased sharply until a specific capacity of 38 mAh g_C^{-1} and then smoothly reached the cutoff charge voltage of 4.2 V. However, RL113 showed flat-type cell voltage behavior between 3.6 and 4.2 V, except for the initially precipitous

drop at 1 mAh g_C^{-1}. The other prelithiated cells exhibited similar specific capacity–cell voltage profiles during the first cycle. A spike-like variation was observed at 7 and 1 mAh g_C^{-1} in the profiles of the RL0 and RL113 cells, respectively, which indicates the pristine Li-ion release behavior of ternary LTMOs [50, 51]. However, the electrolyte decomposition associated with SEI film formation (reduction reaction) occurred at the anode during the first charging. The electrolyte decomposition during the first charging process occurred simultaneously at both electrodes in RL0; in particular, the electrolyte decomposition reaction at the anode–electrolyte interface was more active, that is, by floating the anode potential and lowering the cell voltage. This behavior was hardly observed in RL113 because the electrolyte decomposition on the anode side was achieved through prelithiation.

At the beginning of the first charge, a decrease in the cell voltage followed by a precipitous drop was observed for the NCM523|HC8/N-Si2 cells with lower cutoff anodic specific capacity. These voltage variations implied insufficient SEI film formation through prelithiation when the cutoff anodic specific capacity was less than 300 mAh g_A^{-1}. The SEI film is generally formed at 0.4–1.0 V vs. Li/Li^+ on the anode potential, as mentioned in the previous prelithiation section. The anode potential operates around the reaction potential of SEI film formation, thereby lowering the cell voltage, which was similar to the cell voltage behavior of RL0. Conversely, higher cutoff anodic specific capacity during prelithiation provided the NCM523|HC8/N-Si2 cells with higher operating cell voltage. The RL113 had a higher operating cell voltage than that of RL38 (the difference in the voltage was ~0.1 V). During the subsequent discharge (Figure 5d), all the prelithiated cells operated with average voltage of 3.5–3.6 V. Li plating on the anode surface in full-cells commonly corresponds to charge or discharge voltage profiles [33, 35]. An appropriate and undisturbed charge–discharge profile was observed for each prelithiated cell. Thus, prelithiation with low to high cutoff anodic specific capacity is not likely

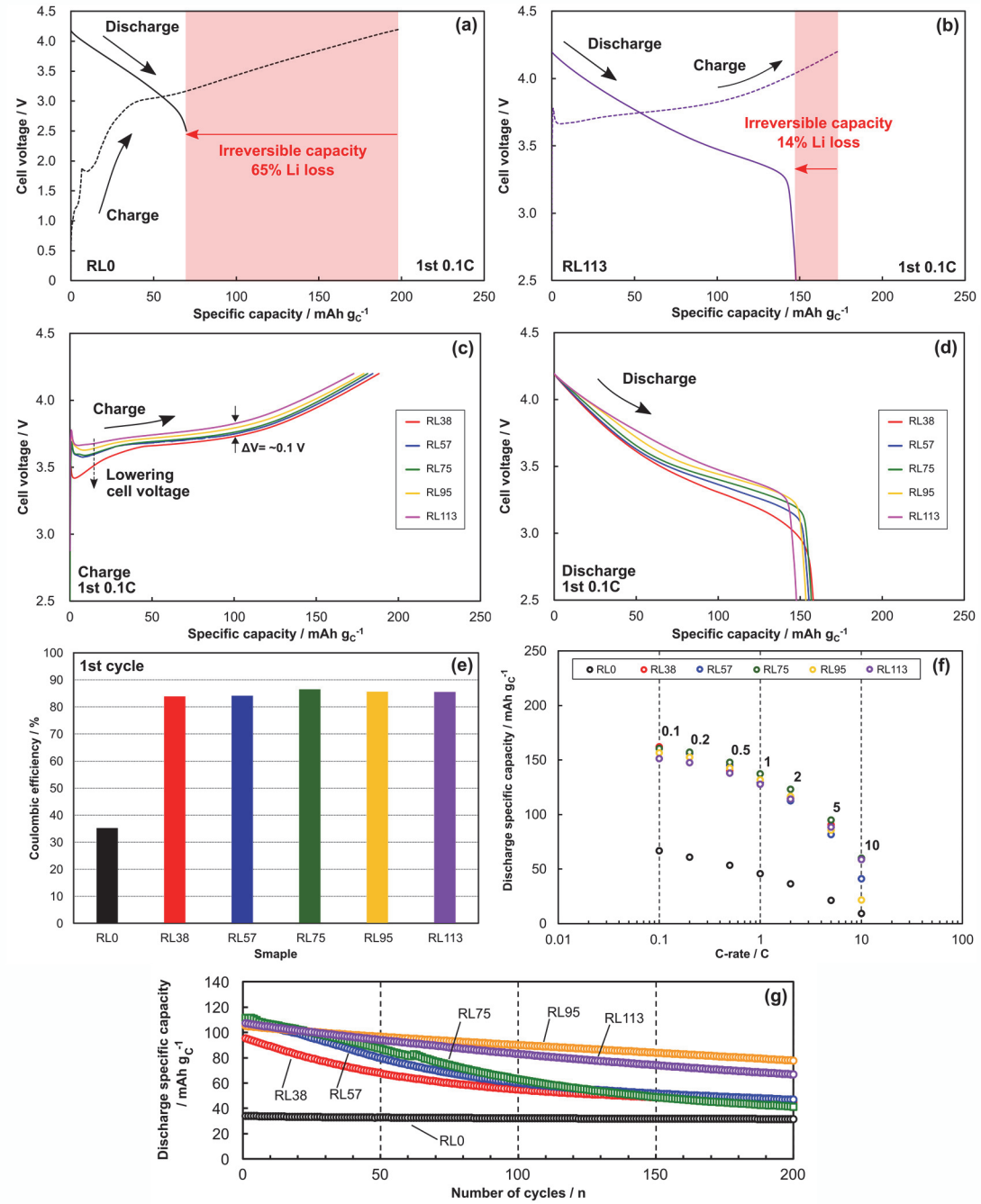

Figure 5. Full-cell performance of the NCM523|HC8/N-Si2 cells with different R_L values. (a, b) first-cycle cell voltage curves of (a) RL0 and (b) RL113, (c, d) a comparison of first-cycle profile for (c) charge and (d) discharge, and (e) the corresponding CEs. (f) rate and (g) cycling performance of the NCM523|HC8/N-Si2 cells.

to result in Li plating on the anodes. The prelithiated NCM523|HC8/N-Si2 cells showed higher CEs (>83%) in the first cycle than that of the cell without prelithiation (RL0; 35.2%; Figure 5e). Therefore, prelithiation helped alleviate the Li loss on the HC8/N-Si2 anode, regardless of the

cutoff anodic specific capacity during prelithiation.

A similar rate performance was observed for the prelithiated NCM523|HC8/N-Si2 cells in the C-rate range of 0.1–10 C (Figure 5f). The discharge-related specific capacity at <5 C was comparable with that of the prelithiated cells. At 10 C, all the cells showed different discharge-related specific capacities; that of RL95 was the lowest among the delithiated cells. This can be attributed to the severe operating condition under 10 C charge–discharge cycling for the NCM523|NC8/N-Si2 cells. The cycling performance tests revealed that RL95 and RL113 exhibited superior performance for 200 cycles at 2 C. The capacity retentions of the prelithiated NCM523|HC8/N-Si2 cells were 47.1%, 42.1%, 37.0%, 74.0%, and 62.3% for RL38, RL57, RL75, RL95, and RL113, respectively. Despite the high discharge-related specific capacity observed during the initial cycle, the charge–discharge cycling at 2 C damaged the prelithiated cells with <0.75 R_L over 200 cycles. These prelithiated cells showed low capacity retention. However, the capacity retention dramatically improved for R_L greater than or equal to 0.95. The excessive pre-lithiation of the HC8/N-Si2 anode, which increased the number of Li ions inside the cell, assisted in enhancing the cycling performance of the NCM523|HC8/N-Si2 cell. RL0 displayed a negligible rate and cycling performance owing to the significant consumption of active Li ions caused by the SEI film formation on the anode.

Figure 6 shows Ragone plots of the prelithiation-free cell (RL0) and the NCM523|HC8/N-Si2 cell with optimal full-cell performance. The representative specific energy and specific power data of previously reported cells were used for comparison [24, 48, 49, 52–54]. Essentially, the prelithiation of the HC8/N-Si2 anode enabled the NCM523|HC8/N-Si2 cell to exhibit higher specific energy over a wide power range (35–3081 W kg_{C+A}^{-1}). High specific energies of 121 and 348 Wh kg_{C+A}^{-1} were exhibited at 3081 and 35 W kg_{C+A}^{-1}, respectively. The NCM523|HC8/N-Si2 cell showed a superior energy release capability until <1619 W kg_{C+A}^{-1}, compared with that of the previously reported cells with a single active material in the anode.

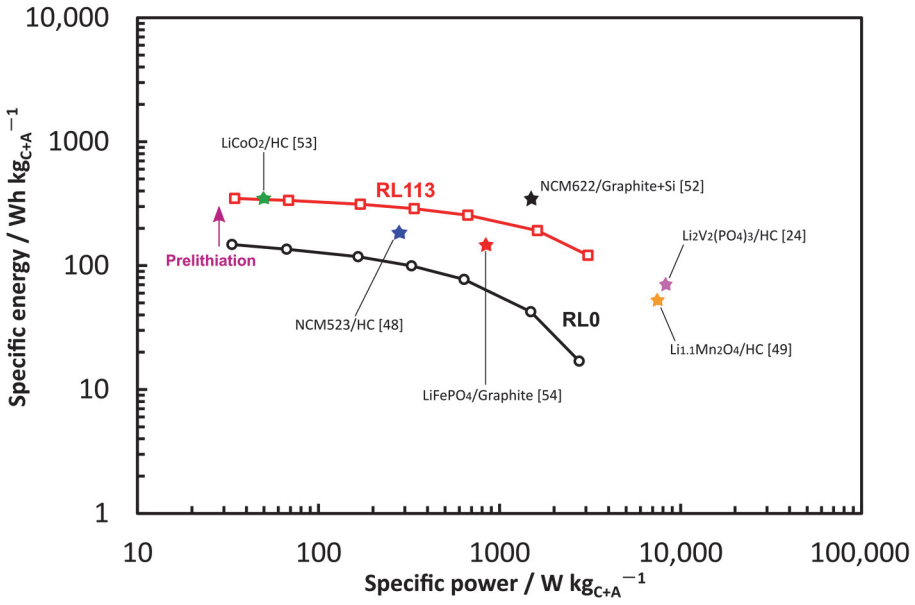

Figure 6. Ragone plots of the NCM523|HC/N-Si cell with optimal full-cell performance and the prelithiation-free cell.

Considering the decrease in specific energy corresponding to specific powers of 35 to 3081 W kg_{C+A}^{-1}, acceptable specific energies can be expected in the ultrahigh-power region (~10,000 W kg_{C+A}^{-1}). Consequently, the power capability can be further improved by replacing graphite with HC8/N-Si2 and subjecting the anode to excessive prelithiation. In future studies, I will attempt to develop an LIB with ultrahigh-power capability by pairing the excessively prelithiated HC8/N-Si2 anode and a high-rate cathode based on $LiNi_{0.5}Mn_{1.5}O_4$, carbon-coated $LiFePO_4$ or other surface-modified metal oxides.

4. 3. 6 *Effects of Blend Ratio and Excessive Prelithiation on Performance of HC/N-Si Composite*

The HC/N-Si composite anodes exhibited higher specific capacities at the higher N-Si mass ratio. The N-Si mass of ~20% yielded the HC8/N-Si2 composite anode that exhibited a maximum specific capacity of 531 mAh g_A^{-1} at 0.1 C. In the estimation of the specific capacity of the composite anode, the specific capacities of HC and N-Si were determined to 150 and 381 mAh g_A^{-1}, respectively. The addition of a small amount of N-Si enhanced the specific capacity of the anode. The rate performance was improved compared with that of graphite. HC, which

has a disordered structure with several single graphene sheets, can rapidly and easily access and store Li ions. Owing to the Li-alloying mechanism, N-Si stored numerous Li ions in the Si particles, thereby offering a dramatically high specific capacity and severe volume expansion during the lithiation, as well as low electrical conductivity. The low electrical conductivity and poor electrical contact were improved by adding HC and acetylene black [25, 26]. Therefore, the electrochemical properties of HC and N-Si and their lithiation mechanism helped boost the performance of the HC/N-Si composite anodes.

SEM observations and EDX elemental mapping revealed the electrode structure and elemental distribution of the HC8/N-Si2 composite anode. The composite anode was constructed using two main active materials—0.1 μm-sized N-Si and 10 μm-sized HC—and other inactive materials (acetylene black and PAA binder). The large HC particles were dispersed in the coating layer and surrounded by the nanosized materials (N-Si and acetylene black) and the binder. Both the active materials were firmly joined through acetylene black and binder, as revealed by SEM analysis. Additionally, certain N-Si particles were densely packed in the air space created by the HC particles. During lithiation, the airspace helped alleviate the mechanical stress caused by the volume expansion of N-Si. Moreover, the buffer effects derived from HC and acetylene black during lithiation mitigated the severe volume expansion of N-Si. Therefore, the use of two types of anode-active materials with different particle sizes and the introduction of a combination of two carbon materials facilitated the creation of an electrode structure with less mechanical stress and decent electrochemical properties.

Anode activation with the formation of the SEI film was preliminarily completed by conducting prelithiation prior to full-cell assembly. Following the incorporation of the prelithiated HC8/N-Si2 composite anode into the full cell, the NCM523|HC8/N-Si2 cells operated favorably in the first cycle, as they exhibited higher CEs than the prelithiation-free NCM523|HC8/N-Si2 cell (RL0). The Li ions injected via prelithiation reacted with the electrolyte at the anode–electrolyte interface and negated the irreversible capacity drop that occurred during the first charging

process. However, residual Li ions likely existed on the anode side; therefore, the full cell had excess Li ions in either the cathode or anode. Furthermore, the prelithiated cells exhibited a difference in Max_C_{Li} before the first charging process. At the start of the first charging process, Li ions were already present in the anode, and the primary Li ions were transferred from the cathode. In this storage state, the anode probably operated at a high utilization rate for Li-ion storage. The utilization rate of the anode depended on the cutoff anodic specific capacity during prelithiation; the higher the cutoff anodic specific capacity, the higher the utilization rate of the anode. At R_L higher than 0.95, the anodes of RL95 and RL 113 were overcharged and could not be confirmed to cause Li plating at the anode. In HC8/N-Si2 anode, HC and N-Si exhibited the durability of Li plating owing to their physical property and electrochemical performance. The former was indicative of the disorder of single graphene sheets, and the Li storage sites such as micro-/nanopores and void spaces between the graphene sheets. Li plating hardly occurred during charging at such storage sites. The latter could be explained using the Li alloying mechanism, where the Si is alloyed with certain Li ions at high operating potentials versus Li/Li^+ (~0.2 V vs. Li/Li^+) during the charging. The operating potential did not result in Li plating. Therefore, all prelithiated cells could favorably operate at the beginning of the first charge–discharge cycle without Li plating.

The RL95 and RL113 exhibited excellent capacity retention in the cycling performance tests conducted for 200 cycles at 2 C. Their capacity retention was dramatically improved compared with that of the other cells. This was due to the alleviation of the volume expansion of N-Si, followed by anode operation limited by the high utilization rate. Song et al. reported that the electrical conductivity of alloyed Si was higher than that of bare Si [29]. The alloyed Si helped realize the high utilization rate of the composite anode. Thus, the HC/N-Si composite anode is recommended for operation with a high utilization rate for Li storage. Moreover, the electrochemical properties of HC assisted in retaining the specific capacity during the charge–discharge cycling. Additionally, the Li storage in the interlayer of the graphene sheets and micropores in the randomly arranged sheets inhibited the volume expansion of N-Si in the

anode. While the cycling performance improved, the rate performance was independent of the anode utilization rates, which were varied using different cutoff anodic specific capacities during prelithiation. Compared with the prelithiation-free cell (RL0), the discharge-related specific capacity was boosted with the application of prelithiation, regardless of the cutoff anodic specific capacity. Preliathion enhanced the specific capacity of the NCM523|HC8/N-Si2 cells, and the Li ions injected via prelithiation rarely affected their rate performances. Thus, prelithiation affected only the cycling performance of the NCM523|HC8N-Si2 cells.

4. 4 Summary

Blended active materials were prepared by mixing HC and N-Si during anode fabrication. In the half-cell evaluation, excellent rate performance and enhanced specific capacity (531 mAh g_A^{-1}) were obtained for the anode prepared at an HC/N-Si mass ratio of 8:2. The electrode structure, which comprised 10 μm sized HC and 0.1 μm sized N-Si, provided buffer space during Li-ion uptake and release. Prior to full-cell assembly, anode activation with SEI film formation was achieved by conducting prelithiation in an HC8/N-Si2|Li half-cell intended for prelithiation. During prelithiation, the lithiation capacity was controlled by setting the cutoff anodic specific capacity (200–600 mAh g_A^{-1}). The prelithiated NCM523|HC8/N-Si2 cells operated effectively in the first cycle, during which the CE was boosted to >83%. In contrast, the NCM523|HC8/N-Si2 cell without prelithiation did not work favorably in the galvanostatic charge–discharge tests. The cycling performance of the NCM523|HC8/N-Si2 cells was affected by the anode utilization rate, which was dominated by the prelithiation process conducted at different cutoff anodic specific capacities. The excessive prelithiation of the anode ($R_L > 0.95$) and the consequently achieved higher anode utilization rates assisted in realizing a high capacity retention (>62.3%) for 200 cycles at 2 C. The rate performance was independent of the anode utilization rate. The prelithiated NCM523|HC8/N-Si2 cell with an R_L value of 1.13 showed optimal energy-release capability over a wide power range (35–3081 W kg_{C+A}^{-1}), compared with that of previously reported cells. Therefore, the excessively prelithiated NCM523|HC8/N-Si2 cell is anticipated to expedite the development of high-power LIB cells with graphite-

replacement materials.

Reference

[1] Y. Miao, P. Hynan, A. von Jouanne, A. Yokochi, Current Li-ion battery technologies in electric vehicles and opportunities for advancements. *Energies* 12 (2019) 1074.

[2] H. Li, Practical evaluation of Li-ion batteries. *Joule* 3 (2019) 908–919.

[3] B.D. McCloskey, Expanding the Ragone plot: Pushing the limits of energy storage. *J. Phys. Chem. Lett.* 6 (2015) 3592–3593.

[4] E. Buiel, J.R. Dahn, Li-insertion in hard carbon anode materials for Li-ion batteries. *Electrochim. Acta* 45 (1999) 121–130.

[5] H. Shobukawa, J. Alvarado, Y. Yang, Y. S. Meng, Electrochemical performance and interfacial investigation on Si composite anode for lithium ion batteries in full cell. *J. Power Sources* 359 (2017) 173–181.

[6] J.-H. Kim, M.-J. Jung, M.-J. Kim, Y.-S. Lee, Electrochemical performances of lithium and sodium ion batteries based on carbon materials. *J. Ind. Eng. Chem.* 61 (2018) 368–380.

[7] V. G. Khomenko, V. Z. Barsukov, Characterization of silicon- and carbon-based composite anodes for lithium-ion batteries. *Electrochim. Acta* 52 (2007) 2829–2840.

[8] J. W. Fergus, Recent developments in cathode materials for lithium ion batteries. *J. Power Sources* 195 (2010) 939–954.

[9] M. L. Terranova, S. Orlanducci, E. Tamburri, V. Guglielmotti, M. Rossi, Si/C hybrid nanostructures for Li-ion anodes: An overview. *J. Power Sources* 246 (2014) 167–177.

[10] K. Eom, T. Joshi, A. Bordes, I. Do, T. F. Fuller, The design of a Li-ion full cell battery using a nano silicon and nano multi-layer graphene composite anode. *J. Power Sources* 249 (2014) 118–124.

[11] N. Kobayashi, Y. Inden, M. Endo, Silicon/soft-carbon nanohybrid material with low expansion for high capacity and long cycle life lithium-ion battery. *J. Power Sources* 326 (2016) 235–241.

[12] K. Kierzek, J. Machnikowski, Factors influencing cycle-life of full Li-ion cell built from

Si/C composite as anode and conventional cathodic material. *Electrochim. Acta* 192 (2016) 475–481.

[13] C. Ge, Z. Fan, J. Zhang, Y. Qiao, J. Wang, L. Lingd, Novel hard carbon/graphite composites synthesized by a facile in situ anchoring method as high-performance anodes for lithium-ion batteries. *RSC Adv.* 8 (2018) 34682–34689.

[14] K. Yao, R. Liang, J. P. Zheng, Freestanding flexible Si nanoparticles–multiwalled carbon nanotubes composite anodes for Li-ion batteries and their prelithiation by stabilized Li metal powder. *J. Electrochem. Energy Convers. Storage* 13 (2016) 011004.

[15] B. Hu, S. Jiang, I. A. Shkrob, J. Zhang, S. E. Trask, B. J. Polzin, A. Jansen, W. Chen, C. Liao, Z. Zhang, L. Zhang, Understanding of pre-lithiation of poly(acrylic acid) binder: Striking the balances between the cycling performance and slurry stability for silicon-graphite composite electrodes in Li-ion batteries. *J Power Sources* 416 (2019) 125–131.

[16] H. J. Kim, J.-S. Kim, S.-W. Song, Uniform distribution of siloxane-grafted SiO_x nanoparticles in micron hard-carbon matrix for high-rate composite anode in Li-ion batteries. *J. Solid State Chem.* 270 (2019) 479–486.

[17] X. Zhong, Y. Wei, Y. Guo, C. Cui, T. Zhai, H. Li, Double the energy storage of hard carbon anode for Li-ion batteries via a simple blending strategy. *Electrochim. Acta* 336 (2020) 135729.

[18] K. H. Kim, J. Shon, H. Jeong, H. Park, S.-J. Lim, J. S. Heo, Improving the cyclability of silicon anodes for lithium-ion batteries using a simple pre-lithiation method. *J. Power Sources* 459 (2020) 228066.

[19] H. Park, N. Yoon, D. H. Kang, C. Young, J. K. Lee, Electrochemical characteristics and energy densities of lithium-ion batteries using mesoporous silicon and graphite as anodes. *Electrochim. Acta* 357 (2020) 136870.

[20] H. Li, W. Ji, Z. He, Y. Zhang, J. Zhao, Distinct capacity fade modes of nickel-rich/graphite-SiO_x power lithium ion battery. *J. Energy Storage* 47 (2022) 103830.

[21] W.-J. Huang, J.-Y. Zheng, J.-J. Liu, R. M. Yang, F. X. Cheng, H. B. Suo, H. Guo, S. B. Xia, Boosting rate performance of $LiNi_{0.8}Co_{0.15}Al_{0.05}O_2$ cathode by simply mixing lithium iron

phosphate. *J. Alloys Compd.* 827 (2020) 154296.

[22] K. H. Chen, V. Goel, M. J. Namkoong, M. Wied, S. Müller, V. Wood, J. Sakamoto, K. Thornton, N. P. Dasgupta, Enabling 6C fast charging of Li-ion batteries with graphite/hard carbon hybrid anodes. *Adv. Energy Mater.* 11 (2020) 2003336.

[23] J. Wang, J. L. Liu, Y. G. Wang, C. X. Wang, Y. Y. Xia, Pitch modified hard carbons as negative materials for lithium-ion batteries. *Electrochim. Acta* 74 (2012) 1–7.

[24] Y. Liu, B. Yang, X. Dong, Y. Wang, Y. Xia, A simple prelithiation strategy to build a high-rate and long-life lithium-ion battery with improved low-temperature performance. *Angew. Chem., Int. Ed.* 56 (2017) 16606–16610.

[25] U. Kasavajjula, C. Wang, A. J. Appleby, Nano- and bulk-silicon-based insertion anodes for lithium-ion secondary cells. *J. Power Sources* 163 (2007) 1003–1039.

[26] M. A. Azam, N. E. Safie, A. S. Ahmad, N. A. Yuza, N. S. A. Zulkifli, Recent advances of silicon, carbon composites and tin oxide as new anode materials for lithium-ion battery: A comprehensive review. *J Energy Storage* 33 (2021) 102096.

[27] H. Wu, Y. Cui, Designing nanostructured Si anodes for high energy lithium ion batteries. *Nano Today* 7 (2012) 414–429.

[28] P. Bärmann, M. Diehl, L. Göbel, M. Ruttert, S. Nowak, M. Winter, T. Placke, Impact of the silicon particle size on the pre-lithiation behavior of silicon/carbon composite materials for lithium ion batteries. *J. Power Sources* 464 (2020) 228224.

[29] B. F. Song, A. Dhanabalan, S. L. Biswal, Evaluating the capacity ratio and prelithiation strategies for extending cyclability in porous silicon composite anodes and lithium iron phosphate cathodes for high capacity lithium-ion batteries. *J Energy Storage* 28 (2020) 101268.

[30] M.-S. Wu, P.-C. J. Chiang, J. C. Lin, Electrochemical investigations on advanced lithium-ion batteries by three-electrode measurements. *J. Electrochem. Soc.* 152 (2005) A47–A52.

[31] S. S. Zhang, K. Xu, T. R. Jow, Study of the charging process of a $LiCoO_2$-based Li-ion battery. *J. Power Sources* 160 (2006) 1394–1354.

[32] N. Loeffler, J. von Zamory, N. Laszczynski, I. Doberdo, G.-T. Kim, S. Passerini,

Performance of $LiNi_{1/3}Mn_{1/3}Co_{1/3}O_2$/graphite batteries based on aqueous binder. *J. Power Sources* 248 (2014) 915–922.

[33] C.-S. Kim, K. M. Jeong, K. Kim, C. W. Yi, Effects of capacity ratios between anode and cathode on electrochemical properties for lithium polymer batteries. *Electrochim. Acta* 155 (2015) 431–436.

[34] S. Liu, L. Xiong, C. He, Long cycle life lithium ion battery with lithium nickel cobalt manganese oxide (NCM) cathode. *J. Power Sources* 261 (2014) 285–291.

[35] Y. Abe, S. Kumagai, Effect of negative/positive capacity ratio on the rate and cycling performances of $LiFePO_4$/graphite lithium-ion batteries. *J. Energy Storage* 19 (2018) 96–102.

[36] H. Sun, X. He, J. Ren, J. Li, C. Jiang, C. Wan, Hard carbon/lithium composite anode materials for Li-ion batteries. *Electrochim. Acta* 52 (2007) 4312–4316.

[37] H. Wang, C. Lai, Y. Xiao, X. Ai, A new lithium-ion battery with $LiNi_{0.8}0Co_{0.15}Al_{0.05}O_2$ cathode and lithium pre-doping hard carbon anode. *Mater. Lett.* 160 (2015) 250–254.

[38] I. H. Son, J. H. Park, S. Park, K. Park, S. Han, J. Shin, S.-G. Doo, Y. Hwang, H. Chang, J. W. Choi, Graphene balls for lithium rechargeable batteries with fast charging and high volumetric energy densities. *Nat. Commun.* 8 (2017) 1561.

[39] X. Zhang, C. Fan, S. Han, Improving the initial Coulombic efficiency of hard carbon-based anode for rechargeable batteries with high energy density. *J. Mater. Sci.* 52 (2017) 10418–10430.

[40] T. L. Kulova, A. M. Skundin, Irreversible capacity elimination via immediate contact of carbon with lithium metal. *J. Solid State Electrochem.* 8(1) (2003) 59–65.

[41] Y. Abe, T. Saito, S. Kumagai, Effect of prelithiation process for hard carbon negative electrode on the rate and cycling behaviors of lithium-ion batteries. *Batteries* 4(4) (2018) 71.

[42] Sigma-Aldrich, High-performance silicon anode. Available online: https://www.sigmaaldrich.com/JP/ja/product/aldrich/918334 (accessed on 19th February 2022).

[43] V. Agubra, J. Fergus, Lithium ion battery anode aging mechanisms. *Materials* 6 (2013) 1310–1325.

[44] S. Jeong, X. Li, J. Zheng, P. Yan, R. Cao, H. J. Jung, C. Wang, J. Liu, J.-G. Zhang, Hard carbon coated nano-Si/graphite composite as a high performance anode for Li-ion batteries. *J. Power Sources* 329 (2016) 323–329.

[45] J. Ni, Y. Huang, L. Gao, A high-performance hard carbon for Li-ion batteries and supercapacitors application. *J. Power Sources* 223 (2013) 306–311.

[46] M. H. Parekh, V. P. Parikh, P. J. Kim, S. Misra, Z. Qi, H. Wang, V. G. Pol, Encapsulation and networking of silicon nanoparticles using amorphous carbon and graphite for high performance Li-ion batteries. *Carbon* 148 (2019) 36–43.

[47] T. Mu, Z. Zhang, Q. Li, S. Lou, P. Zuo, C. Du, G. Yin, Scalable submicron/micron silicon particles stabilized in a robust graphite-carbon architecture for enhanced lithium storage. *J. Colloid Interface Sci.* 555 (2019) 783–790.

[48] S. Jiang, Q. Ji, S. Yun, Z. Zhang, Q. Jiang, H. C. Chen, Tuning the microstructures of uniform carbon spheres by controlling the annealing conditions for high-performance lithium-ion full batteries and lithium-ion capacitors. *J. Energy Storage* 39 (2021) 102625.

[49] H. Yu, X. Dong, Y. Pang, Y. Wang, Y. Xia, High power lithium-ion battery based on spinel cathode and hard carbon anode. *Electrochim. Acta* 228 (2017) 251–258.

[50] W. Simonetti, G. Maresca, G. B. Appetecchi, G.-T. Kim, N. Loeffler, S. Passerini, Towards $Li(Ni_{0.33}Mn_{0.33}Co_{0.33})O_2$/graphite batteries with ionic liquid-based electrolytes. I. Electrodes' behavior in lithium half-cells. *J. Power Sources* 331 (2016) 426–434.

[51] Y. Ding, R. Wang, L. Wang, K. Cheng, Z. Zhao, D. Mu, B. Wu, A short review on layered $LiNi_{0.8}Co_{0.1}Mn_{0.1}O_2$ positive electrode material for lithium-ion batteries. *Energy Procedia* 105 (2017) 2941–2952.

[52] C.-S. Kim, K. M. Jeong, K. Kim, C.-W. Yi, Effects of capacity ratios between anode and cathode on electrochemical properties for lithium polymer batteries. *Electrochim. Acta* 155 (2015) 431–436.

[53] Y. Sun, G. Ning, C. Qi, J. Li, X. Ma, C. Xu, Y. Li, X. Zhang, J. Gao, An advanced lithium

ion battery based on a sulfur-doped porous carbon anode and a lithium iron phosphate cathode. *Electrochim. Acta* 190 (2016) 141–149.

[54] J.-S. Zheng, L. Zhang, A. Shellikeri, W. Cao, Q. Wu, J. P. Zheng, A hybrid electrochemical device based on a synergetic inner combination of Li ion battery and Li ion capacitor for energy storage. *Sci. Rep.* 7 (2017) 41910.

[55] J. Ma, J. Sung, Y. Lee, Y. Son, S. Chae, N. Kim, S.-H. Choi, J. Cho, Strategic pore architecture for accommodating volume change from high Si content in lithium-ion battery anodes. *Adv. Energy Mater.* 10 (2020) 1903400.

Chapter 5

Role of SiO_x in Rice-Husk-Derived Anodes for LIBs

5. 1 Introduction

Approximately 150 million tons of RH are generated annually and globally as agricultural waste [1]. RH is composed of approximately 80 mass% organic material (lignin, cellulose, hemicellulose, and others), and the rest are mainly silicon oxides (SiO_x, $0< x <2$) [2]. Rice, a silicicolous plant, adsorbs $Si(OH)_4$ from the soil for growth and accumulates SiO_x in its husk [3]. RH is not preferred as a fuel because it produces a large amount of SiO_x-derived ash during combustion. Thus, the utilization of RH has been limited to agricultural applications such as fertilizer additives, stockbreeding mats, and bed soil. On the other hand, RH, being intrinsically a composite of organic material and inorganic SiO_x itself, can be easily transformed into a C/SiO_x composite through simple heat treatment under inert conditions (carbonization).

LIBs have been used as power sources in various industrial applications, such as smartphones, industrial robots, electric vehicles, and grid-scale electricity storage systems. Graphite, HC, Si, and SiO_x have been used as anodic active materials (AMs) in LIBs [4–10]. Anodic AMs operate using several Li storage mechanisms (insertion, conversion, and alloying reactions) [8, 11–14]. Intercalation compounds, such as carbon materials, follow the intercalation mechanism, which facilitates Li-ion insertion (reduction) and extraction (oxidation) [11]. This mechanism provides a good conductive pathway, smooth Li-ion transport, and strong robustness during cyclic Li-ion insertion and extraction. Alloying compounds, such as Si and Sn, follow the alloying mechanism when they react with Li, which can lead to dramatically higher specific capacities for Li storage than those for the insertion mechanism [14]. High specific capacities are also obtainable by the conversion mechanism associated with the reactions of transition metal oxides and Li. However, large irreversible capacities and positive anode potentials are induced by this mechanism compared to the other mechanisms.

Low electrode potential, high specific capacity for Li-ion uptake and release, good cycle stability, low toxicity, low cost, and natural abundance are required for anodic AMs. Graphite, which follows the insertion mechanism, is still mainly used in commercial LIBs because of its low and flat potential profile, low irreversible capacity, low cost, and accumulated experience. However, it has drawbacks, including a limited specific capacity of 372 mAh g^{-1}, small margin for Li deposition or dendrite formation, and moderate cycle life [11, 15]. Si, which follows the alloying mechanism, is anticipated to supersede graphite because of its very high specific capacity (4200 mAh g^{-1} at full Li alloying) [14]. However, it undergoes a large volume expansion during Li-ion uptake and release (~280%) [16], causing the cracking of Si particles and thus, repeated formation of a SEI. Repeated SEI formation consumes Li ions in the electrolyte and increases the irreversible capacity of the Si anode. Moreover, cracking can induce the delamination of Si particles from the electrode, leading to capacity fading of the cell. Therefore, the sole use of Si in LIB anodes is still rare for commercial LIBs. However, the use of SiO_x has been an alternative countermeasure to increase the anode capacity of cells. High specific capacities of 1965 and 2043 mAh g^{-1} were obtained for SiO_2 and SiO, respectively [7, 17]. The reduction reaction of SiO_x with Li ions can produce lithium silicate (Li_xSiO_y) and lithium oxide (Li_2O), leading to a smaller volume expansion at succeeding cycles of Li-ion uptake and release and thus, higher cycle stability [17]. However, SiO_x has a lower electrical conductivity than C and Si, requiring a high-level conductive agent (e.g., carbon black) to fabricate the anode. Thus, C/SiO_x composites have attracted much attention as anodic AMs for LIBs [18–21].

For sustainable development goals, biomass-derived materials are viable options for next-generation LIB anodes that require high environmental compatibility. As mentioned above, C/SiO_x composites can be readily produced from RH via simple carbonization. RH-derived C/SiO_x composites have been investigated for application as LIB anodes. Ju et al. stated that RH-derived C/SiO_x exhibits a large irreversible capacity of 46.7% CE at the initial Li-ion

insertion and extraction [22]. Kumagai et al. also reported ~53% CE at the initial Li-ion uptake and release [17]. The large irreversible capacity of RH-derived C/SiO_x has been demonstrated elsewhere [15, 20–23]. In addition, the Li-ion insertion and extraction properties of carbon materials produced by removing almost all SiO_x from carbonized RH were also evaluated [24, 25]. Although SiO_x undergoes reduction reactions with Li ions and thereby increases the irreversible capacity, the CE of the carbon material is not high (~60%) [15, 18]. SiO_x in RH acts as a template to produce micro- and mesoporous structures in the resultant carbon material [26]. The passivation of Li ions in the produced pores, as well as SEI formation on the increased surface area, is responsible for the large irreversible capacity [20, 23]. To overcome the large irreversible capacity of RH-derived C/SiO_x, a pre-lithiation process that provides sufficient Li ions to the anodic AMs can be a realistic choice [27–32]. Up to now, the Li-ion insertion and extraction properties of RH-derived C/SiO_x or C have been evaluated in the half-cell configuration where infinite Li ions can be provided by the Li metal electrode (counter and reference electrodes). However, for actual LIB full-cells, the large irreversible capacity of the anode has a decisive effect on the charge-discharge performance because a significant amount of Li ions can be consumed within and on the anode, and additional Li ions cannot be supplied from the outside. Although several studies have focused on the feasibility of RH-derived C/SiO_x as a LIB anodic AM, its electrochemical performance in a full-cell configuration has not been reported thus far. The role of SiO_x in LIB full-cell performance is also unknown.

In the present study, C/SiO_x was produced by heating RH under N_2 and then immersing the carbonized RH in NaOH solution. By adjusting the immersion temperature and time, C/SiO_x composites with different SiO_x contents were prepared as LIB anodic AMs. The physical properties of the prepared samples were evaluated by thermogravimetric analysis, particle size analysis, and N_2 adsorption-desorption porosimetry. CR2032-type half-cells and full-cells were assembled to evaluate the Li-ion insertion and extraction properties of C/SiO_x. Pre-lithiation was performed prior to the LIB full-cell assembly. Full-cells with a pre-lithiated or pristine C/SiO_x anode and Li($Ni_{0.5}Co_{0.2}Mn_{0.3}$)O_2 (NCM) cathode were assembled, and their rate and

cycle performance were evaluated. Finally, the role of SiO_x in the C/SiO_x anode in the rate and cycle performance of the assembled full-cells was discussed. To the best of our knowledge, the performance of LIB full-cells with pre-lithiated C/SiO_x anodes has been evaluated for the first time in this study. Revealing the roles of the pre-lithiation process and SiO_x removal in the anode on the performance of LIB full-cells is scientifically novel and industrially and environmentally significant. The knowledge provided in this study is expected to promote the development of eco-friendly LIBs and the effective use of agricultural waste.

5. 2 Experimental

5. 2. 1 *Preparation of C/SiO_x AMs and Their Characterization*

Raw RH (Akitakomachi rice) was provided by a rice farmer in Senboku City, Akita Prefecture, Japan with his permission and used as feedstock for RH-derived C/SiO_x AMs. The raw RH was dried at 100 °C for 10 h to determine the initial mass. Pre-carbonization was conducted in a tubular furnace by heating the raw RH at 600 °C for 1 h under N_2 gas flow at 1 L min^{-1}. The pre-carbonized RH was then immersed in a 1 mol L^{-1} NaOH solution under the following two conditions: (A) immersion temperature: 25 °C, immersion time: 22 h for half-elimination of SiO_x and (B) immersion temperature: 80 °C, immersion time: 10 h for complete elimination of SiO_x. The mass ratio of pre-carbonized RH to the solution was 1:20. The pre-carbonized RH immersed in NaOH solution was rinsed with distilled water until the pH of the used rinse water was reduced to <9. For the pre-carbonized RH that was not immersed in NaOH solution, the rinse consisting of distilled water was also prepared. All rinsed samples were dried at 100 °C for 10 h. For the main carbonization, they were heated to 1000 °C, and the temperature was maintained for 1 h in a similar manner to the pre-carbonization. Grains of the carbonized RH were pulverized using a planetary ball-milling machine with a zirconia vessel and balls (P-6, Fritch Japan Co., Ltd., Japan) at 400 rpm for 20 min, finally providing C/SiO_x AMs with different SiO_x contents.

The production mass yield was calculated based on the masses of the dried raw RH and prepared

Table 1. Physical properties of the C/SiO_x active materials.

	C/SiO_x-45	C/SiO_x-24	C/SiO_x-5
Production mass yield (mass%)	35.5	25.7	21.1
Average particle diameter (μm)	4.6	4.2	4.5
Brunauer–Emmett–Teller specific surface area ($m^2\ g^{-1}$)	44	125	193
Total pore volume ($cm^3\ g^{-1}$)	0.07	0.17	0.23
SiO_x content (mass%)	44.6	23.6	4.8

C/SiO_x AMs. The average particle diameters of the C/SiO_x AMs were measured using a laser diffraction particle size analyzer (SALD-200V, Shimadzu Corp., Japan). The specific surface areas of the C/SiO_x AMs were measured using a gas adsorption analyzer (Autosorb-3B, Quantachrome Instruments Inc., USA). The BET specific surface area was calculated from the obtained nitrogen adsorption-desorption isotherms at −196 °C. The total pore volume was measured using the volume of adsorbed nitrogen at a relative pressure close to 1 as reference. A thermogravimetry system (Thermo Plus EVO TG8120, Rigaku Corp., Japan) was used to heat the C/SiO_x AMs up to 850 °C under air flow (200 mL min^{-1}). The SiO_x content was calculated from the mass of C/SiO_x at 140 and 850 °C. The physical properties of the three types of C/SiO_x AMs are summarized in Table 1. The C/SiO_x AMs are denoted as C/SiO_x-45, C/SiO_x-24, and C/SiO_x-5 based on the SiO_x content. The production mass yield decreased with the SiO_x content and was reduced by ~14% owing to complete SiO_x removal. The particle sizes of the C/SiO_x AMs were adjusted to 4–5 μm. The removal of SiO_x increased the specific surface area and total pore volume, which is related to the decrease in the production mass yield.

5. 2. 2 *Electrode Fabrication*

To fabricate the anode, 80 mass% C/SiO_x, 10 mass% conductive agent (acetylene black, Denka Co., Ltd., Japan), 7.5% sodium carboxymethyl cellulose (Cellogen 7A, DSK Co., Ltd., Japan), and 2.5 mass% styrene–butadiene rubber (TRD2001, JSR Corp., Japan) were dispersed in distilled water and mixed using a planetary centrifugal mixer (AR-100, Thinky Corp., Japan). The uniformly dispersed slurry was coated onto a Cu foil (no surface treatment, *t*20 μm, Hohsen Corp., Japan) using an applicator and dried in an oven at 100 °C for >6 h. The cathode for the full-cell assembly was also fabricated. A ternary LTMO ($LiNi_{0.5}Co_{0.2}Mn_{0.3}O_2$, NCM, Beijing

Easpring Material Technology Co., Ltd., China), acetylene black, and PVDF (KF polymer F #9130, Kureha Corp., Japan) were mixed at a mass ratio of 80:10:10 in N-methylpyrrolidone (Tokyo Chemical Industry Co., Ltd., Japan). The cathode slurry was coated onto an Al foil (no surface treatment, *t*20 μm, Hohsen Corp., Japan) and dried in an oven at 100 °C for >6 h. Both dried electrodes were punched out into ϕ15-mm disks and dried at 140 °C under vacuum for 3 h. The loading masses of the AMs in the cathodes and anodes were respectively 5.57–5.61 and 2.15–2.31 mg cm^{-2}; hence the electrode loading masses were 6.96–7.01 mg cm^{-2} for the NCM cathode and 2.69–2.89 mg cm^{-2} for the C/SiO_x anode. The coating thicknesses of the cathode and anode layers on the current collectors were 42–44 and 31–43 μm, respectively.

5. 2. 3 *Half-Cell Assembly and Pre-Lithiation of the C/SiO_x Electrodes*

The half-cell consisting of the C/SiO_x electrode and Li metal foil (ϕ15 mm, *t*0.2 mm, Honjo Metal Co., Ltd., Japan) was assembled using a CR2032 coin cell (Hohsen Corp., Japan) in an argon-filled glove box. The electrolyte used was 1 mol L^{-1} $LiPF_6$ dispersed in 1:1 v/v% ethylene carbonate/diethyl carbonate (Kishida Chemical Co., Ltd., Japan). The two electrodes separated by a polypropylene separator (ϕ18 mm, 2500, Celgard LLC, USA) were installed in the coin cell after dipping the electrodes and separator in the electrolyte for ~5 s. A Li-ion insertion-extraction test was performed on the coin-type half-cells using a battery charge-discharge system (HJ1020mSD8, Hokuto Denko Corp., Japan). The electrode potential range was 0–2.5 V vs. Li^+/Li, and the current density was 20 mA g_{AM}^{-1}, where g_{AM} is the unit of the mass of the C/SiO_x AM in the electrode. The Li-ion insertion-extraction process was repeated five times. The specific capacities of the C/SiO_x AMs were determined using the half-cell test results as the reference. The cycling stabilities of the C/SiO_x AMs were then evaluated by repeated (100-times) Li-ion insertion-extraction at a current density of 200 mA g_{AM}^{-1} in a similar potential range.

5. 2. 4 *Assembly of the Full-Cells with Pre-Lithiated C/SiO_x Electrode and Their Evaluation*

The specific capacity of the employed NCM AM was 150 mA g^{-1} based on the previous test

results obtained using a half-cell configuration [28]. According to the specific capacity of the C/SiO_x AMs determined in the coin-type half-cell tests, the capacity ratio of the anode to the cathode in the full-cells was adjusted to 1.0−1.1. The pre-lithiation of the C/SiO_x electrode and NCM+C/SiO_x full-cell assembly is illustrated in Figure 1. To prepare the pre-lithiated anode, a half-cell with the C/SiO_x electrode was separately assembled using an SUS304 stainless steel flat-type cell (HS Flat cell, Hosen Corp., Japan). The flat-type half-cell consisting of the C/SiO_x electrode, the above-mentioned Li metal foil, separator (ϕ23 mm), and electrolyte (1 mL) was assembled. The C/SiO_x electrode was pre-lithiated in an assembled flat-type half-cell. The potential of the C/SiO_x electrode decreased at a current density of 40 mA g_{AM}^{-1}, delivering Li ions to the C/SiO_x AM. The pre-lithiation sequence was stopped when the electrode potential reached 0 V vs. Li^+/Li. Following pre-lithiation, the flat-type half-cell was introduced into an argon-filled glove box. The pre-lithiated C/SiO_x electrode was carefully extracted from the flat-type half-cell. Coin-type full-cells were then fabricated using the NCM cathode and pre-lithiated or unlithiated C/SiO_x anode in a similar manner to the coin-type half-cells.

The C-rate was employed to represent the current density of the full-cells. 1 C is defined as 150 mA g_{CAM}^{-1}, where g_{CAM} is the unit of the mass of the cathodic AM. The cell voltage range used for the charge-discharge sequences of the full-cells was 2.5–4.2 V. Charge-discharge cycling at 0.1 C was first performed three times for cell stabilization. Following cell stabilization, the rate performance of the full-cells was evaluated, during which the C-rate was increased stepwise

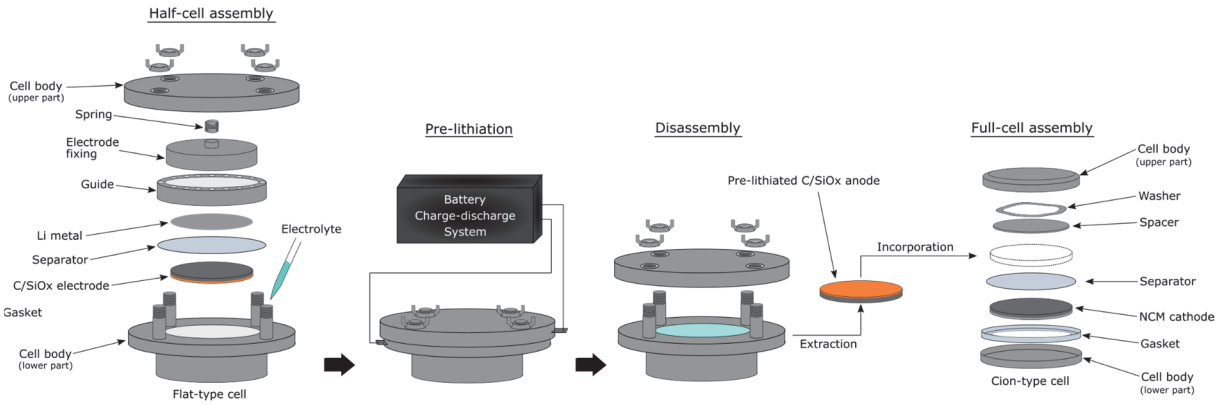

Figure 1. Pre-lithiation of the C/SiO_x anode and $Li(Ni_{0.5}Co_{0.2}Mn_{0.3})O_2$ (NCM)+C/SiO_x full-cell assembly.

from 0.1 to 10 C, and then decreased to 0.1 C. The charge-discharge process was repeated five times at each C-rate. The cycle performance of the full-cells was then evaluated by repeating the charge-discharge cycles at 2 C. The full-cell performance was represented by the cathode specific capacity (time integral of the cell current divided by the mass of cathode AM in units of mAh g_{AM}^{-1}).

5. 3 Results and Discussion

5. 3. 1 *Li-ion Insertion and Extraction Properties of C/SiO_x AMs*

Figure 2 shows the initial Li-ion insertion and extraction properties of the C/SiO_x AMs at 20 mA g_{AM}^{-1}, and their cycling stabilities at 200 mA g_{AM}^{-1} in the half-cell configuration. In the first cycle, C/SiO_x-5 exhibited the highest Li-ion insertion specific capacity of 752 mAh g_{AM}^{-1}. A comparative Li-ion insertion specific capacity (~650 mAh g_{AM}^{-1}) was observed for C/SiO_x-45 and C/SiO_x-24. All C/SiO_x AMs displayed a Li-ion extraction specific capacity of <410 mAh g_{AM}^{-1}, which was much lower than those for Li-ion insertion. The initial CEs of C/SiO_x-45, C/SiO_x-24, and C/SiO_x-5 were 63.0%, 54.1%, and 50.2%, respectively, indicating that the initial CE decreases with decreasing SiO_x content. The CEs increased with the number of cycles. In the fifth cycle, C/SiO_x-45 had the highest Li-ion extraction specific capacity (420 mAh g_{AM}^{-1}), while C/SiO_x-24 had the lowest one (298 mAh g_{AM}^{-1}). C/SiO_x-5 displayed a maximum specific capacity of 380 mAh g_{AM}^{-1}. The apparent specific capacity of the C/SiO_x AMs was determined as 400 mAh g_{AM}^{-1}. These results demonstrate that SiO_x is beneficial for increasing the specific capacity of C/SiO_x AMs. On the other hand, partial removal of SiO_x is detrimental to maintaining the specific capacity. Then, the cycling stabilities of C/SiO_x AMs were evaluated at 200 mA g_{AM}^{-1}. The specific capacities for Li-ion extraction from all C/SiO_x AMs decrease significantly within the initial 10 cycles in the half-cell configuration where ample Li-ions are

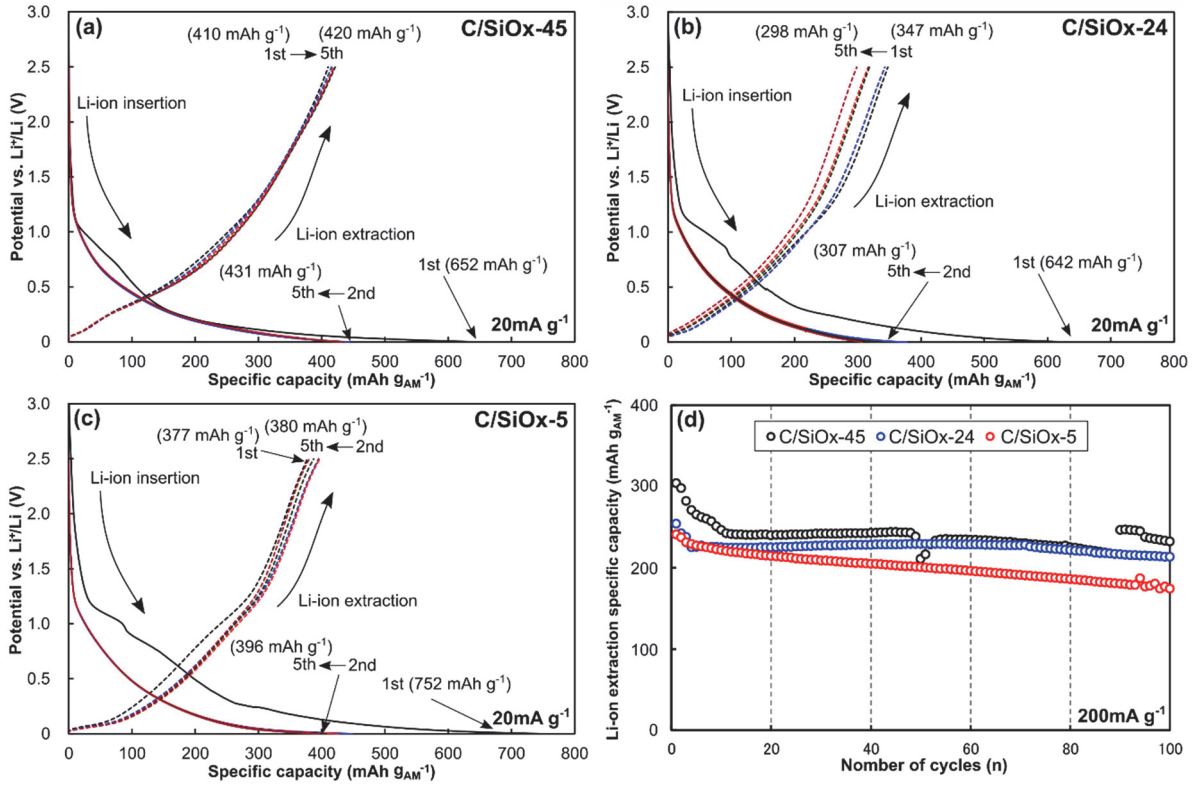

Figure 2. Initial Li-ion insertion and extraction properties of (a) C/SiO_x-45, (b) C/SiO_x-24, and (c) C/SiO_x-5 in a coin-type half-cell configuration at 20 mA g_{AM}^{-1}, and (d) their cycling stabilities at 200 mA g_{AM}^{-1} in the half-cell configuration in the 0–2.5 V (vs. Li^+/Li) electrode potential range.

delivered, after which they plateau during the remaining 100 cycles.

5. 3. 2 *Pre-Lithiation of the C/SiO_x Electrodes*

The C/SiO_x AMs were pre-lithiated prior to full-cell assembly. The Li-ion insertion profiles of the C/SiO_x AMs in the flat-type half-cells are shown in Figure 3. C/SiO_x-45 and C/SiO_x-24 displayed a similar Li-ion insertion specific capacity of ~680 mAh g_{AM}^{-1}, while C/SiO_x-5 had a higher specific capacity of 832 mAh g_{AM}^{-1}. The C/SiO_x AMs exhibited different profiles at the first Li-ion insertion, and their potential levels decreased with increasing SiO_x content. The Li-ion insertion specific capacities of the C/SiO_x AMs obtained here were higher than those obtained using the coin-type half-cell, which can be attributed to the ample amount of electrolyte (1 mL) covering the electrodes.

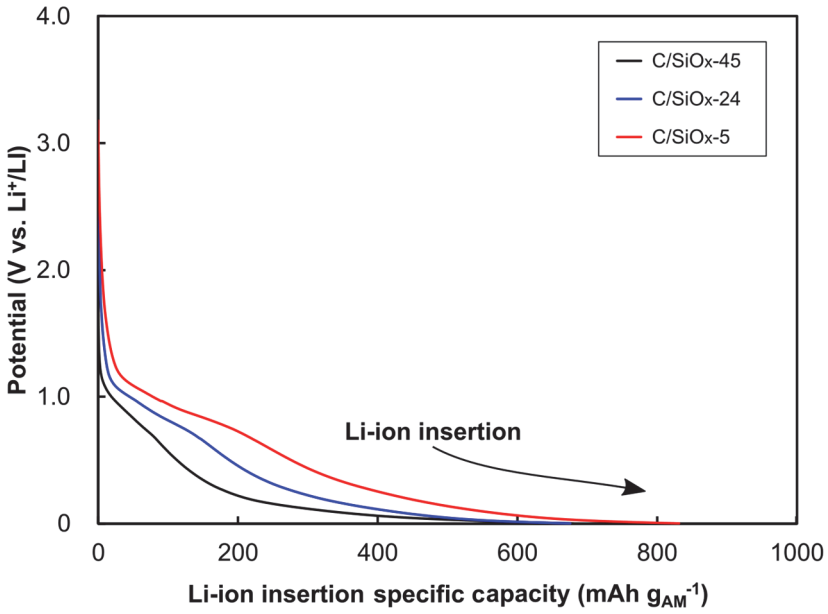

Figure 3. Li-ion insertion profiles of the C/SiO_x active materials during pre-lithiation.

5. 3. 3 *Performance of the NCM+C/SiO_x Full-Cells*

Full-cells with the NCM cathode and pre-lithiated C/SiO_x anode were fabricated. A full-cell incorporating the unlithiated C/SiO_x-45 anode (NCM+C/SiO_x-45 without pre-lithiation) was also fabricated and evaluated. The charge-discharge specific capacities and CEs of the full-cells during the initial three cycles at 0.1 C are summarized in Table 2. In the first cycle, a large difference between the charge and discharge specific capacities (176 and 17 mAh g_{CAM}^{-1}, respectively) and a very low CE of 9.6% were observed for NCM+C/SiO_x-45 without pre-lithiation. Even after the succeeding cycles, the discharge specific capacity was ~20 mAh g_{CAM}^{-1}. By pre-lithiating the C/SiO_x anodes, the CEs of the full-cells significantly increased up to ~85 % in the first cycle. All full-cells with pre-lithiated anodes (pre-lithiated full-cells) exhibited stable charge-discharge profiles and very high CEs during the initial three cycles. In the 2nd cycle, the discharge specific capacities of the pre-lithiated full-cells reached the apparent specific capacity of the NCM cathode (150 mAh g_{CAM}^{-1}), indicating negligible loss of Li ions from the cathode.

Table 2. Charge (C_C) and discharge (C_D) specific capacities and Coulombic efficiencies (CEs) of the $Li(Ni_{0.5}Co_{0.2}Mn_{0.3})O_2$ (NCM)+C/SiO_x full-cells at the initial 3 cycles at 0.1 C.

Sample	1st			2nd			3rd		
	C_C (mAh g_{CAM}^{-1})	C_D (mAh g_{CAM}^{-1})	CE (%)	C_C (mAh g_{CAM}^{-1})	C_D (mAh g_{CAM}^{-1})	CE (%)	C_C (mAh g_{CAM}^{-1})	C_D (mAh g_{CAM}^{-1})	CE (%)
NCM+C/SiO_x-45	158	135	85.4	149	147	98.7	151	149	98.7
NCM+C/SiO_x-24	169	143	84.6	150	148	98.7	152	149	98.0
NCM+C/SiO_x-5	168	143	85.1	154	152	98.7	156	153	98.1
NCM+C/SiO_x-45 without pre-lithiation	176	17.0	9.7	30.1	19.6	65.1	28.6	20.9	73.0

Following the initial three cycles, the rate performance of all full-cells was evaluated at a current density of 0.1–10 C and is shown in Figure 4. Except for NCM+C/SiO_x-45 without pre-lithiation, the full-cells displayed similar levels of discharge specific capacity up to 2 C. At higher current densities (5 and 10 C), a higher SiO_x content led to a higher discharge specific capacity. The discharge specific capacities of NCM+C/SiO_x-45, NCM+C/SiO_x-24, and NCM+C/SiO_x-5 at 10 C were 60, 43, and 31 mAh g_{CAM}^{-1}, respectively. The CEs of the pre-lithiated full-cells were ~100%, except during the first cycle at each C-rate. The discharge specific capacity of NCM+C/SiO_x-45 without pre-lithiation was much lower than those of the pre-lithiated full-cells throughout the rate test. The cell voltage-specific capacity profiles of NCM+C/SiO_x-45 and NCM+C/SiO_x-24 exhibited slope-like variations, while NCM+C/SiO_x-5 maintained a higher cell voltage (allowing narrow plateau regions) than the others at low current densities (up to 2 C). Maintaining a high cell voltage increases the density of the energy delivered during the charge and discharge processes. At high current densities (>2 C), the residual SiO_x in the anode was effective in sustaining the cell capacity.

The cycling performance of the full-cells at 2 C is shown in Figure 5. The highest discharge specific capacity was displayed by NCM+C/SiO_x-45 in the 1st cycle and NCM+C/SiO_x-5 in the final cycle. All full-cells showed a gradual decrease in capacity with the number of cycles. The capacity retentions of NCM+C/SiO_x-45, NCM+C/SiO_x-24, and NCM+C/SiO_x-5 after 800 cycles were 47.5%, 61.7%, and 60.7%, respectively. The presence of SiO_x in the anode led to a ~13% difference in the retention of the cell specific capacity. The largest decrease was observed

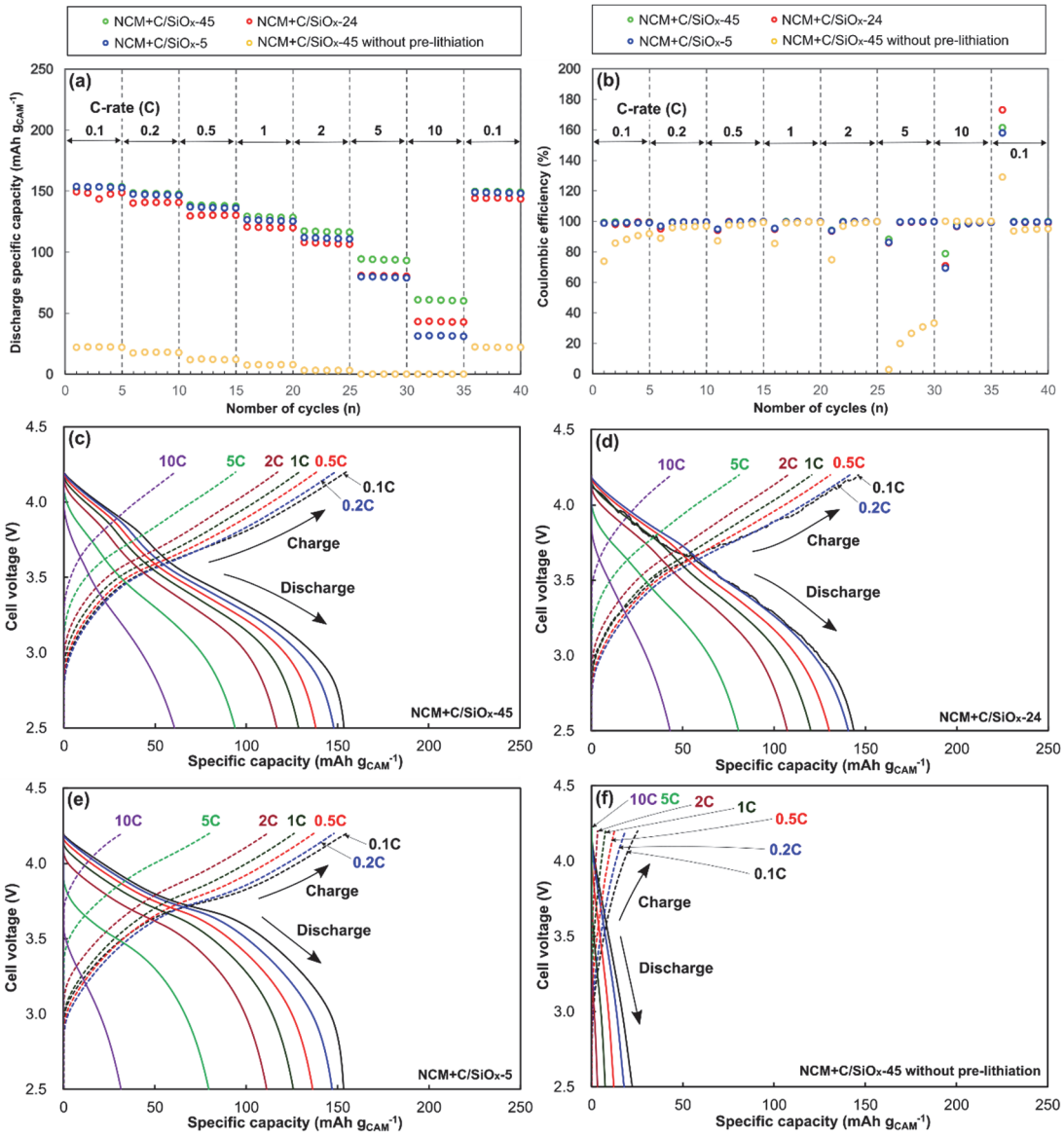

Figure 4. Rate performance of the $Li(Ni_{0.5}Co_{0.2}Mn_{0.3})O_2$ (NCM)+C/SiO_x full-cells. (a) Discharge specific capacity and (b) Coulombic efficiency at different C-rates. Cell voltage-specific capacity profiles of the full-cells: (c) NCM+C/SiO_x-45, (d) NCM+C/SiO_x-24, (e) NCM+C/SiO_x-5, and (f) NCM+C/SiO_x-45 without pre-lithiation. The profiles of the 3rd cycle at each C-rate are shown. The cell voltage range was 2.5–4.2 V.

for NCM+SiO_x-45, which has the highest level of SiO_x. The discharge specific capacity of NCM+C/SiO_x-45 without pre-lithiation was negligible throughout the 800 cycles, suggesting that pre-lithiation is essential for RH-derived C/SiO_x AMs. Cycle aging was alleviated when the SiO_x in the anode was removed completely or partially. However, NCM+C/SiO_x-24 showed

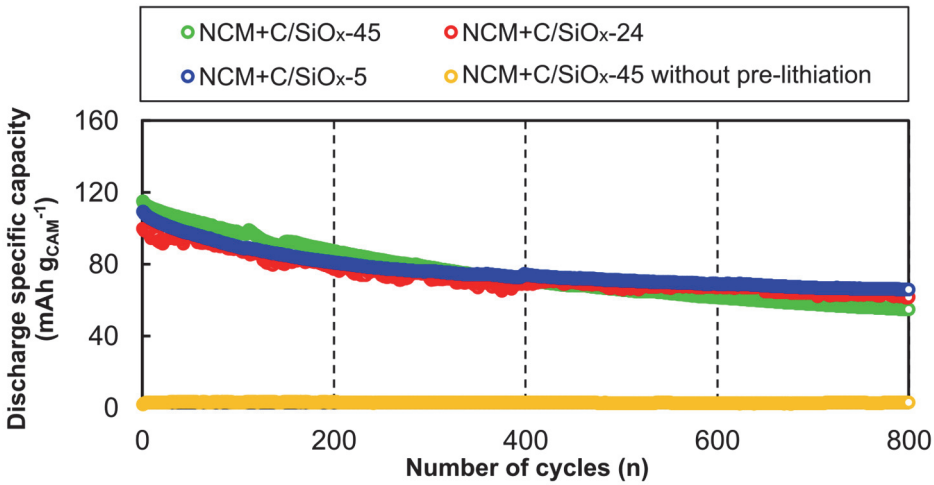

Figure 5. Cycling performance of the $Li(Ni_{0.5}Co_{0.2}Mn_{0.3})O_2$ (NCM)+C/SiO_x full-cells. The cell voltage range was 2.5–4.2 V, and the charge-discharge current density was 2 C (300 mA g_{CAM}^{-1}).

an unstable variation in the discharge specific capacity up to the ~400th cycle.

5. 3. 4 *Effects of SiO_x in the Anode on the Full-Cell Performance*

The number of oxygen atoms (x) in SiO_x in the RH carbonized at 1000°C was found to be close to 2 [17]. Under this assumption, the SiO_x in C/SiO_x AMs can react with Li ions according to the following chemical formulae [Eqs. (5.1) to (5.4)] [21]:

Reversible reactions (Li-ion insertion and extraction)

$$5SiO_2 + 4Li^+ + 4e^- \leftrightarrow 2Li_2Si_2O_5 + Si \quad (5.1)$$

$$Si + xLi^+ + xe^- \leftrightarrow Li_xSi \quad (5.2)$$

Irreversible reactions (Li-ion insertion only)

$$SiO_2 + 4Li^+ + 4e^- \rightarrow 2Li_2O + Si \quad (5.3)$$

$$2SiO_2 + 4Li^+ + 4e^- \rightarrow Li_4SiO_4 + Si \quad (5.4)$$

In the half-cell configuration, the reversible (Li-ion extraction) capacities of C/SiO_x-45 and C/SiO_x-5 were 420 and 380 mAh g_{AM}^{-1}, respectively. These results indicate that the specific capacities of C and SiO_x were 375 and 475 mAh g_{AM}^{-1}, respectively. Based on the specific

capacity of SiO_2 (1965 mAh g^{-1}) [7], the irreversible reactions in Eqs. (5.3) and (5.4) dominate. However, approximately one-quarter of SiO_x was responsible for the reversible specific capacity for Li-ion insertion and extraction via Eqs. (5.1) and (5.2). On the other hand, C/SiO_x-24 had the lowest specific capacity of 298 mAh g_{AM}^{-1}. Sodium silicates such as Na_2SiO_3 are likely produced during SiO_x leaching, i.e., immersion in NaOH solution [20]. They are inactive for Li-ion uptake and release, which reduced the specific capacity of C/SiO_x-24. C/SiO_x AMs with a lower SiO_x content exhibited a lower initial CE. The removal of SiO_x from C/SiO_x AMs increased the specific surface area (44 m^2 g^{-1} for C/SiO_x-45 and 193 m^2 g^{-1} for C/SiO_x-5) because micro- and mesopores were produced at the trace of SiO_x [26]. As pores develop in RH-derived anodic AMs, more Li ions can be passivated within the pores [20, 23]. Thus, the lower the SiO_x content, the lower the initial CE.

The physical properties of the C/SiO_x AMs affected the rate and cycle performance of the NCM+C/SiO_x full-cells. Pre-lithiation was demonstrated to be required for LIBs with RH-derived anodic AMs. Owing to pre-lithiation, all full-cells displayed a high discharge specific capacity of ~150 mAh g_{CAM}^{-1} at 0.1 C. At the increased C-rates of 5 and 10 C, the discharge specific capacity was more retained when C/SiO_x-45 was used as the anode, indicating that the time response of the reversible reactions of SiO_x with Li ions [Eqs. (5.1) and (5.2)] is higher than that of the remaining C component. During the cycle test, the full-cell with the higher SiO_x content could not retain the initial cell specific capacity, and unstable capacity variation was observed for NCM+C/SiO_x-24. Although the SiO_x component in C/SiO_x AM provided a higher time rate for Li-ion insertion and extraction, the uptake and release of Li ions in SiO_x [Eqs. (5.1) and (5.2)] seem to cause a large volume expansion, thereby leading to structural decay in the anode. The unstable variation of NCM+C/SiO_x-24 could be explained by the formation of inactive sodium silicates during SiO_x leaching.

The textural and electrochemical properties of RH-derived AMs intended for use in LIB anodes are summarized in Table 3. The reversible specific capacities of RH-derived AMs produced in

the present study are lower than those reported in the relevant literature. However, C/SiO_x-45, produced through two-step carbonization, exhibited the highest CE (63.0%) among all AMs, and the CEs of C/SiO_x-24 and C/SiO_x-5 are also high compared to those of the other AMs. A trade-off relationship between specific capacity and CE seems to be closely related to porosity, which is represented by the specific surface area or the total pore volume of the AM. Pre-lithiation was shown to be essential for the RH-derived AMs produced here when employed in a LIB full-cell, suggesting that pre-lithiation is necessary for all anodic AMs produced from RH for stable operation in LIB full-cells.

In the present study, the partial removal of SiO_x using the NaOH solution likely produced a sodium silicate byproduct, which is inactive for Li-ion uptake and release. This byproduct formation rather destabilized the cycle performance of the full-cell. It was shown that the specific capacity of the SiO_x component was 100 mAh g_{AM}^{-1} higher than that of the C component in the RH-derived anodic AM. In addition, the time response of the SiO_x component for Li-ion uptake and release was also higher, thereby delivering the highest rate performance to the NCM+C/SiO_x full-cells. However, the SiO_x component reduced the specific capacity retention of the full-cells during the cycle test. Judging from the minor difference in the specific capacity retention (~13% in 800 cycles), significant effort to completely remove SiO_x, excellent rate performance provided by SiO_x, and formation of sodium silicate byproduct, it is not strongly necessary to remove SiO_x from the RH-derived AM intended for LIB anodes. The important task of the present study was to develop sustainable and eco-friendly LIB anode materials. In this sense, it is preferrable to preserve SiO_x to avoid using a strong alkaline solution for SiO_x leaching and strong acid for neutralization. The high production yield due to SiO_x preservation (~14 mass% higher than that for SiO_x removal) is also beneficial for industrial applications.

Table 3. Comparing the textural and electrochemical properties of RH-derived AMs intended for the in LIB anodes

Sample	Preparation notes	Content of Si-based materials (mass%)	SA* ($m^2\ g^{-1}$)	V_{total}** ($cm^3\ g^{-1}$)	$CE_{Initial}$*** (%)	C_R**** (mAh g^{-1})	Ref.
C/SiO_x-45	Carbonization, rinse, and carbonization	45 (SiO_x)	44	0.07	63.0	420 @20 mA g^{-1}	This work
C/SiO_x-24	Carbonization, immersion in NaOH solution at 25 °C, rinse, and carbonization	24 (SiO_x)	125	0.17	54.1	298 @20 mA g^{-1}	This work
C/SiO_x-5	Carbonization, immersion in NaOH solution at 80 °C, rinse, and carbonization	5 (SiO_x)	193	0.23	50.2	380 @20 mA g^{-1}	This work
Nano-Si/C	Addition of Mg into RH, carbonization, and neutralization using HCl solution	18 (Si)	-	-	59.6	560 @100 mA g^{-1}	18
Activated carbon	Carbonization, chemical activation using NaOH, and neutralization	-	2176	0.91	45.8	608 @0.2 C	20
C/SiO_2	Addition of ZnCl into RH, carbonization, and neutralization using HCl solution	57 (SiO_2)	1191	0.40	-	~750 @200 mA g^{-1}	21
SiO_x/C	Carbonization	-	-	-	46.7	582 @100 mA g^{-1}	22
C/SiO_2	Formic acid treatment, hydrothermal processing, carbonization, and SiO_x removal with ammonium hydrogen fluoride	-	243	0.41	49.8	~400 @75 mA g^{-1}	23
Porous C	Immersion in H_2SO_4 solution, hydrothermal processing, carbonization, and immersion in NaOH solution, and neutralization	-	332	-	43.8	~757 @74 mA g^{-1}	33

* Specific surface area; ** Total pore volume; *** Initial Coulombic efficiency; **** Reversible specific capacity.

5. 4 Summary

RH-derived C/SiO_x AMs with 45, 24, and 5 mass% SiO_x were prepared by heat treatment and immersion in a NaOH solution. C/SiO_x AMs that were pre-carbonized at 600°C, then subjected to SiO_x leaching, and finally carbonized at 1000 °C were evaluated as Li-ion battery anodes in half-cell and full-cell configurations. The specific capacities of the C and SiO_x components were 375 and 475 mAh g^{-1}, respectively, indicating that only about one-quarter of SiO_x was responsible for the reversible specific capacity for Li-ion insertion and extraction. C/SiO_x AMs with a lower SiO_x content exhibited a lower initial CE for Li-ion insertion and extraction because of Li passivation within the pores developed at the trace of the removed SiO_x. Full-cells with an NCM cathode and C/SiO_x anode were assembled. Owing to the low initial CE (<65%), pre-lithiation was essential to attain a stable anodic operation for the C/SiO_x AMs. All full-cells exhibited a high initial CE (~85%) and high discharge specific capacity (~150 mAh g_{CAM}^{-1}) at 0.1 C. At the increased C-rates of 5 and 10 C, a higher SiO_x content in the full-cell led to a higher cell specific capacity retention, revealing that the reversible reactions of SiO_x with Li ions are faster than those of the C component. The full-cell with C/SiO_x-45 exhibited the largest decrease in cell specific capacity (47.5% retention) during the cycle test, while the other full-cells exhibited ~60% retention. All results indicated that the SiO_x component in the RH-derived AMs enhances the specific capacity and rate performance, while inducing structural decay owing to the volume expansion of SiO_x. Considering the higher production yield, enhanced specific capacity and rate stability due to SiO_x, acceptable cycle performance degradation, and operational effort, cost, and eco-friendliness of SiO_x removal, the preservation of SiO_x is recommended when carbonized RHs are utilized as LIB anodes.

Reference

[1] R. Chen, S. S. C. Congress, G. Cai, W. Duan, S. Liu, Sustainable utilization of biomass waste-rice husk ash as a new solidified material of soil in geotechnical engineering: A review. *Constr. Build. Mater.* 292 (2021) 123219.

[2] S. Kumagai, et al. Lithium-ion capacitor using rice husk-derived cathode and anode active

materials adapted to uncontrolled full-pre-lithiation. *J. Power Sources* 437 (2019) 226924.

[3] D. S. Jung, M.-H. Ryou, Y. J. Sung, S. B. Park, J. W. Choi, Recycling rice husks for high-capacity lithium battery anodes. *Proc. Natl. Acad. Sci. U. S. A.* 110 (2013) 12229–12234.

[4] M. A. Azam, N. E. Safie, A. S. Ahmad, N. A. Yuza, N. S. A. Zulkifli, Recent advances of silicon, carbon composites and tin oxide as new anode materials for lithium-ion battery: A comprehensive review. *J. Energy Storage* 33 (2021) 102096.

[5] B. F. Song, A. Dhanabalan, S. L. Biswal, Evaluating the capacity ratio and prelithiation strategies for extending cyclability in porous silicon composite anodes and lithium iron phosphate cathodes for high capacity lithium-ion batteries. *J. Energy Storage* 28 (2020) 101268.

[6] Y. Abe, S. Kumagai, Effect of negative/positive capacity ratio on the rate and cycling performances of $LiFePO_4$/graphite lithium-ion batteries. *J. Energy Storage* 19 (2018) 96–102.

[7] H. Shobukawa, J. Alvarado, Y. Yang, Y. S. Meng, Electrochemical performance and interfacial investigation on Si composite anode for lithium ion batteries in full cell. *J. Power Sources* 359 (2017) 173–181.

[8] H. J. Kim, et al. Controlled prelithiation of silicon monoxide for high performance lithium-ion rechargeable full cells. *Nano Lett.* 16 (2016) 282–288.

[9] X. Yang, et al. The contradiction between the half-cell and full-battery evaluations on the tungsten-coating $LiNi_{0.5}Co_{0.2}Mn_{0.3}O_2$ cathode. *Electrochim. Acta* 180 (2015) 604–609.

[10] N. Loeffler, et al. Performance of $LiNi_{1/3}Mn_{1/3}Co_{1/3}O_2$/graphite batteries based on aqueous binder. *J. Power Sources* 248 (2014) 915–922.

[11] Q. Liu, et al. Understanding undesirable anode lithium plating issues in lithium-ion batteries. *RSC Adv.* 6 (2016) 88683–88700.

[12] C. Wang, et al. A robust strategy for crafting monodisperse $Li_4Ti_5O_{12}$ nanospheres as superior rate anode for lithium ion batteries. *Nano Energy* 21 (2016) 133–144.

[13] T. Yi, et al. Approaching high-performance lithium storage materials by constructing hierarchical $CoNiO_2$@CeO_2 nanosheets. *Energ. Environ. Mater.* 4 (2021) 586–595.

[14] J. Hassoun, G. Derrien, S. Panero, B. Scrosati, A nanostructured Sn-C composite lithium battery electrode with unique stability and high electrochemical performance. *Adv. Mater.* 20 (2008) 3169–3175.

[15] L. Dawei, et al. Adjusting ash content of char to enhance lithium storage performance of rice husk-based SiO_2/C. *J. Alloys Compd.* 854 (2021) 156986.

[16] T. Eguchi, K. Sawada, M. Tomioka, S. Kumagai, Energy density maximization of Li-ion capacitor using highly porous activated carbon cathode and micrometer-sized Si anode. *Electrochim. Acta* 394 (2021) 139115.

[17] S. Kumagai, Y. Abe, M. Tomioka, M. Kabir, Suitable binder for Li-ion battery anode produced from rice husk. *Sci. Rep.* 11 (2021) 15784.

[18] H. Chu, Q. Wu, J. Huang, Rice husk derived silicon/carbon and silica/carbon nanocomposites as anodic materials for lithium-ion batteries. *Colloids Surf. A Physicochem. Eng. Aspects* 558 (2018) 495–503.

[19] S. E. Wang, I.-S. Y. C. Jang, Kang, J. Chun, D.-S. Jung, Residual silica removal and nanopore generation on industrial waste silicon using ammonium fluoride and its application to lithium-ion battery anodes. *Chem. Eng. J.* 419 (2021) 129389.

[20] Y. Kaifeng, J. Li, H. Qi, C. Liang, High-capacity activated carbon anode material for lithium-ion batteries prepared from rice husk by a facile method. *Diam. Relat. Mater.* 86 (2018) 139–145.

[21] J. Cui, et al. High surface area C/SiO_2 composites from rice husks as a high-performance anode for lithium ion batteries. *Powder Technol.* 311 (2017) 1–8.

[22] Y. Ju, et al. SiO_x/C composite from rice husks as an anode material for lithium-ion batteries. *Electrochim. Acta* 191 (2016) 411–416.

[23] L. Wang, Z. Schnepp, M. M. Titirici, Rice husk-derived carbon anodes for lithium ion batteries. *J. Mater. Chem. A* 1 (2013) 5269–5273.

[24] M. K. Rybarczyk, et al. Hard carbon derived from rice husk as low cost negative electrodes in Na-ion batteries. *J. Energy Chem.* 29 (2019) 17–22.

[25] X. Fan, et al. Fe_3O_4/rice husk-based maco-/mesoporous carbon bone nanocomposite as

superior high-rate anode for lithium ion battery. *J. Solid State Electrochem.* 21 (2017) 27–34.

[26] S. Kumagai, M. Sato, D. Tashima, Electrical double-layer capacitance of micro- and mesoporous activated carbon prepared from rice husk and beet sugar. *Electrochim. Acta* 114 (2013) 617–626.

[27] L. Jiao, et al. An advanced lithium ion battery based on a high quality graphitic graphene anode and a $Li[Ni_{0.6}Co_{0.2}Mn_{0.2}]O_2$ cathode. *Electrochim. Acta* 259 (2018) 48–55.

[28] Y. Abe, T. Saito, S. Kumagai, Effect of prelithiation process for hard carbon negative electrode on the rate and cycling behaviors of lithium-ion batteries. *Batteries* 4 (2018) 71.

[29] I. H. Son, et al. Graphene balls for lithium rechargeable batteries with fast charging and high volumetric energy densities. *Nat. Commun.* 8 (2017) 1561.

[30] J. Libich, J. Máca, J. Vondrák, O. Čech, M. Sedlaříková, Irreversible capacity and rate-capability properties of lithium-ion negative electrode based on natural graphite. *J. Energy Storage* 14 (2017) 383–390.

[31] J. Zhang, X. Liu, J. Wang, J. Shi, Z. Shi, Different types of pre-lithiated hard carbon as negative electrode material for lithium-ion capacitors. *Electrochim. Acta* 187 (2016) 134–142.

[32] Z. Wang, et al. Application of stabilized lithium metal powder (SLMP®) in graphite anode—A high efficient prelithiation method for lithium-ion batteries. *J. Power Sources* 260 (2014) 57–61.

[33] K. Yu, et al. Preparation of porous carbon anode materials for lithium-ion battery from rice husk. *Mater. Lett.* 253 (2019) 405–408.

Chapter 6

Conclusions

6. 1 Conclusions

The charging and discharging performances of advanced LIBs using eco-friendly and economical active materials have been elucidated. The knowledge accumulated in Chapters 3–5 can contribute to the development of academic fields associated with green concept LIBs. The obtained results partially contribute to the realization of a carbon-neutral society due to the sustainable approaches for electrode material preparations. In the following sections, the major outcomes and conclusions from each chapter are summarized.

Chapters 1 and 2

The chapters presented the current state and challenges of active materials in LIB electrodes. Focusing on material preparation for LIB electrodes, academic approaches needed to address these challenges were considered. Research conducted on active materials in LIB cathodes and anodes is described in the subsequent chapters.

Chapter 3

Using pyrolysis to recycle whole battery stacks without exposure to air, three rare metals (Co, Ni, and Mn) were successfully recovered from waste LIB stacks. The recovered rare metals were utilized to fabricate LIB cathodes, which were evaluated using LIB half- and full cells. The recycled rare metals demonstrated acceptable performance, with slightly lower lithiation specific capacity but much higher capacity retention than a commercial material of NCM523. Chemical analyses revealed that the recycled active materials contained metallic impurities of Al, Cu, and Fe, totaling 4 mass%, along with excessive Li and residual F. Surprisingly, co-existing metallic impurities seemed to contribute to a partial improvement in performance, although the lithiation specific capacity decreased slightly. This successful demonstration of sustainable LIB fabrication through rare metal recycling provides valuable insights into reliable

and efficient recycling methodologies and concepts for sustainable material supply.

Chapter 4

The effects of excessive prelithiation on an HC/N-Si composite anode in LIBs were investigated by prelithiating the anode with different cutoff anodic specific capacities (200–600 mAh g^{-1}) prior to full cell assembly. The full cells containing an NCM523 cathode and the prelithiated HC/N-Si anode successfully operated during the initial charging-discharging cycle, regardless of the cutoff anodic specific capacities. Higher cutoff anodic specific capacities in the prelithiation resulted in higher anode utilization rates during full-cell operation. While higher anode utilization rates, triggered by cutoff anodic specific capacities above 500 mAh g^{-1}, are likely to impact cycling performance, rate performance was independent of anode utilization rates. These findings suggest that excessive prelithiation is an effective strategy for achieving stable and superior operation of LIBs with 8:2 HC/N-Si composite anodes.

Chapter 5

Sustainable and eco-friendly fabrication of LIB anodes was achieved by utilizing agricultural waste from RH with simple heat and chemical treatments. The RH was carbonized through a two-step heating process, with SiO_x removed by immersing it in a NaOH solution after the first heating process to evaluate the anodic performance of RH-derived anodes with varying SiO_x content. The RH-derived anodes were successfully incorporated in LIBs and demonstrated stable operation during long charging-discharging cycles, owing to prelithiation. The study demonstrated the effectiveness of the C/SiO_x anodes, with different SiO_x contents affecting current rate dependence and cycling behavior. Ultimately, the RH-derived C/SiO_x was found to be a valuable and sustainable active material for LIBs.

Publications and Presentations Associated with This Dissertation

Original Papers

[1] ○Y. Abe, I. Saito, M. Tomioka, M. Kabir, S. Kumagai, "Effects of excessive prelithiation on full-cell performance of Li-ion batteries with a hard-carbon/nanosized-Si composite anode", *Batteries*, Vol. 8(11), 210 (17 pages), November, 2022.

[2] ○Y. Abe, K. Sawa, M. Tomioka, R. Watanabe, T. Yodose, S. Kumagai, "Electrochemical performance of $LiNi_{1/3}Co_{1/3}Mn_{1/3}O_2$ cathode recovered from pyrolysis residue of waste Li-ion batteries", *Journal of Electroanalytical Chemistry*, Vol. 922, 116761 (11 pages), October, 2022.

[3] T. Eguchi, R. Sugawara, Y. Abe, M. Tomioka, S. Kumagai, "Impact of full prelithiation of Si-based anodes on the rate and cycle performance of Li-ion capacitors", *Batteries*, Vol. 8(6), 49 (14 pages), May, 2022.

[4] ○Y. Abe, M. Tomioka, M. Kabir, S. Kumagai, "Role of SiO_x in rice-husk-derived anodes for Li-ion batteries" *Scientific Reports*, Vol. 12, 975 (10 pages), January, 2022.

[5] S. Kumagai, Y. Abe, M. Tomioka, M. Kabir, "Suitable binder for Li-ion battery anode produced from rice husk", *Scientific Reports*, Vol. 11, 15784 (13 pages), August, 2021.

Review Paper

[1] 安部勇輔，熊谷誠治 (2022.4)「もみ殻由来 C/SiO_x 負極を用いるリチウムイオン電池」『アグリバイオ』6 巻 4 号 pp. 73–77. 北隆館

International Conferences

[1] Y. Abe, M. Nemoto, M. Tomioka, S. Kumagai, "Rice husk as a worthful source of battery materials for high-performance Li-ion battery anodes", The 9th International Conference

on Materials Engineering for Resources (ICMR2021), B-5, Online, October, 2021.

[2] K. Sawa, Y. Abe, S. Kumagai, R. Watanabe, T. Yodose, Electrochemical performance of NCM cathode recycled from waste lithium-ion batteries, The 9th International Conference on Materials Engineering for Resources (ICMR2021), CP-20, Online, October, 2021.

Domestic Conferences

[1] 熊谷悠希，安部勇輔，富岡雅弘，熊谷誠治「ハイニッケル系リチウムイオン電池における正極活物質塗工層の高密度化」令和 5 年電気学会全国大会, 名古屋大学, 名古屋市 (2023.3)

[2] 澤賢佑，高橋瑛斗，安部勇輔，熊谷誠治，渡邊亮栄，淀瀬達也「熱分解したリチウムイオン電池から再生した不純物含有 NCM111 の電気化学特性」第 63 回電池討論会，福岡国際会議場，福岡市 (2022.11)

[3] 高橋瑛斗，澤賢佑，安部勇輔，富岡雅弘，熊谷誠治「リサイクル正極材料を用いたリチウムイオン電池の充放電特性」第 6 回秋田ヒューマン・エネルギー研究会, オンライン (2022.8)

[4] 澤賢佑，高橋瑛斗，安部勇輔，熊谷誠治，渡邊亮栄，淀瀬達也「再生正極材における Li 含有率が Li イオン電池の充放電特性に及ぼす影響」2022 年度電気関係学会東北支部連合大会，オンライン (2022.8)

[5] 山川裕大，安部勇輔，富岡雅弘，熊谷誠治「ナノ Si 電極の組成がその Li イオン吸蔵放出特性に及ぼす影響」日本素材物性学会令和 4 年度（第 32 回）年会，オンライン (2022.6)

[6] 高橋瑛斗，澤賢佑，安部勇輔，熊谷誠治，渡邊亮栄，淀瀬達也「廃リチウムイオン電池から再生した三元系正極材のリチウム含有率がその電気化学特性に及ぼす影響」日本素材物性学会令和 4 年度（第 32 回）年会，オンライン (2022.6)

[7] 澤賢佑，高橋瑛斗，安部勇輔，熊谷誠治，渡邊亮栄，淀瀬達也「廃 Li イオン電池から再生した三元系正極材を用いる Li イオン電池の充放電特性」日本素材物性学会令和 4 年度（第 32 回）年会，オンライン (2022.6)

[8] 熊谷悠希，安部勇輔，富岡雅弘，熊谷誠治「Ni 高含有遷移金属酸化物における電極製造時のプレス圧力が電気化学特性に及ぼす影響」日本素材物性学会令和 4 年度（第 32 回）年会，オンライン (2022.6)

[9] 安部勇輔，熊谷悠希，富岡雅弘，熊谷誠治「短時間放電法による三元系 Li イオン電池正極の出力性能評価」日本素材物性学会令和 4 年度（第 32 回）年会，オンライン (2022.6)

[10] 澤賢佑，安部勇輔，熊谷誠治，渡邊亮栄，淀瀬達也「廃 Li イオン電池から再生した $LiNi_{1/3}Co_{1/3}Mn_{1/3}O_2$ の電気化学特性」令和 4 年電気学会全国大会，オンライン

(2022.3)

[11]安部勇輔，根本優樹，富岡雅弘，熊谷誠治「ハーフセルとフルセルによる Li イオン電池のもみ殻炭負極評価」2021 年度電気関係学会東北支部連合大会，オンライン (2021.8)

[12]大滝隼一朗，澤賢佑，安部勇輔，富岡雅弘，熊谷誠治「NCA 正極を用いたリチウムイオン電池のプレコンディショニング条件」日本素材物性学会令和 3 年度（第 31 回）年会，オンライン (2021.6)

[13]安部勇輔，根本優樹，富岡雅弘，熊谷誠治「もみ殻炭を用いる Li イオン電池フルセルの充放電特性に及ぼすシリカの影響」日本素材物性学会令和 3 年度（第 31 回）年会，オンライン (2021.6)

Related Presentations

[1] 遠藤幸太郎，安部勇輔，富岡雅弘，熊谷誠治「異種活性炭添加による電気二重層キャパシタ電極の劣化抑制」令和 5 年電気学会全国大会，名古屋大学，名古屋市 (2023.3)

[2] 藤本一輝，安部勇輔，富岡雅弘，熊谷誠治「高電圧充放電試験後の電気二重層キャパシタのインピーダンス特性」2022 年度電気関係学会東北支部連合大会，オンライン (2022.8)

[3] 遠藤幸太郎，安部勇輔，富岡雅弘，熊谷誠治「異種活性炭を添加した電気二重層キャパシタ電極の特性評価」2022 年度電気関係学会東北支部連合大会，オンライン (2022.8)

[4] 藤本一輝，安部勇輔，富岡雅弘，熊谷誠治「イオン液体を電解液に用いることによる電気二重層キャパシタの高エネルギー密度化」日本素材物性学会令和 4 年度（第 32 回）年会，オンライン (2022.6)

[5] 遠藤幸太郎，安部勇輔，富岡雅弘，熊谷誠治「異なる種類の活性炭を電極に用いる電気二重層キャパシタの充放電特性」日本素材物性学会令和 4 年度（第 32 回）年会，オンライン (2022.6)

Related Papers Previously Published by the Author

[1] Y. Abe, N. Hori, S. Kumagai, “Electrochemical impedance spectroscopy on the performance degradation of $LiFePO_4$/graphite lithium-ion battery due to charge-discharge cycling under different C-rates”, *Energies*, Vol. 12(23), 4507 (14 pages), November, 2019.

[2] S. Kumagai, Y. Abe, T. Saito, T. Eguchi, M. Tomioka, M. Kabir, D. Tashima, “Lithium-ion

capacitor using rice husk-derived cathode and anode active materials adapted to uncontrolled full-pre-lithiation", *Journal of Power Sources*, Vol. 437, 226924 (14 pages), October, 2019.

[3] Y. Abe, T. Saito, S. Kumagai, "Effect of prelithiation process for hard carbon negative electrode on the rate and cycling behaviors of lithium-ion batteries", *Batteries*, Vol. 4(4), 71 (16 pages), December, 2018.

[4] Y. Abe, S. Kumagai, "Effect of negative/positive capacity ratio on the rate and cycling performances of $LiFePO_4$/graphite lithium-ion batteries", *Journal of Energy Storage*, Vol. 19, 96–102 (7 pages), October, 2018.

[5] T. Saito, H. Fujiwara, Y. Abe, S. Kumagai, "Hard carbon/SiO_x composite active material prepared from phenolic resin and rice husk for Li-ion battery negative electrode", *International Journal of the Society of Materials Engineering for Resources*, Vol. 23(2), 142–146 (5 pages), September, 2018.

Acknowledgment

This dissertation is based on the research outcomes of the author's graduate studies at the Graduate School of Engineering Science, Akita University. The completion of this doctoral dissertation was made possible with the significant contributions of numerous individuals who were involved in this research.

I am deeply grateful to Professor Seiji Kumagai, my supervisor, for providing me with the opportunity to pursue this study. His guidance throughout the two-and-a-half years of research has helped me grow into a full-fledged researcher. I firmly believe that, without his guidance, this dissertation would not have been completed, and the academic achievements would not have contributed to the development of the field of electrical engineering. I would like to express my gratitude to him once again.

I would like to acknowledge Professor Katsubumi Tajima, Professor Okawa Hirokazu, and Associate Professor Mahmudul Kabir for their valuable advice and guidance in writing this dissertation. Additionally, I would like to express my gratitude to Mr. Ryoei Watanabe and Mr. Tatsuya Yodose from DOWA ECO-SYSTEM Co., Ltd. for their assistance in preparing samples and conducting chemical analyses, which were crucial for research presented in Chapter 3. This research was a collaborative effort between Akita University and DOWA ECO-SYSTEM Co., Ltd. and was financially supported by the Dowa Techno Fund. Finally, I acknowledge the donor of the farm family in Senboku City, Akita Prefecture, for generously providing rice husks as the starting material for research presented in Chapter 5.

I would like to express my gratitude to Lecturer Yukihiro Yoshida from Akita University and Lecturer Masahiro Tomioka from the National Institute of Technology, Nagano College, for

their valuable comments and advice throughout my research. I would also like to thank Assistant Professor Takuya Eguchi from Nihon University, who was a former graduate of the doctoral course at Akita University, for his daily stimulating discussions and encouragement during my time in the laboratory. Finally, I acknowledge Mr. Akihiro Nakajima, a technical staff, for his technical support during the research process.

I am grateful to the electrical engineers at TAIHEIYO CEMENT Corp., where I worked from 2019 to 2021, for their invaluable coaching and guidance in acquiring practical skills and knowledge related to electrical engineering. Their guidance not only helped me grow as a specialist with work experience but also complemented the research capacities I developed at Akita University.

Finally, I would like to express my sincere gratitude to my family for their unwavering physical and psychological support, as well as their financial assistance, over the past 29 years. Their unconditional love and support allowed me to pursue my academic and professional goals with confidence. I am grateful for their constant encouragement and for trusting me to make the right decisions for my career. Without their support, I could not have accomplished what I have today. I dedicate my academic achievements as an expression of gratitude and a testament to their unwavering support and belief in me. I am proud to be their son. Thank you very much.

令和五年九月
安部勇輔